Investigation of Multicomponent Transport Phenomena in Nafion 117 and Crosslinked Polyether-based Membranes via In Situ ATR FTIR Spectroscopy

by

Breanna Marie Dobyns

A dissertation submitted to the Graduate Faculty of
Auburn University
in partial fulfillment of the
requirements for the Degree of
Doctor of Philosophy

Auburn, Alabama
August 8, 2020

Transport, multicomponent, in situ, ATR FTIR spectroscopy

Approved by

Bryan Beckingham, Chair, Assistant Professor of Chemical Engineering, Auburn University
Andrew Adamczyk, Assistant Professor of Chemical Engineering, Auburn University
Allan David, Associate Professor of Chemical Engineering, Auburn University
Daniel Miller, Materials Staff Scientist/Engineer, Lawrence Berkeley National Laboratory
Kyle Schulze, Reader, Associate Professor of Mechanical Engineering, Auburn University

Abstract

This dissertation focuses on understanding transport and co-transport behavior for a series of species in dense, hydrated polymer membranes. The rate of solute transport through a membrane, permeability, is a fundamental property when selecting a membrane for an application of interest. However, it is challenging to characterize multicomponent transport using traditional techniques. This work investigates the transport of multiple components through polymeric membranes via a facile, in situ technique that combines the advantages of in situ characterization with spectroscopy; in situ ATR FTIR spectroscopy. Using this technique, the transport behavior of a series of alcohols and sodium acetate is investigated. The transport behavior of alcohols and their complex mixtures are probed as phenomena such as flux coupling and competitive sorption make prediction of multicomponent transport from single component data challenging, and is poorly understood. First, multicomponent transport in Nafion™ 117, a commercially significant cation exchange membrane that has been researched extensively, is investigated for alcohols and complex mixtures of alcohols. Furthermore, a series of PEGDA membranes with varied fractional free volume and PEGDA-PEA-AMPS membranes of varied charge and hydrophobicity were synthesized and characterized for their permeability to methanol, sodium acetate, and their binary mixtures. Large deviations were observed between single component permeability and permselectivity compared to those extracted from multicomponent experiments, with variations of up to a factor of 11, demonstrating the importance of this characterization and technique for investigating membrane transport behavior. Overall, while much remains to be learned in this field, the fundamental understanding gained herein advances our understanding of the role of co-solutes, and membrane characteristics on transport behavior.

Acknowledgements

My time in grad school has been incredible! I love my research, the friends that I made, and the work I accomplished. I am so very thankful to Auburn University for accepting me, and from there, thank you so much Bryan for being such a great boss!!! I know that there were times I almost quit, and times I'm sure you wish I had, but I will never be able to thank you enough! Everything that I have learned from you has helped me immensely, in research, in dealing with people, and in being an adult! From there, I'd like to thank my group mates. Michael, thank you for being such a wonderful friend through these 5 years, and not getting too mad at me when I yell at you. Luca, thank you for all of your help and for being such an honest friend and constant in my life. If I need the truth, you are who I ask! Vinita, I love you and adore how sweet you are, I hope we stay friends forever. Bradley, although I don't know you that well considering you just started, it was really fun while it lasted. Finally, Sneha! I miss you terribly sweet girl and am so happy we became such amazing friends while you were here! Now I would like to thank my family. Mom, thank you for believing in me more than anyone else, always, and for all of your support and love. Tiff, thank you for all of your help relaxing whenever I came home, and showing me such an amazing time! Jack, thank you for being such a sweetheart and always making me laugh. And Ginger, thank you for all of the help you've given me! I loved hanging out with you over COVID and you have no idea how much you helped me with this dissertation! To my man, Brian, thank you so much for all of your love, support, and stress relieving efforts, however futile they may have been. I love you so much! Granny, thank you for all of your emotional and financial support, you are always there for me when I need you! Dad, I love and miss you, and hope you know just how thankful I am that you were my father. To my wonderful animals, thank you for being my number one stress relief and always such sweehearts! Now I would like to thank my committee

members for all of their help and support in this work. After my Prelim, I was terrified to defend, but I am so excited to have made it to this and I could not have done it without all of your help! Again, THANK YOU! And to everyone I missed, I hope you forgive me, ha this document is due today and I just want to be done!

Table of Contents

List of Tables

List of Figures

List of Abbreviations and Variables

$\alpha_{i/j}$: Selectivity of i over j

A: Area of membrane available for transport

A_i: Measured absorbance of component i

c_i: Concentration of species i

$\frac{dc_i}{dx}$: Concentration gradient of species i through the thickness of the membrane

$\frac{d\mu_i}{dx}$: Gradient of the chemical potential of species i through the thickness of the membrane

D_0: Pure solvent's diffusion coefficient

D_i: Diffusivity coefficient of species i

$\varepsilon_{i,\lambda}$: Effective extinction coefficient of component i at wavenumber λ

ϵ: Extinction coefficient

J_i: Flux of component i in g/cm^2 s

k: "Front factor" for the "upper bound polymers" line in the Robeson plot

K_i: Solubility coefficient of species i

l: Membrane thickness

l: Path length of a beam through a solution

ΔL: Dimensional swelling in membrane thickness

L_i: Coefficient of proportionality

L_S: Membrane thickness after solution uptake equilibration

L_W: Membrane thickness after equilibration with water

m_W: Mass of the hydrated membrane

m_D: Mass of the dry membrane

m_S: Mass of the solute swollen membrane

n: Slope of the log-log Robeson plot for the separation of interest

n_i: Number of polymer molecules in solution

p_i^0: Reference pressure of species i

P: Power of an electromagnetic radiation beam within the absorbing medium

P_0: Radiant power of an electromagnetic radiation beam

P_i or P_j: Permeability of component i or j

π_{sw}: Swelling pressure

π_{mix}: Mixing pressure

π_{el}: Elastic deformation pressure of the polymer chains

ϕ_1: Volume fraction of water

ϕ_m: Volume fraction of the polymer

R: Gas constant

S: solute uptake

t: time for permeation experiment

T: Absolute temperature

v_1^0: Molar volume of pure water

v_2: Volume fraction of the solvent

V: Volume of the receiver and donor cells in the diffusion cell apparatus

W: Water uptake

χ: "Flory-Huggins interaction parameter" or the thermodynamic interaction parameter between a particular solvent and polymer pair

γ_i: Activity coefficient of species i

γ_1: Activity coefficient correction to compensate for the non-ideality of the polymer-water mixture

Chapter 1: Introduction

1.1. Objective

Polymers are found everywhere in today's world. They make up the human body as well as what people wear, use, and even eat. Polymers are long chains of repeating units, termed mers, connected by covalent bonds. Polymeric molecules exist naturally as well as synthetically, but synthetic polymers have only been produced within the last 110 years. A critical application for polymeric materials is polymer-based membranes, which are used in a plethora of applications today, such as fuel cells, dialysis, and water purification. According to Baker's Membrane Technology and Applications, "[t]he most important property of membranes is their ability to control the rate of permeation of different species".[1] Current standard processes that utilize a polymer membrane are forward osmosis, reverse osmosis, electrodialysis, reverse electrodialysis, capacitive deionization, and pressure-retarded osmosis.[1] These membrane-based processes are vital as they have a lower carbon footprint and higher energy efficiency than other separation processes, such as distillation.

Small synthetic differences easily modify polymeric membranes, but the physics behind solute transport, particularly small solute transport, through these membranes is poorly understood in the literature. There are several in situ, probe-based techniques to characterize solute transport through membranes that explain single component phenomena adequately, but they are unusable for multiple component mixtures. Multiple component solute experiments have rarely been performed in the past due to the difficulty of these experiments. Herein, we establish and utilize a facile technique to study multiple solute transport simultaneously through polymeric membranes.

Through *in situ* attenuated-total-reflectance Fourier-transform infrared (ATR FTIR) spectroscopy, the concentration of multiple solutes can be quantified in solution. As solutes transport through a membrane, the spectrophotometer collects spectra enabling independent calculation of each solute's concentration in the solution, requiring only pure solute calibrations. This technique preempts the need to periodically collect aliquots and analyze their composition ex situ, a time-consuming process with additional complications. In this dissertation, this approach is leveraged to investigate multicomponent solute transport in the commercially available cation exchange membrane Nafion^{TM} 117 as well as a series of fabricated membranes with controlled and tunable properties.

This dissertation first evaluates the capability of using ATR FTIR spectroscopy to determine solute concentrations in complex mixtures and, ultimately, their permeability from complex mixtures through membranes. The transport of various solutes and their complex mixtures through Nafion^{TM} 117 membranes are then characterized and evaluated in the context of solution-diffusion transport behavior. Lastly, two series of synthetic polymer membranes are evaluated. First, poly(ethylene glycol) diacrylate [PEGDA] is crosslinked in the presence of varied water content to vary the amount of fractional free volume (FFV) in the membrane. Second, copolymers of PEGDA, 2-phenoxyethyl acrylate [PEA], and 2-acrylamido-2-methyl-1-propanesulfonic acid [AMPS] are synthesized with differing amounts of bound ions. The characteristics of these two synthesized systems as polymeric membranes are examined to better understand how membrane chemistry and the presence of co-permeants impact membrane transport processes.

1.2. Organization

This dissertation is organized as follows. Chapter 2 provides background information and molecular transport theories used to describe solute transport in polymer membranes. Chapter 3 details the synthesis and characterization methods used herein. Chapter 4 describes a novel technique for calibrating and benchmarking ATR FTIR spectroscopy for the subsequent permeability experiments. Chapter 5 details transport experiments for a series of alcohols through Nafion^{TM} 117. Chapters 6 and 7 describe the synthesis of PEGDA membranes of varied fractional free volume and PEGDA-PEA-AMPS membranes of varied ion content, respectively, and the transport behavior of these membranes to methanol and sodium acetate. Finally, Chapter 8 details current conclusions and future work related to this dissertation.

1.3. References

1. Baker RW. *Membrane Technology and Applications*. John Wiley & Sons, Ltd; 2012. doi:10.1002/9781118359686

Chapter 2: Background

Polymeric thin films, and specifically polymeric membranes, are widely used today as they can be synthesized from polymers with a wide range of properties and fabricated using numerous techniques for meeting the specifications of the desired application. They have many advantages to traditional separation techniques (like distillation) as they may have lower energy, lower carbon footprints, and efficiently separate specific molecules over others (while distillation is simply separation based upon differences in volatility). While there are many benefits to membrane processes, many challenges remain. One significant challenge in polymer membrane science is the characterization of small molecule transport from complex, multicomponent mixtures through membranes, the primary focus of this dissertation. This chapter provides a general background to polymeric membranes, membrane applications (fuel cells in particular), and molecular transport behavior through polymeric thin films.

2.1. Polymer Membranes

Improving efficiency and sustainability of the so-called water-energy nexus, or further, the water-energy-food nexus, is a societal grand challenge.[1–4] The 'water-energy nexus' is a term used to describe the vast amounts of clean water needed to produce, extract, and refine energy and also the vast amounts of energy required to extract, transport, and clean water.[1] In other words, clean water is needed to produce energy, but energy is needed to clean water. Figure 2.1 shows a depiction of the water-energy nexus.

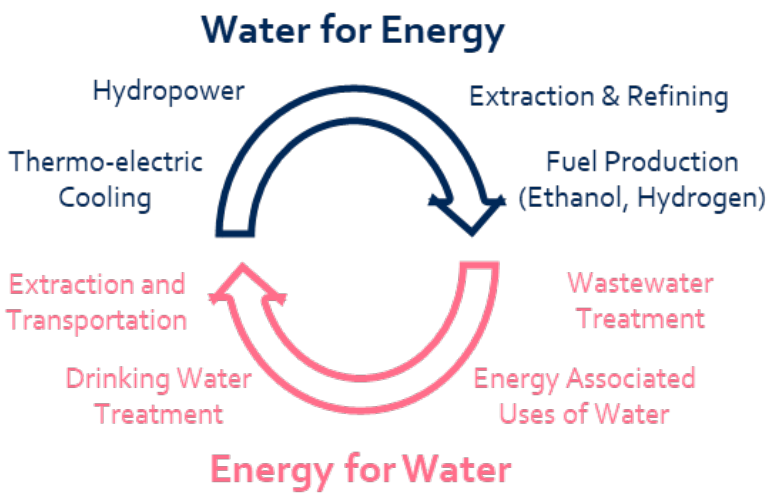

Figure 2.1. Depiction of the water-energy nexus.[1]

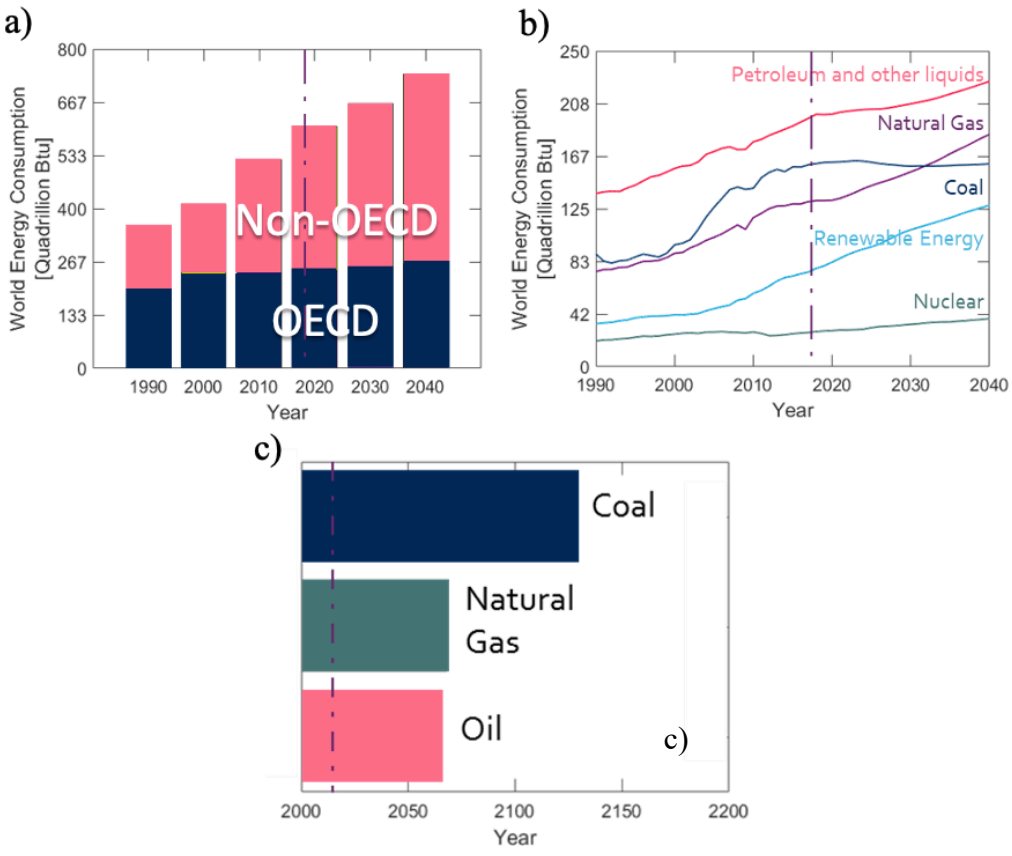

Figure 2.2. The environmental protection agency's projected outlook of a) world energy consumption vs. year of non-OECD and OECD countries, b) world energy consumption vs. year of energy sector, and c) coal, natural gas, and oil reserves.[5]

Three of the International Energy Agency's World Energy Outlook projections are presented in Figure 2.2.[5] Figure 2.2a shows the prediction for energy consumption by the organization for economic cooperation (OECD) and non-OECD countries by year.[5] Notably, it is mostly the non-OECD countries that will increase their energy consumption in the future, as the non-OECD countries are the reason for the increase in the last ~30 years. Figure 2.2b shows the projected world energy consumption by energy sector: petroleum and other liquids, natural gas, renewable energy, and nuclear energy needs will increase while the demand for coal is projected to be constant and/or fall. However, coal is the only fossil fuel that will still be available after 2070 (Figure 2.2c). The dotted purple lines in Figure 2.2 indicate where we were when this was published in 2017.[5–8]

Another side of the nexus is water purification. According to the U.S. Geological Survey's water science school, Earth's surface is 71% water.[19] However, of that water, only 3% is freshwater, and of that freshwater, only 0.3% is readily available for human consumption, as depicted in Figure 2.3. Therefore, better ways to clean water are needed, and, relatedly, better ways to produce the required energy to do so.[9]

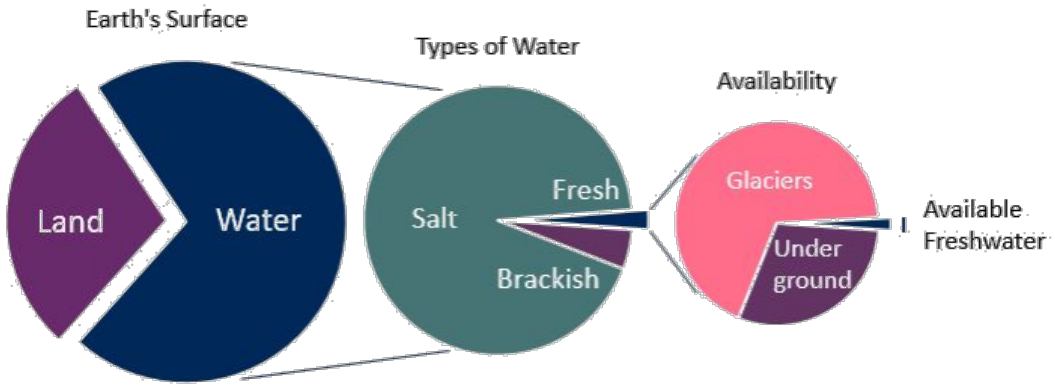

Figure 2.3. Available freshwater on Earth's surface.[9]

The water-energy nexus describes the current world need for efficient, facile techniques for cleaning water and generating energy. Polymers can be utilized for both water purification and energy production as sorbents or membrane materials. Polymers are molecules made from many (poly) repeating units (mers). They are found everywhere, from the paint on your walls, to the food that we eat, to the DNA we are composed of. Natural polymers are ubiquitous (for example, rubber, proteins, and our DNA), but synthetic polymers with the exact specifications have only been accomplished in the last 110 years.[10] From rubbery to glassy, hydrophobic to hydrophilic, dense to porous, polymeric membranes can be synthesized for a specific application and range of solutes, within reason. Polymeric membranes are used for a wide variety of applications: from fuel cells to biomedical applications to water purification, and many processes utilize membranes: reverse osmosis, forward osmosis, electrodialysis, reverse electrodialysis, capacitive deionization, and pressure-retarded osmosis. Polymeric membranes have a small carbon footprint and are more energy-efficient when compared to traditional separation techniques (e.g., distillation). Nevertheless, there are multiple areas (i.e., chemical stability, fouling resistance, and small molecule transport[11]) that need to be studied more thoroughly.

There are a variety of different types of membrane materials, from ceramic to ionic liquid to polymeric.[11–14] Figure 2.4 shows a so-called Robeson Plot constructed for polymeric and ionic liquid membranes and compares membrane selectivity and permeability. Permeability is a gauge of a membrane's efficiency for transporting molecules, and selectivity is simply the ratio of the permeabilities of two components of interest, as shown in Equation 2.1.

$$\alpha_{ij} = \frac{P_i}{P_j} \qquad 2.1$$

The Robeson Plot, in Figure 2.4, plots the selectivity of CO_2 over N_2 versus CO_2 permeability. In essence, they are comparing the membrane's ability to separate these species to the membrane's productivity of the more concentrated gasses. The higher the selectivity, the greater that component's (here CO_2) flux through the membrane relative to the other element (here N_2). However, as shown in Figure 2.4, selectivity and permeability tend to be inversely related, and designing materials which display improvements in both are a focus of considerable research.[15–17] For instance, Lin and Freeman characterized the solubility, diffusivity, and permeability of multiple gases through poly(ethylene oxide) (PEO) membranes with varied temperature and pressure.[18] They found high CO_2/N_2 selectivity of 140, a much greater selectivity than all of the polymers shown in Fig. 2.4, at a permeability of 8.1 Barrers, indicating that these membranes will separate CO_2 and N_2 streams more efficiently, with decent production rates, than any of the membranes on the Robeson plot in Figure 2.4.[18]

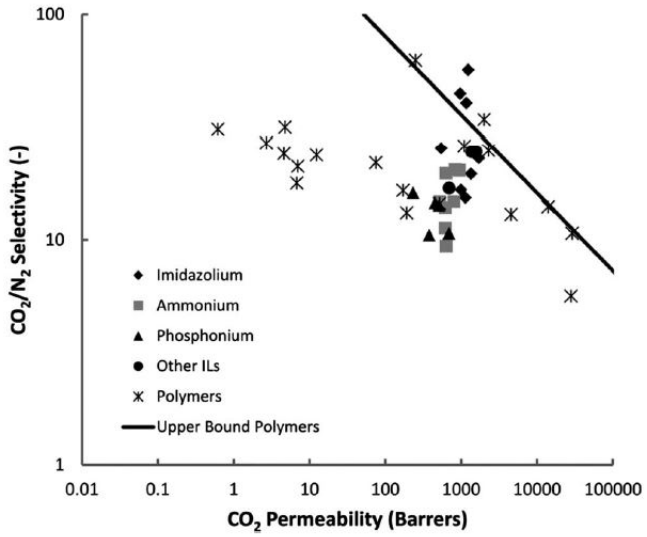

Figure 2.4. A Robeson plot of the permeability of carbon dioxide of different types of polymer membranes[19–21] and ionic liquid membranes[22] versus their preference for CO_2 when compared to N_2 (aka their selectivity).[16]

The solid black line in Figure 2.4 is termed the "upper bound" and is described by Equation 2.2[19,20]

$$P_i = k\alpha_{ij}^n \tag{2.2}$$

where α_{ij} is the selectivity of i over j, P_i is the permeability of component i, P_j is the permeability of component j, k is the "front factor", and n is the slope of the log-log plot for the separation of interest.[19,20] The selectivity, α_{ij}, of certain species over others is incredibly important for many different applications. For example, water purification via reverse osmosis (discussed in detail below), the water must transport (permeate) through the thin film while ionic species (salt) must not. In this application, the selectivity for water over salt must be high to produce drinking water with very low salt content for human consumption. Further, a high permeability is sought to provide large quantities of purified water to meet societal demands without requiring many membranes of low permeability, and thereby higher cost.

For cleaning water, membranes utilizing convective transport (the random Brownian transport of molecules via diffusion, as well as transport along fluidic currents via advection) are used in nanofiltration, ultrafiltration, and microfiltration.[23] Porous membranes are utilized to simply filter particles of specific sizes, as shown in Figure 2.5. These different types of filtration membranes separate a range of particle sizes over six orders of magnitude! The difference between these types of membrane filtration is simply in the size of the particles being excluded and, consequently, the size of the membrane pores, as can be seen from Figure 2.5, except for reverse osmosis, which will be discussed shortly.

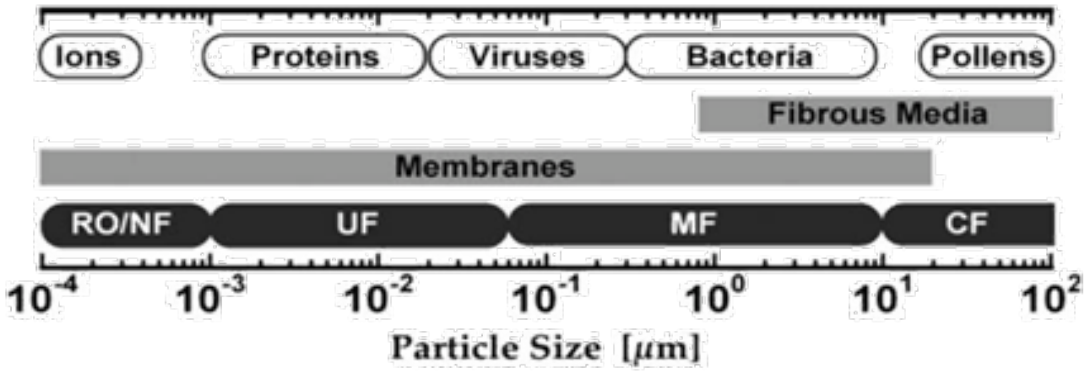

Figure 2.5. Particles and their sizes removed by reverse osmosis (RO), nanofiltration (NF), ultrafiltration (UF), microfiltration (Mf), and conventional filtration (CF).[24]

Conventional filtration is generally used in water treatment for the removal of substantial organic matter and other particulates. Microfiltration removes bacteria, larger viruses, sediment, algae, and all protozoan cysts.[25] Ultrafiltration removes smaller species such as plastics, silica, smog, endotoxins, proteins, silt, and viruses.[26] Nanofiltration is comparatively new and is typically applied to wastewater treatment for the removal of very small species such as arsenic, dyes, pesticides, and soil leachate.[23] All of these filtration methods can be used in the power, refinery, petrochemical, chemical, oil/gas, mining/metals, food/beverage, and municipal industries based upon the size of the solid particles that need to be removed from liquid streams.[26]

While nanofiltration can desalinate water, the very small pores tend to become obstructed over time, so-called membrane fouling, leading to the need for cleaning or complete replacement of the membrane.[26–29] Reverse osmosis is another membrane technology that can remove these very small species, though it works using different separation principles (depicted in Figure 2.6), and it too can have fouling issues. Reverse osmosis uses a semipermeable membrane that selectively permeates water and uses applied pressure to the lower-concentrated water solution (salt-water

solution, low water concentration) to drive water transport to the higher-concentrated solution (pure water, high water concentration). The semipermeable membrane is typically a thin, dense polymer layer supported on a porous membrane that provides strength and durability. The dense polymer layer prevents ions from transporting through the membrane.

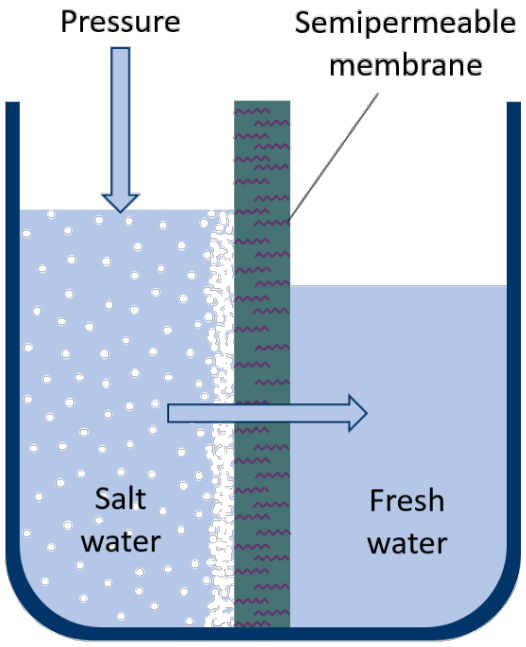

Figure 2.6. Reverse osmosis depiction.

Dense polymeric membranes such as the thin selective layers in RO membranes do not contain pores, and therefore, there is no convective flow. Dense membranes are greatly researched today for a variety of applications. Liang et al. synthesized dense polyvinyl butyral (PVB) polymeric membranes for use in lithium-ion batteries. These membranes showed excellent characteristics for this particular application, and they mention how they are promising candidates for the polymer electrolyte within lithium-ion batteries.[30] Another dense polymeric membrane system was synthesized with imidazolium by Carlisle et al. and showed good pure component selectivity for CO_2/H_2. These membranes were the first dense ionenes but exhibited similar selectivity/permeability relationships as many other polymers.[31]

Nafion™ is a highly utilized, dense, commercially-available cation exchange membrane introduced by DuPont in the 1960s. There has been a considerable amount of research on these membranes as they are an ideal candidate for fuel cells in general,]direct methanol fuel cells in particular.[32–45] Nafion™ has a polytetrafluoroethylene (PTFE) backbone, which is the same chemical makeup of Teflon®, and polyvinylfluoroether sulfonate side chains, which enable the transport of hydrophilic species. The chemical structure of Nafion™ is shown in Figure 2.7. The PTFE backbone ensures the membrane is chemically and thermally stable, while the side chains provide water and proton transport pathways.

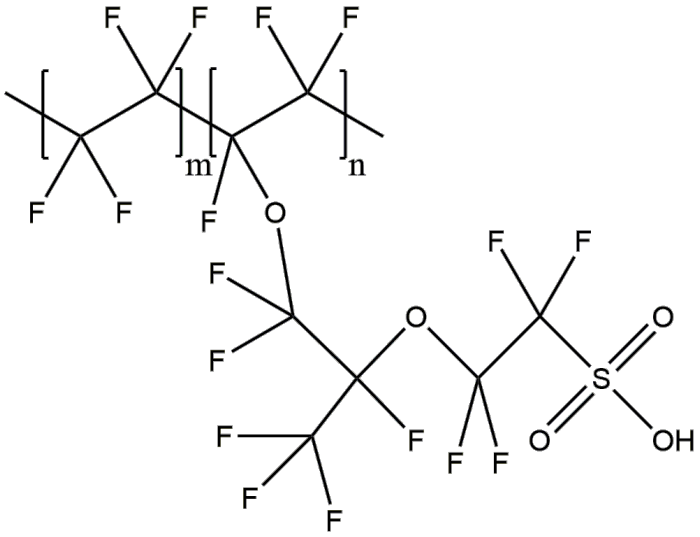

Figure 2.7. Chemical Structure of Nafion™ 117.

Nafion™ and other ion exchange membranes are integral components of many applications including electrolyzers and fuel cells.[37,40,46–50] In this dissertation, the transport behavior of a series of solutes in hydrated Nafion™ 117 is investigated (Chapter 5), as understanding this behavior is critical to understanding device performance. Additional details are provided in Chapter 5, while the following sections give a general overview of fuel cells and artificial photosynthesis devices.

2.2. Fuel Cells

Fuel cells convert reactants into high-value products via catalytic reduction driven by an electrical current. They do not need recharging as with batteries and do not run down, as long as the electrodes are not degraded. Oxidation of a hydrogen source occurs at the platinum anode, and reduction of an oxygen source occurs at the porous cathode. An electrolyte between the electrodes must transport protons while hindering the transport of the reduction products. The released electrons then flow through an electric circuit. Figure 2.8 is a depiction of a solid oxide fuel cell (SOFC). Hydrogen enters on the side of the anode (on the left) and is split into protons and electrons. The electrons are passed through an electric circuit to the cathode. Oxygen enters on the right (the side of the cathode) and is split into oxygen ions. The electrolyte in the middle not only separates the electrodes but also must have good ionic conductivity to combine the proton and oxygen ions, synthesizing water. The issue with these types of fuel cells, however, is that they must be used at high temperatures and they need pure hydrogen supplied to the anode, increasing both operational costs and the cost of the equipment.[51]

Some of the issues with solid oxide fuel cells can be alleviated by the use of other reactants and/or other electrolytes. Figure 2.9 gives an overview of current fuel cell types being investigated, their operating temperatures, their effectiveness, their reactants, and their products. The SOFC's (solid oxide fuel cells[51]), MCFC's (molten carbonate fuel cells[51]), and PAFC's (phosphoric acid fuel cells[51]) require very high temperatures, while every fuel cell shown requires a hydrogen supply to the anode, except the DMFC's (direct methanol fuel cells[51–53]). SOFC's, MCFC's, and DMFC's produce CO_2 while PAFC's and DMFC's are below 50% efficient. Proton exchange or polymer

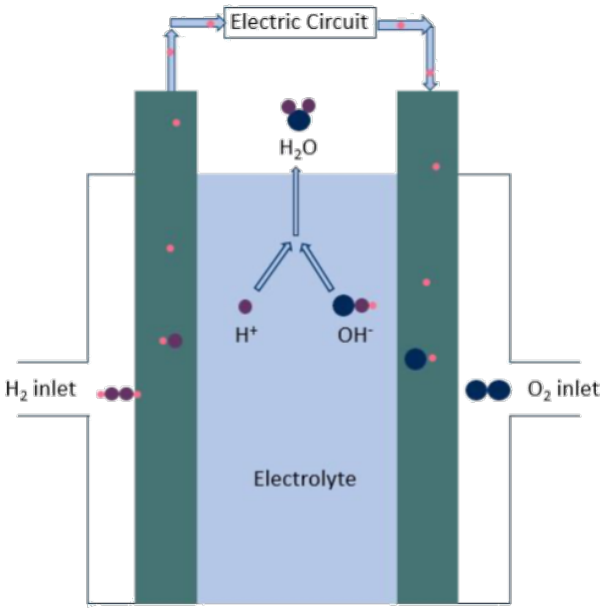

Figure 2.8. Depiction of a solid oxide fuel cell.

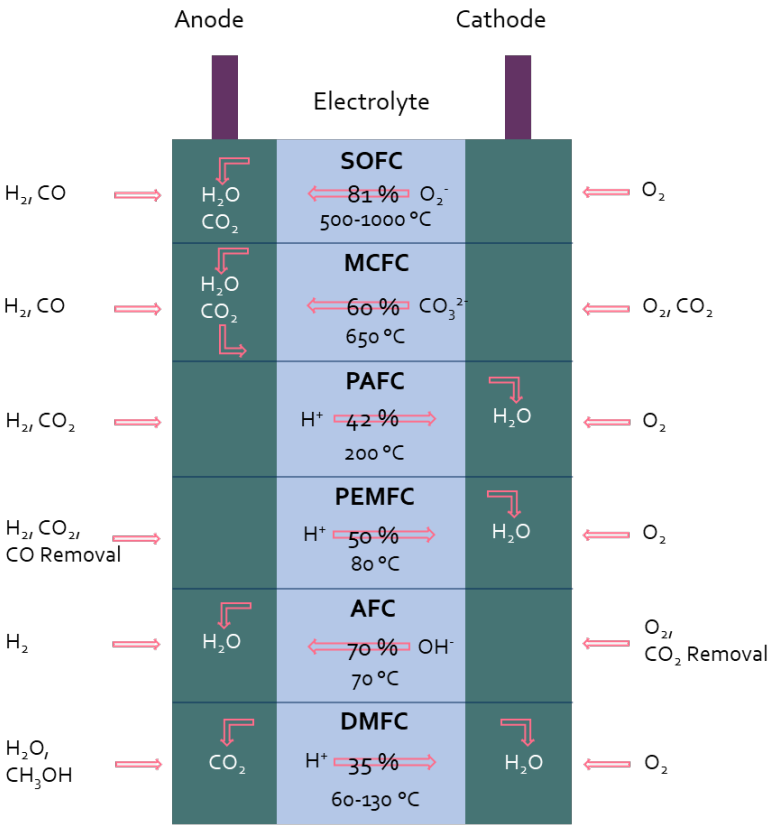

Figure 2.9. Current fuel cells being researched. Reactants, products, operation temperature, and efficiency are included.

electrolyte fuel cells (PEMFC's) perform at 80 °C, need pure hydrogen, reduce CO_2 and CO, and are 50% effective, seemingly the best candidate thus far.[51,54,55]

One solution for removing the necessity of pure hydrogen as a feedstock is direct methanol fuel cells (DMFC), which rely on methanol and water as the reactants. DMFCs operate at lower temperatures; however, they are only 35% efficient and synthesize CO_2. This is less desirable as mitigation of CO_2 production and release to the environment is a current challenge concerning global warming. While current fuel cell technologies present many advantages to traditional energy sources, there is still much room for the improvement of these devices.[51–57]

2.2.1. CO_2 Reduction

As was mentioned previously, one type of device reduces CO_2 to produce chemical products. A general schematic of a CO_2 reduction device is shown in Figure 2.10.[58] Artificial photosynthesis is the reduction of carbon dioxide as the oxygen input and the oxidation of water as the hydrogen input, utilizing sunlight to power the system. Of the greenhouse gases in the atmosphere, carbon dioxide makes up over 75%, shown in Figure 2.11a. Figure 2.11b shows the carbon dioxide emissions by sector and transportation accounts for over a quarter of the human CO_2 emissions.[59] These devices synthesize high-value fuels and/or high-value chemical products from the electrochemical reduction of CO_2 and have particular membrane requirements: they must be ionically conductive, have excellent mechanical and thermal stability, and have low permeability to CO_2 reduction reactants (CO_2 and O_2 gases) and products (aqueous species).[56,60,61]

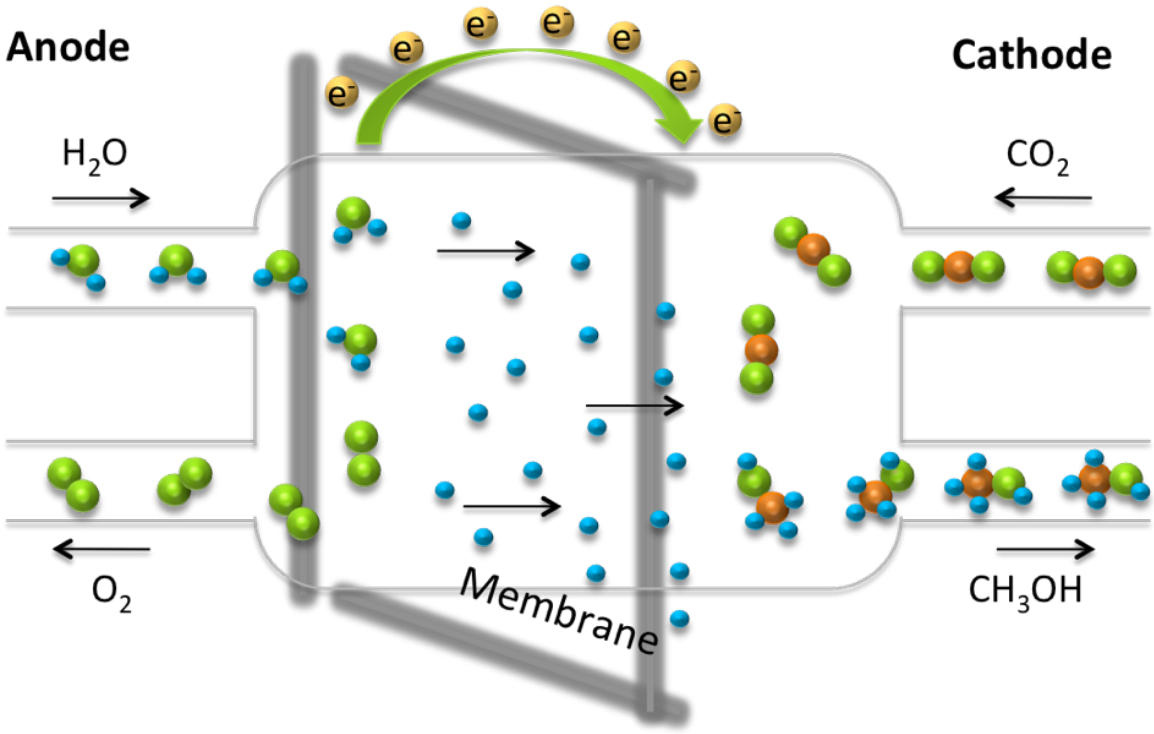

Figure 2.10. CO_2 reduction device.[58]

Table 2.1 gives a list of reported CO_2 reduction products.[60] In this dissertation, the transport behavior of the CO_2 reduction products acetone, ethanol, methanol, n-propanol, and sodium acetate will be investigated for different membranes in Chapters 4 - 7.[58,60]

Figure 2.12 shows an artificial photosynthetic closed-loop system for transportation. Utilizing water, sunlight, and CO_2, carbon-based fuels can be fed to our transportation vehicles. Then, the CO_2 emissions can be recycled back into the device, making an emission-free system that reduces CO_2 and powers our vehicles. This would be a fantastic solution to the current deplenishing fossil fuel and greenhouse gas emission issues.

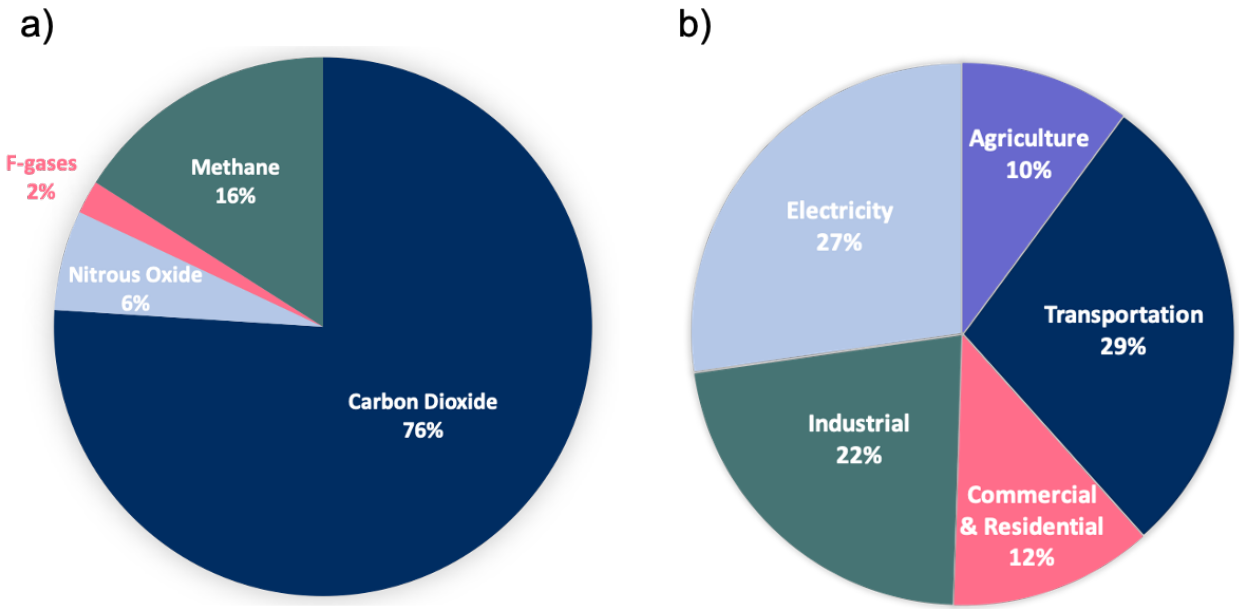

Figure 2.11. Current CO_2 statistics. a) human greenhouse gas emissions and b) CO_2 emissions by sector.[59]

Table 2.1. CO_2 reduction liquid products.[60]

# of e⁻s	Liquid Products
2	Formate
4	Formyl Radical
6	Methanol
6	Glyoxal
8	Acetate
8	Glycoaldehyde
10	Ethylene Glycol
10	Acetaldehyde
12	Ethanol
14	Hydroxyacetone
16	Acetone
16	Allyl Alcohol
16	Propionaldehyde
18	n-Propanol

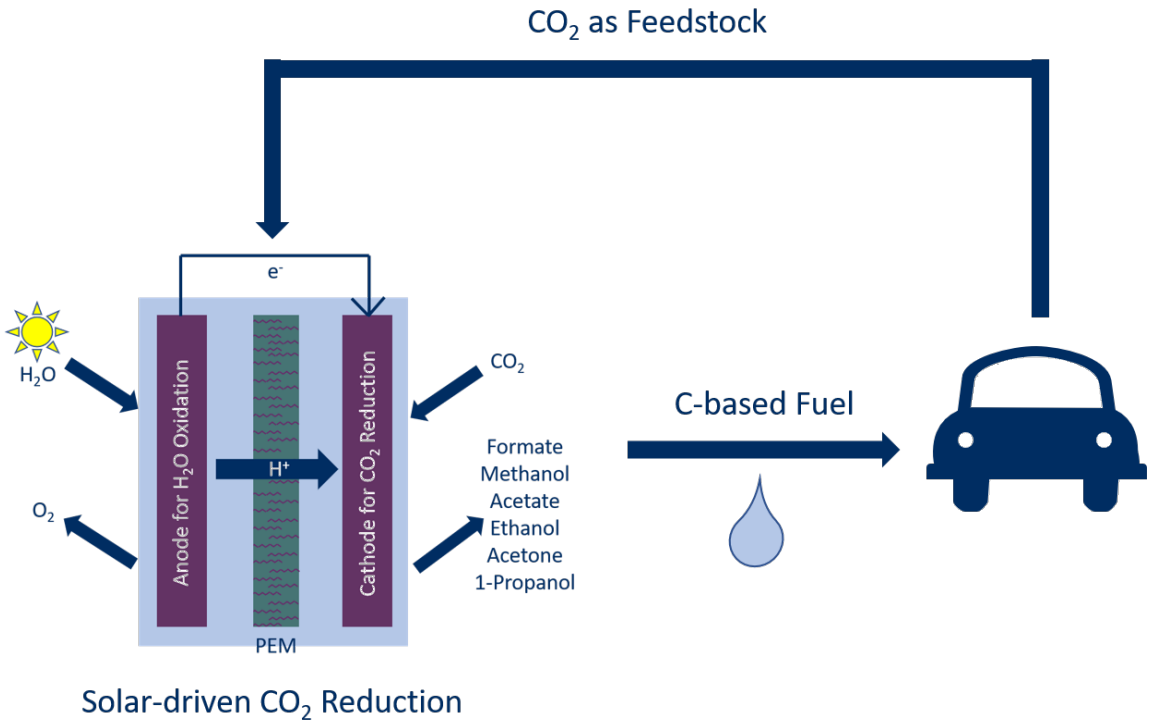

Figure 2.12. Closed-loop artificial photosynthetic transportation system.[62]

2.3. Solute Transport through Polymeric Thin Films

The two modes of molecular transport through a membrane are convective and diffusive flow. Solutes can transport through porous media by both convective and diffusive flow. In systems with convective flow (such as porous membranes), the diffusive contribution is comparatively negligible. In the dense polymer membranes of interest for artificial photosynthesis devices, solutes transport through this dense media strictly by diffusion, as there are no pores in which convective flow can occur. The diffusive flux in these membranes is through passive transport, which is transport based on a gradient as the driving force for the mass transfer.[63,64] This kind of transport does not require any added energy, it merely relies on the given gradient and the permeability of the membrane to the molecule(s). In many cases, the gradient exists between solutions of different solute concentrations, and molecules move from the solution of higher concentration to the solution of lower concentration.

There are multiple models for describing the transport of molecules through membranes, depending on their structure. The two most well-known are the pore-flow model and the solution-diffusion model. The pore-flow model (Figure 2.13) is what most envision when they think about transport through a membrane. In this model, only molecules small enough to fit within the membrane pores are allowed to pass through the membrane, and separation occurs based on differences in molecular size between species that can and cannot pass through the membrane.[65]

In the pore-flow model, the solvent activity, γ_i, remains constant from the upstream solution, within the membrane, and to the downstream solution. Meanwhile, the chemical potential, μ_i, and pressure, p, are reduced through the membrane as shown schematically in Figure 2.14.[65]

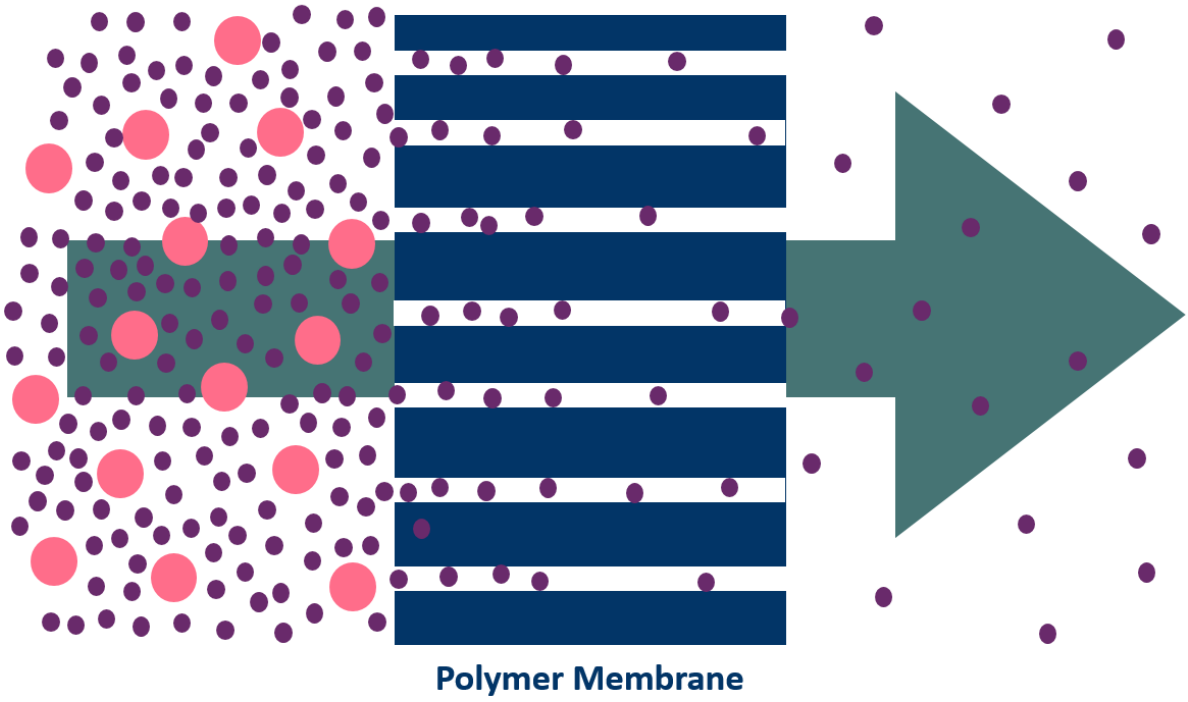

Figure 2.13. Depiction of the Pore-Flow Model.

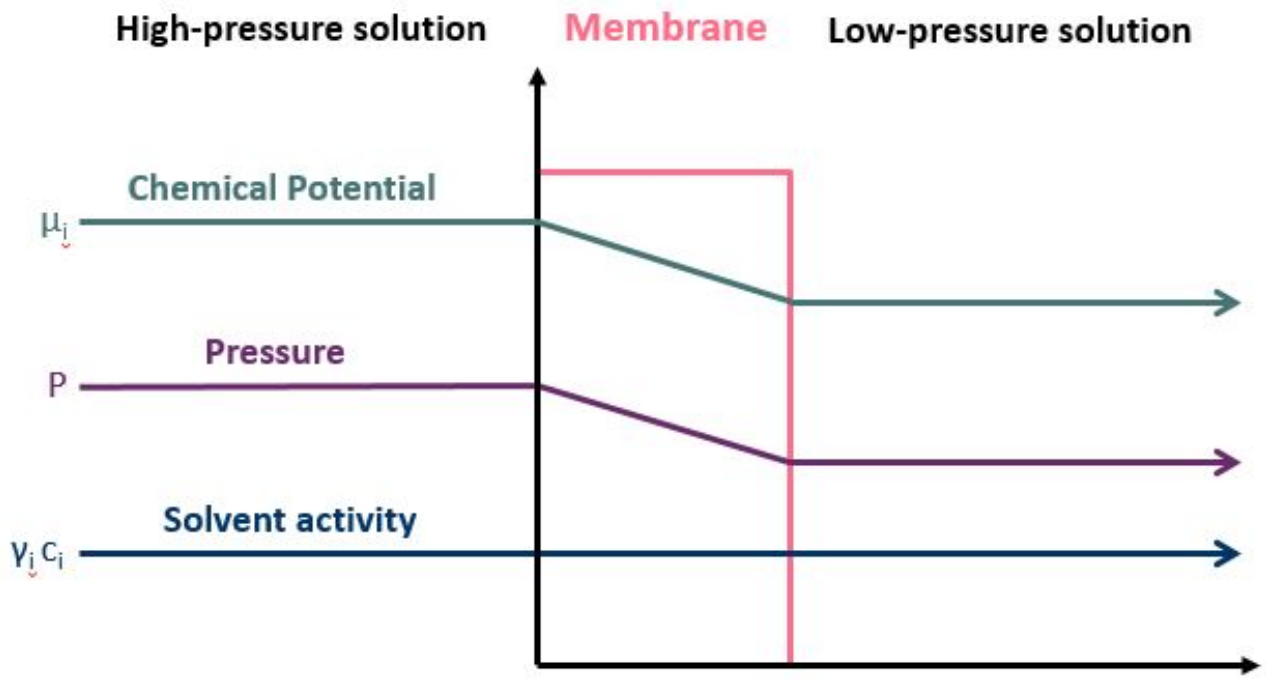

Figure 2.14. A plot of chemical potential, pressure, and solvent activity through a membrane according to the Pore-Flow Model.[65]

While porous membranes are highly useful for many applications, they solely partition solutions based upon shape and size, which limits potential applications. Additionally, these membranes must typically be pretreated and regularly cleaned to prevent the formation of and/or removal of pore blockages (i.e., membrane fouling). This cleaning process can be harsh, and lead to changes in the membrane structure which may require membrane replacement.[66]

The Solution-Diffusion Model describes the transport behavior for dense polymer membranes and is shown schematically in Figure 2.15.[65]. In dense polymer membranes, molecules do not move through open pores as these membranes are non-porous. Instead, the diffusing species absorb into the membrane from the solution at the upstream face, diffuse through the membrane by moving through the membrane fractional free volume (discussed further below) and then desorb from the membrane at the downstream face. This transport of different species is due to differences in chemical potential (via temperature, concentration, etc.) between the upstream solution and downstream solution.

Similar to the pore flow model, the chemical potential, μ_i, decreases through the membrane and reaches a minimum when it reaches the downstream solution where it remains constant. However, in the Solution-Diffusion Model, the solvent activity, γ_i, also decreases through the membrane at the same rate as the chemical potential, but then returns to the upstream solution value in the downstream solution because the solvent activity is the same in each solution even though it decreases through the membrane. The pressure, p, stays constant throughout the membrane but drops to the low-pressure solution level once the molecule is no longer in the membrane.

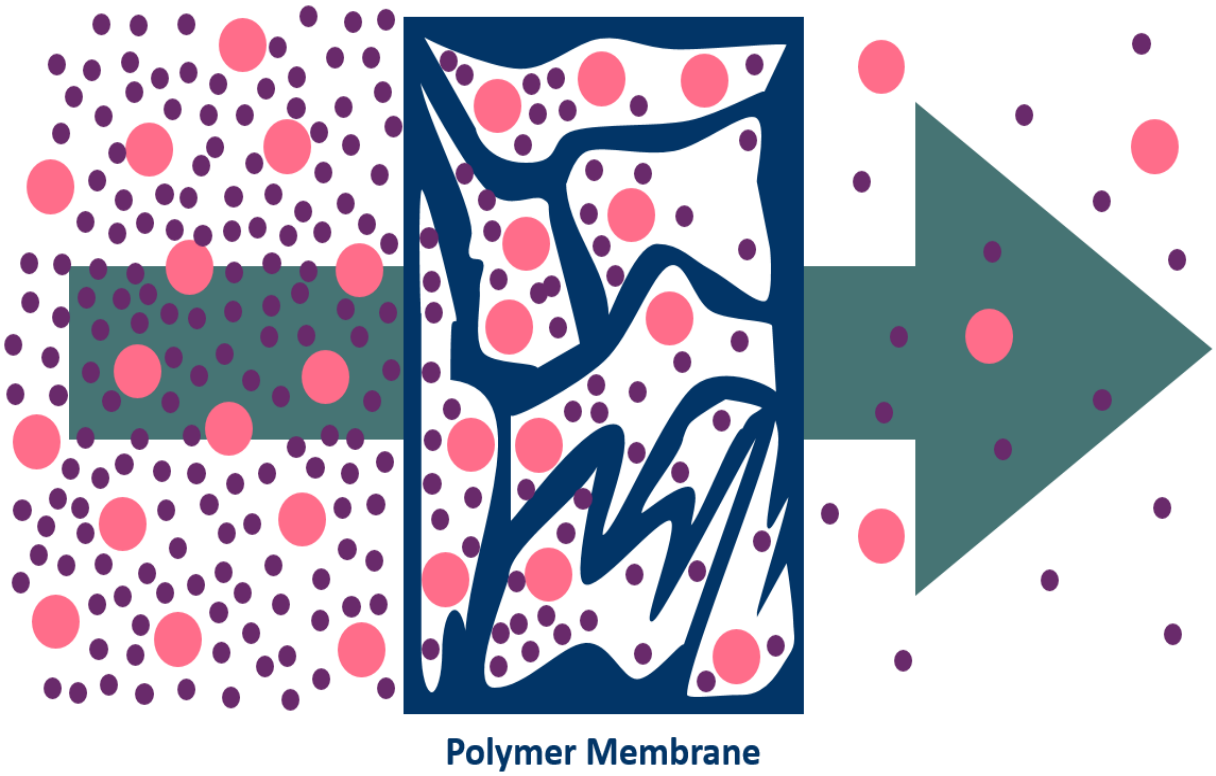

Figure 2.15. Depiction of the Solution-Diffusion Model

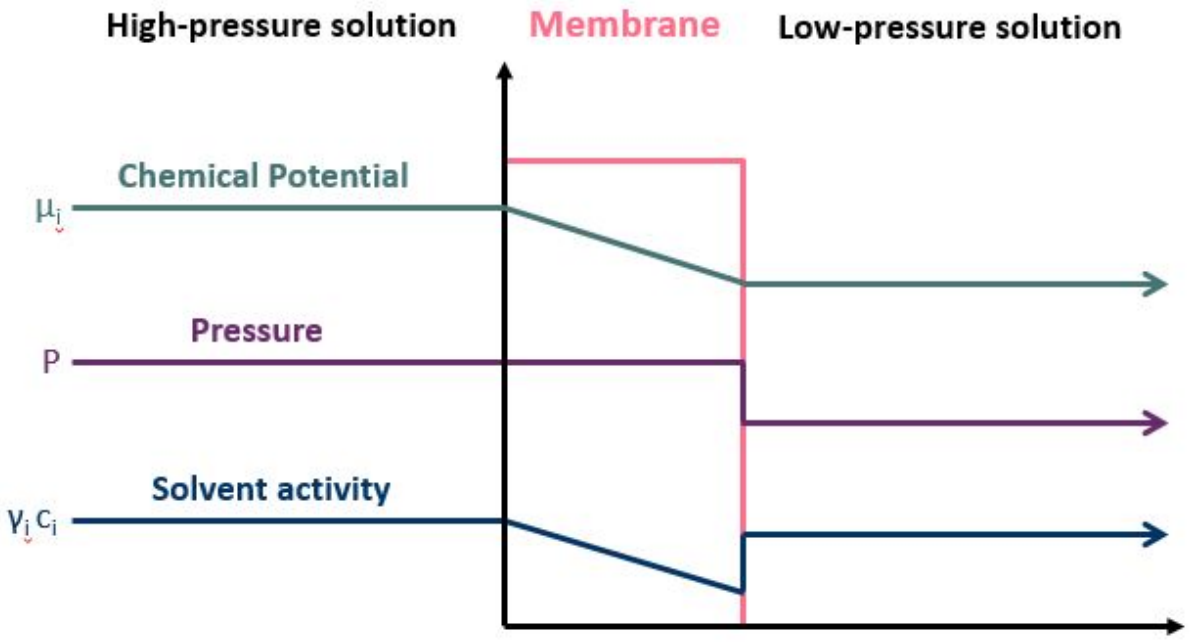

Figure 2.16. A plot of chemical potential, pressure, and solvent activity through a membrane according to the Solution-Diffusion Model.[65]

Species move through these dense membranes by diffusing through the fractional free volume between the polymer chains, as shown in Figure 2.17. This free volume is present because two chains cannot occupy the same volume, but they also do not pack due to van der Waals interactions and steric effects. In the solution diffusion model, the solute sorbs into the membrane based on the thermodynamic solubility, diffuses through the membrane due to polymer reptation/segmental motion based on the kinetic diffusivity, and finally, desorbs from the membrane into the downstream solution, again, due to solubility.

The solution-diffusion model is described by Equation 2.3, where the productivity of the membrane, or permeability P_i, is the product of the thermodynamic solubility, K_i, and the kinetic diffusivity, D_i.

$$P_i = D_i K_i \tag{2.3}$$

Polymer chains can be liquid in solution; however, when they are bonded together, "crosslinked", they form a polymer network, as shown in Figure 2.18. The more a membrane (polymer network) swells, the further the polymer chains are from each other, and the easier it is for solute molecules to diffuse through the membrane because there is more free volume between the polymer chains. However, the more such a membrane swells, the more the polymers stretch as polymer swelling is a competition between the van der Waals repulsions of the chains and the elastic forces attempting to keep the polymer chains together.[67] The stretching of these chains is incredibly important for transport behavior, as the further the chains are from each other, the larger the transport area, and, therefore, the higher the water uptake and larger the permeability of solutes.

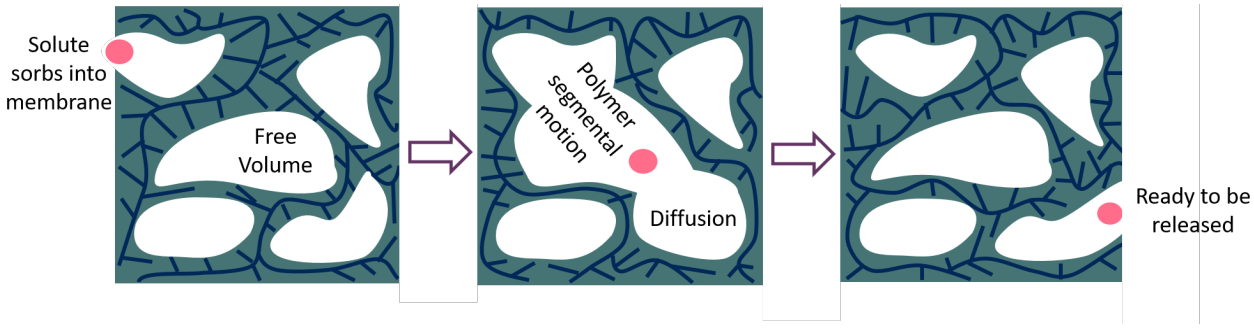

Figure 2.17. Fractional free volume representation. The solute sorbs into the membrane, diffuses through based upon polymer segmental motion, and desorbs from the membrane into the downstream solution.[68]

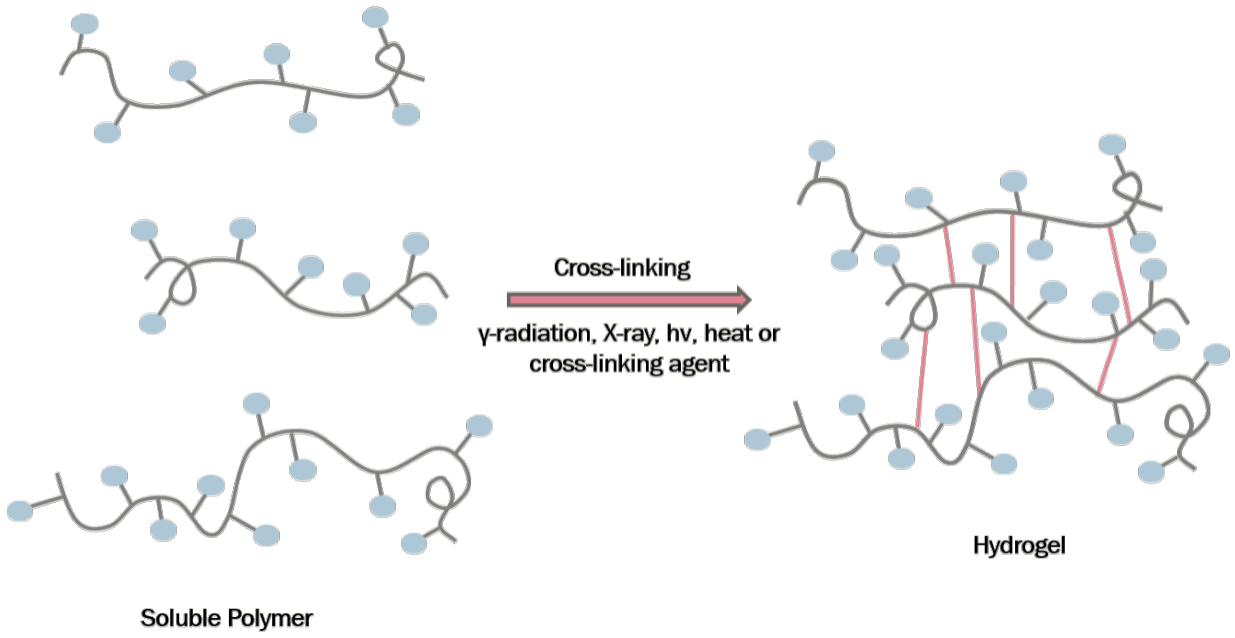

Figure 2.18. Representation of the crosslinking microstructure from soluble polymer to hydrogel.

The Solution-Diffusion Model applies to membranes used in applications such as dialysis, pervaporation, reverse osmosis, and most gas separation membranes.[65] Dialysis is the transport of solutes through a membrane based solely upon a concentration gradient (unless an external electric field is applied, then it is termed electrodialysis).[69] Pervaporation is the separation of components through a membrane based upon their permselectivity to the membrane and differences in their vapor pressures. Pervaporation is a separation process that has a liquid feed on one side of the membrane and vacuum pressure on the other side such that the component(s) that permeate through the membrane are vaporized on the downstream side and, typically, later condensed back to the liquid phase.[70,71] Reverse osmosis is the separation of components through a membrane from low concentration to high concentration because of an applied external pressure.[72]

To study transport in dense polymer membranes, an understanding of the relevant transport phenomena is necessary. The following provides a summation description of the derivation resulting in a concise equation that incorporates experimentally accessible variables for determining membrane permeability. To begin, the driving force for the movement of a permeate through a membrane in each of these applications is the gradient in its chemical potential which, for steady-state operations, can be described by Fick's first law (Equation 2.4),

$$J_i = -L_i \frac{d\mu_i}{dx} \tag{2.4}$$

where J_i is the flux of component i in g/cm^2 s, $\frac{d\mu_i}{dx}$ is the gradient of the chemical potential of species i through the thickness of the membrane, and L_i is the coefficient of proportionality which links the chemical potential gradient with the flux of component i. The chemical potential can be influenced by, among other factors, concentration, temperature, and pressure. By limiting Equation

2.4 to gradients in concentration and pressure, the chemical potential can be expressed by Equation 2.5.

$$d\mu_i = RTdln(\gamma_i n_i) + v_i dp \tag{2.5}$$

For liquid and solid phases (incompressible phases), the volume does not change with pressure, and the reference pressure, p_{i_0}, can be set to be the vapor pressure, $p_{i_{sat}}$

$$\mu_i = \mu_{i_0} + RTln(\gamma_i n_i) + v_i(p_i - p_i^0) = \mu_{i_0} + RTln(\gamma_i n_i) + v_i(p - p_{i_{sat}}) \tag{2.6}$$

Equating the chemical potential of the feed solution to that of the feed side of the membrane (Equation 2.7) and substituting into Equation 2.6 leads to Equation 2.8 and, ultimately, Equation 2.9 upon rearrangement.

$$\mu_{i_0} = \mu_{i_{0(m)}} \tag{2.7}$$

$$\mu_i^0 + RTln(\gamma_{i_0}^L n_{i_0}) + v_i(p_0 - p_{i_{sat}}) = \mu_i^0 + RTln(\gamma_{i_{0(m)}} n_{i_{0(m)}}) + v_i(p_0 - p_{i_{sat}}) \tag{2.8}$$

$$ln(\gamma_{i_0}^L n_{i_0}) = ln(\gamma_{i_{0(m)}} n_{i_{0(m)}}) \tag{2.9}$$

For membrane transport by the solution-diffusion model, the concentration gradient is the driving force for mass transport through the membrane. By removing the natural logarithm and rearranging Equation 2.9 (Equation 2.10), and substituting for concentration (by $c_i = m_i \rho n_i$) Equation 2.11 is derived.

$$n_{i_{0(m)}} = \frac{\gamma_{i_0}^L}{\gamma_{i_{0(m)}}} \cdot n_{i_0} \tag{2.10}$$

$$c_{i_{0(m)}} = \frac{\gamma_{i_0}^L \rho_m}{\gamma_{i_{0(m)}} \rho_m} \cdot c_{i_0} \tag{2.11}$$

A sorption coefficient, K_i^L is then defined (Equation 2.12) to give the simple result shown in Equation 2.13.

$$K_i^L = \frac{\gamma_{i_0}^L \rho_m}{\gamma_{i_{0(m)}} \rho_m} \tag{2.12}$$

$$c_{i_{0(m)}} = K_i^L \cdot c_{i_0} \tag{2.13}$$

This procedure is repeated on the permeate side of the membrane, to give Equation 2.14.

$$c_{i_{\ell(m)}} = K_i^L \cdot c_{i_\ell} \tag{2.14}$$

Following (Equation 2.15) is the form of Fick's First Law that includes the concentration gradient (dc_i) along the thickness of the membrane (dx).

$$J_i = -\frac{RTL_i K_i}{c_i} \cdot \frac{dc_i}{dx} \tag{2.15}$$

The prefactor can then be replaced by the diffusion coefficient, D_i (Equation 2.16) and integrated (Equation 2.17)

$$J_i = -D_i K_i \frac{dc_i}{dx} \tag{2.16}$$

The limits of integration are from 0 to l for traversing the entire membrane thickness and from c_1 to c_2 for c_i.

$$J_i \int_0^\ell dx = -D_i K_i \int_{c_1}^{c_2} dc_i \tag{2.17}$$

Equation 2.18 is obtained upon integration of Equation 2.17,

$$J_i = -D_i K_i \frac{(c_2 - c_1)}{\ell} \tag{2.18}$$

When multiplied by the area, this result can be simplified to express the volume and concentration gradient with respect to time, both in regards to the downstream side of the membrane.

$$AJ_i = -D_i K_i \frac{(c_2 - c_1)A}{\ell} = V_2 \frac{dc_2}{dt} \tag{2.19}$$

The permeability coefficient, P_i, is equal to the product of the diffusivity coefficient, D_i, and the solubility coefficient, K_i. This equation is termed the Solution-Diffusion Model, as previously discussed.[11,73]

$$P_i = D_i K_i \tag{2.20}$$

Equation 2.21 and 2.22 show the changes in concentration at certain times

$$\text{At t=0:} \quad (V_1 + V_2)c_{av} = V_1 c_1^0 + V_2 c_2^0 \tag{2.21}$$

$$\text{At t=t:} \quad (V_1 + V_2)c_{av} = V_1 c_1 + V_2 c_2 \tag{2.22}$$

Equation 2.23 shows the limits of the integrals to be taken from Equation 2.19 with Equation 2.20 substituted in

$$\int_0^t -\frac{P_i A}{V_2 l}\, dt = \int_{c_2^0}^{c_2} \frac{1}{(c_2 - c_1)}\, dc_2 \tag{2.23}$$

Substituting c_1 from Equation 2.22 into Equation 2.23, rearranging and integrating from time 0 to time t gives the following equation, the "final equation" according to Geankoplis.[74]

$$\frac{c_{av} - c_2}{c_{av} - c_2^0} = exp\left[-\frac{P_i(V_1 + V_2)t}{(\ell/A)(V_1 V_2)}\right] \tag{2.24}$$

Experimentally, the volumes of the cells upstream and downstream of the membrane are equal (Equation 2.25)

$$V = V_1 = V_2 \tag{2.25}$$

Taking the natural logarithm on both sides of Equation 2.24, and substituting in Equation 2.25 results in Equation 2.26,

$$ln\left(\frac{c_{av}-c_2}{c_{av}-c_2^0}\right)=-\frac{P_i 2At}{V\ell} \tag{2.26}$$

where $c_2^0 = C_{i_0}$, $c_2 = C_{i_t}$, and $c_{av} = \frac{C_{i_0}}{2} + \frac{C_{i_t}}{2}$ which, when substituted into Equation 2.26, gives Equation 2.27.

$$ln\left(\frac{\frac{C_{i_0}}{2}+\frac{C_{i_t}}{2}-C_{i_t}}{\frac{C_{i_0}}{2}+\frac{C_{i_t}}{2}-C_{i_0}}\right)=-\frac{P_i 2At}{V\ell} \tag{2.27}$$

Simplification of the argument within the natural results in Equation 2.28.

$$ln\left(1-\frac{2C_{i_t}}{C_{i_0}}\right)=P_i\left(-\frac{2At}{V\ell}\right) \tag{2.28}$$

Equation 2.28 is the so-called "Yasuda Model" derived by H. Yasuda et. al in 1968.[75] This model equation incorporates only variables that are known or experimentally measured from a diffusion-cell experiment except for the permeability coefficient, P_i. Therefore, the permeability can be calculated if the beginning concentration in the donor cell, C_{i_0}, concentration at time *t* within the receiving cell, C_{i_t}, volume of the cells, *V*, area of the face of the membrane, *A*, thickness of the membrane, *l*, and time, *t*, are known. The Yasuda Model will be used in the remainder of this work for determining permeability from diffusion cell experiments.

The Yasuda Model is also a useful equation for understanding how experimental variables will influence the experimental measurements. One lens for this is to think about the impact of each parameter individually on experimental time (*t*) for the downstream solution to reach the desired

concentration (C_{it}), i.e., constant left-hand side of Equation 2.28. The thickness of the membrane (l) is inversely proportional to the time such that the thicker the membrane, the longer the experiment. Similarly, the larger the volume of the cells, the longer the experiment (inversely proportional). The larger the membrane area, the quicker the experiment (proportional). Lastly, the more permeable the membrane, the quicker the experiment (proportional).

Determination of the permeability of a membrane to solutes using the solution-diffusion model requires a diffusion-cell apparatus, shown in Figure 2.19. The membrane is held between a donor and a receiver cell, the donor cell originally contains a known amount of solute(s) (1 M in this work), and the receiver cell originally contains pure DI water. The cells are jacketed for temperature control and well mixed. The receiver cell's solute concentration must be determined over time to calculate the membrane's permeability to that solute.

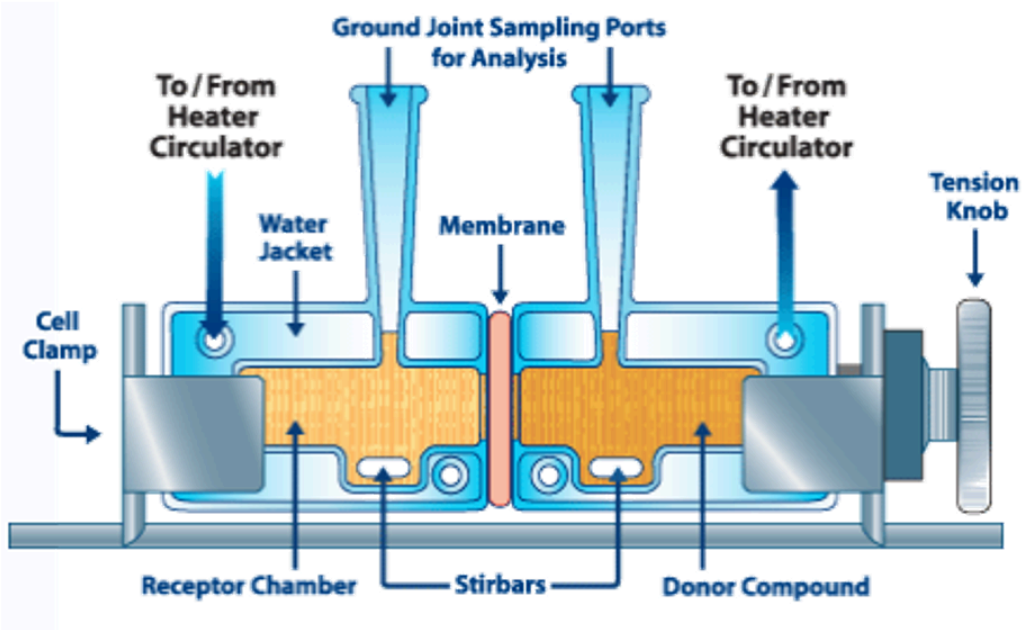

Figure 2.19. Common diffusion-cell apparatus depiction. The membrane is held between a donor cell on the right and a receiver cell on the left. The cells are thermally jacketed and well mixed. The receiver chamber is tested overtime for the concentration of the solutes that transported through the membrane.[58,75–80]

Generally, *in situ* characterization via probe-based systems like pH[81,82] or conductivity[83–86] are used to characterize solute permeability as these probes can determine an overall change in solution over time, shown in Figure 2.20a and b, respectively. However, these probe-based systems can only observe solution changes, not species-specific changes, and, therefore, can only be used for a single solute at a time. These measurements do not take into account solute-solute interactions or multiple solute-membrane interactions. *Ex situ* characterization via gas chromatography[87,88], mass spectrometry[89], and attenuated total reflectance Fourier-transform infrared (ATR FTIR) spectroscopy[90] can quantify changes in multiple species in solution, however, are arduous on the researcher and open to significant error due to the aliquotic sampling needed. Also, the aliquots open the downstream solution to a continually changing volume, making calculations incredibly difficult (see Equation 2.28), and can introduce additional driving forces for transport through the membrane such as hydrostatic pressure differences.

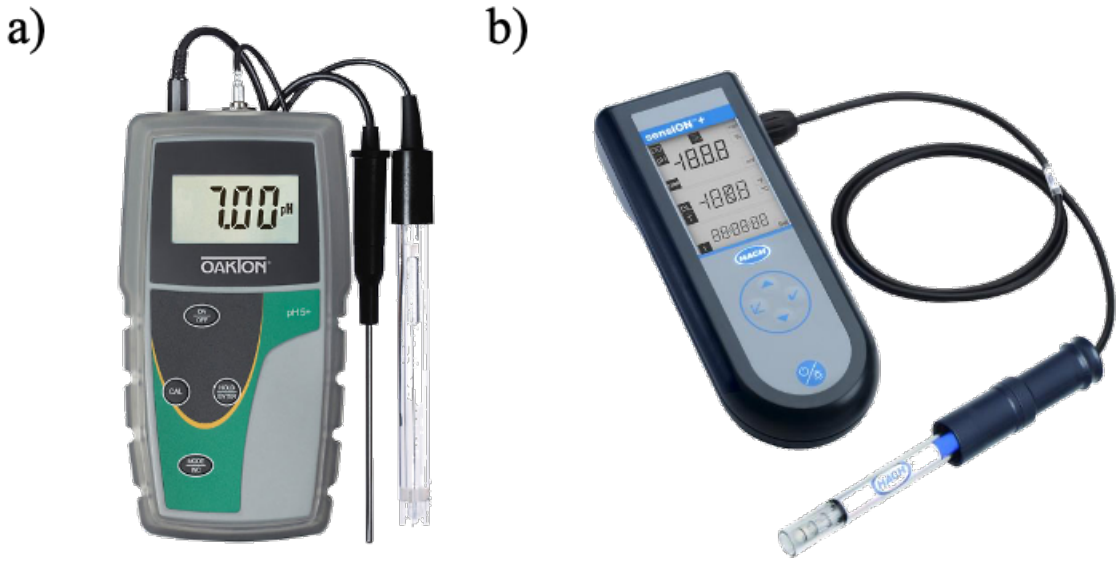

Figure 2.20. a) pH probe[81,82] and b) conductivity probe.[83–86]

In this work, a newly adopted technique that incorporates the advantages of an *in situ* probe-based technique and *ex situ* characterization technique is utilized.[77,91,92] In particular, fiber-optic cable-based ATR FTIR spectroscopy is used to collect downstream solution concentrations of multiple simultaneously transporting species with high accuracy. This technique is described in detail in Chapter 3 (experimental details) and Chapter 4 (implementation).

There are multiple models to characterize transport through polymeric films that calculate the diffusivity of a component based upon polymer volume fraction and other known or measurable parameters. The Mackie-Meares Model, Equation 2.29, is based on tortuosity, the simple cubic lattice model, and similar size sites for the polymer and solvent segments. In other words, it is strictly based upon geometric obstructions to solute flow[93–95]

$$\frac{D}{D_0} = \frac{(1-\phi)^2}{(1+\phi)^2} \tag{2.29}$$

where D is the diffusion coefficient, D_0 is the pure solvent's diffusion coefficient, and ϕ is the volume fraction of the polymer. This model assumes that the polymer and solvent segments are similarly sized, which is not universally, or even generally, the case.

Another model to calculate diffusivity from known parameters is the Flory-Rehner model, which defines the swelling pressure, p_{sw}, by Equation 2.30, completely disregarding electrostatic interactions,

$$\pi_{sw} = \pi_{mix} + \pi_{el} \tag{2.30}$$

where p_{mix} is the mixing pressure and p_{el} is the elastic deformation pressure of the polymer chains.[96] However, when studying the membranes and solutes in this work, the electrostatic interactions

between solutes or the solutes and membranes are important. Equation 2.31 can also be used for describing transport behavior in such systems,

$$ln\gamma_1\phi_1 = ln\phi_1 + \phi_m + \chi\phi_m^2 + \frac{\overline{v_1^0}G}{RT}\left(\phi_m^{1/3} - \frac{1}{2}\phi_m\right) \quad (2.31)$$

where ϕ_1 is the volume fraction of water, γ_1 is the activity coefficient correction to compensate for the non-ideality of the polymer-water mixture, ϕ_m is the volume fraction of the polymer, χ is the Flory-Huggins interaction parameter, $\overline{v_1^0}$ is the molar volume of pure water, and G is the bulk modulus of the hydrogel membrane.[97] Equation 2.31 is typically used to calculate the activity coefficient, which is then used in Equation 2.32, derived by Fisher, Hollomon, and Turnbull[98], to determine diffusivity.

$$D = D_0\gamma\left(1 + C\frac{dln\gamma}{dC}\right) \quad (2.32)$$

Both of these models have been shown to evaluate diffusivity based upon specific, measurable parameters. However, for this work, we utilize the Solution-Diffusion model, which, when coupled with well-known solubility experiments and the permeability experiment technology benchmarked herein, calculate diffusivity directly. Therefore, the Mackie-Meares and Flory-Rehner descriptions were not utilized in this work

2.4. References

1. Copeland C, Carter NT. *Energy-Water Nexus: The Water Sector's Energy Use*.; 2017.

2. Deshmukh A, Boo C, Karanikola V, Lin S, Straub A, Tong T, Warsinger D, Elimelech M. Membrane distillation at the water-energy nexus: limits, opportunities, and challenges. *Energy Environ Sci*. 2018;11(5):1177-1196. doi:10.1039/C8EE00291F

3. Hamiche AM, Stambouli AB, Flazi S. A review of the water-energy nexus. *Renew Sustain Energy Rev*. 2016;65:319-331. doi:10.1016/j.rser.2016.07.020

4. Leck H, Conway D, Bradshaw M, Rees J. Tracing the Water–Energy–Food Nexus: Description, Theory and Practice. *Geogr Compass*. 2015;9(8):445-460. doi:10.1111/gec3.12222

5. Birol F. World Energy Outlook 2017. *Int Energy Agency*.

6. Boden TA, Marland G, Andres RJ. Global, Regional, and National Fossil-Fuel CO2 Emissions. *Carbon Dioxide Inf Anal Cent Oak Ridge Natl Lab US Dep Energy Oak Ridge TN USA*. doi:10.3334/CDIAC/00001_V2010

7. Edmonds J, Reilly J. A long-term global energy- economic model of carbon dioxide release from fossil fuel use. *Energy Econ*. 1983;5(2):74-88. doi:10.1016/0140-9883(83)90014-2

8. Wuebbles DJ, Jain AK. Concerns about climate change and the role of fossil fuel use. *Fuel Process Technol*. 2001;71(1):99-119. doi:10.1016/S0378-3820(01)00139-4

9. Shiklomanov I. World fresh water resources. In: Gleick PH, ed. *Water in Crisis: A Guide to the World's Fresh Water Resources*. Oxford University Press; 1993.

10. Utracki LA. History of commercial polymer alloys and blends (from a perspective of the patent literature). *Polym Eng Sci*. 1995;35(1):2-17. doi:10.1002/pen.760350103

11. Baker RW. *Membrane Technology and Applications*. 2nd ed. Membrane Technology and Research, Inc.

12. Alberts B, Johnson A, Lewis J, Raff M, Roberts K, Walter P. Principles of Membrane Transport. In: *Molecular Biology of the Cell*. 4th ed. Garland Science; 2002.

13. Noble RD, Gin DL. Perspective on ionic liquids and ionic liquid membranes. *J Membr Sci*. 2011;369(1):1-4. doi:10.1016/j.memsci.2010.11.075

14. Badwal SPS, Ciacchi FT. Ceramic Membrane Technologies for Oxygen Separation. *Adv Mater*. 2001;13(12-13):993-996. doi:10.1002/1521-4095(200107)13:12/13<993::AID-ADMA993>3.0.CO;2-#

15. Kenarsari SD, Yang D, Jiang G, Fan M. Review of recent advances in carbon dioxide separation and capture. *RSC Adv*. 2013;3(45):22739-22773. doi:10.1039/c3ra43965h

16. Ramdin M, de Loos TW, Vlugt TJH. State-of-the-Art of CO2 Capture with Ionic Liquids. *Ind Eng Chem Res*. 2012;51(24):8149-8177. doi:10.1021/ie3003705

17. Jiang LY, Wang Y, Chung T-S, Qiao XY, Lai J-Y. Polyimides membranes for pervaporation and biofuels separation. *Prog Polym Sci*. 2009;34(11):1135-1160. doi:10.1016/j.progpolymsci.2009.06.001

18. Lin H, Freeman BD. Gas solubility, diffusivity and permeability in poly(ethylene oxide). *J Membr Sci*. 2004;239(1):105-117. doi:10.1016/j.memsci.2003.08.031

19. Robeson LM. The upper bound revisited. *J Membr Sci*. 2008;320(1-2):390-400. doi:10.1016/j.memsci.2008.04.030

20. Robeson LM. Correlation of separation factor versus permeability for polymeric membranes. *J Membr Sci*. 1991;62:165-185. doi:10.1016/0376-7388(91)80060-J

21. Stern SA. Polymers for gas separations: the next decade. *J Membr Sci*. 1994;94(1):1-65. doi:10.1016/0376-7388(94)00141-3

22. Scovazzo P. Determination of the upper limits, benchmarks, and critical properties for gas separations using stabilized room temperature ionic liquid membranes (SILMs) for the purpose of guiding future research - ScienceDirect. *J Membr Sci*. 2009;343(1-2):199-211. doi:10.1016/j.memsci.2009.07.028

23. Ahmad A. L., Ooi B. S., Wahab Mohammad A., Choudhury J. P. Effect of constricted polymerization time on nanofiltration membrane characteristic and performance: A study using the Donnan Steric Pore Flow Model. *J Appl Polym Sci*. 2004;94(1):394-399. doi:10.1002/app.20904

24. Geise Geoffrey M., Lee Hae-Seung, Miller Daniel J., Freeman Benny D., McGrath James E., Paul Donald R. Water purification by membranes: The role of polymer science. *J Polym Sci Part B Polym Phys*. 2010;48(15):1685-1718. doi:10.1002/polb.22037

25. Bottino A, Capannelli C, Del Borghi A, Colombino M, Conio O. Water treatment for drinking purpose: ceramic microfiltration application. *Desalination*. 2001;141(1):75-79. doi:10.1016/S0011-9164(01)00390-3

26. Howe KJ, Clark MM. Fouling of Microfiltration and Ultrafiltration Membranes by Natural Waters. *Environ Sci Technol*. 2002;36(16):3571-3576. doi:10.1021/es025587r

27. Freeman BD, Park HB, McCloskey BD. Water purification membranes with improved fouling resistance. Published online September 13, 2011. Accessed August 5, 2019. https://patents.google.com/patent/US8017050B2/en

28. Ju H, McCloskey BD, Sagle AC, Kusuma VA, Freeman BD. Preparation and characterization of crosslinked poly(ethylene glycol) diacrylate hydrogels as fouling-resistant membrane coating materials. *J Membr Sci*. 2009;330(1):180-188. doi:10.1016/j.memsci.2008.12.054

29. K. Singh A, Singh P, Mishra S, K. Shahi V. Anti-biofouling organic-inorganic hybrid membrane for water treatment. *J Mater Chem*. 2012;22(5):1834-1844. doi:10.1039/C1JM14250J

30. Lian F, Wen Y, Ren Y, Guan H. A novel PVB based polymer membrane and its application in gel polymer electrolytes for lithium-ion batteries. *J Membr Sci*. 2014;456:42-48. doi:10.1016/j.memsci.2014.01.010

31. Carlisle TK, Bara JE, Lafrate AL, Gin DL, Noble RD. Main-chain imidazolium polymer membranes for CO2 separations: An initial study of a new ionic liquid-inspired platform. *J Membr Sci*. 2010;359(1):37-43. doi:10.1016/j.memsci.2009.10.022

32. Bi W, Gray GE, Fuller TF. PEM Fuel Cell Pt/C Dissolution and Deposition in Nafion Electrolyte. *Electrochem Solid-State Lett*. 2007;10(5):101-104. doi:10.1149/1.2712796

33. Cabasso I, Liu Z-Z, Makenzie T. The permselectivity of ion-exchange membranes for non-electrolyte liquid mixtures. II. The effect of counterions (separation of alcohol/water mixtures with nafion membranes). *J Membr Sci*. 1986;28(2):109-122. doi:10.1016/S0376-7388(00)82204-8

34. Chaabane L, Dammak L, Grande D, Larcheet C, Huguet P, Nikonenko SV, Nikonenko VV. Swelling and permeability of Nafion®117 in water–methanol solutions: An experimental and modelling investigation. *J Membr Sci*. 2011;377(1):54-64. doi:10.1016/j.memsci.2011.03.037

35. DeLuca NW, Elabd YA. Nafion®/poly(vinyl alcohol) blends: Effect of composition and annealing temperature on transport properties. *J Membr Sci*. 2006;282(1):217-224. doi:10.1016/j.memsci.2006.05.025

36. Diaz LA, Abuin GC, Corti HR. Methanol sorption and permeability in Nafion and acid-doped PBI and ABPBI membranes. *J Membr Sci*. 2012;411-412:35-44. doi:10.1016/j.memsci.2012.04.013

37. Dimitrova P, Friedrich KA, Stimming U, Vogt B. Modified Nafion®-based membranes for use in direct methanol fuel cells. *Solid State Ion*. 2002;150(1):115-122. doi:10.1016/S0167-2738(02)00267-9

38. Evans CE, Noble RD, Nazeri-Thompson S, Nazeri B, Koval CA. Role of conditioning on water uptake and hydraulic permeability of Nafion® membranes. *J Membr Sci*. 2006;279(1):521-528. doi:10.1016/j.memsci.2005.12.046

39. Hietala S, Maunu SL, Sundholm F. Sorption and diffusion of methanol and water in PVDF-g-PSSA and Nafion® 117 polymer electrolyte membranes. *J Polym Sci Part B Polym Phys*. 2000;38(24):3277-3284. doi:10.1002/1099-0488(20001215)38:24<3277::AID-POLB90>3.0.CO;2-O

40. Hobson LJ, Ozu H, Yamaguchi M, Hayase S. Modified Nafion 117 as an Improved Polymer Electrolyte Membrane for Direct Methanol Fuel Cells. *J Electrochem Soc*. 2001;148(10):A1185-A1190. doi:10.1149/1.1402980

41. Majsztrik P, Bocarsly A, Benziger J. Water Permeation through Nafion Membranes: The Role of Water Activity. *J Phys Chem B*. 2008;112(51):16280-16289. doi:10.1021/jp804197x

42. Mauritz KA, Moore RB. State of Understanding of Nafion. *Chem Rev*. 2004;104(10):4535-4586. doi:10.1021/cr0207123

43. Liang Z, Chen W, Liu J, Wang S, Zhou Z, Li W, Sun G, Xin Q. FT-IR study of the microstructure of Nafion® membrane. *J Membr Sci*. 2004;233(1):39-44. doi:10.1016/j.memsci.2003.12.008

44. Randová A, Hovorka Š, Izák P, Bartovská L. Swelling of Nafion in methanol–water–inorganic salt ternary mixtures. *J Electroanal Chem*. 2008;616(1):117-121. doi:10.1016/j.jelechem.2007.12.018

45. Zawodzinski TA, Smith VT, Springer TE. Water Uptake by and TransportThrough Nafion 117 Membranes. *J Electrochem Soc*. 1993;140(4):7. doi:https://doi.org/10.1149/1.2056194

46. Siracusano S, Baglio V, Lufrano F, Staiti P, Aricò AS. Electrochemical characterization of a PEM water electrolyzer based on a sulfonated polysulfone membrane. *J Membr Sci*. 2013;448:209-214. doi:10.1016/j.memsci.2013.07.058

47. Zhang Y, Zhang H, Zhang Y, Ma Y, Zhong H, Ma H. Facile synthesis of Nafion-stabilized iridium nanoparticles and their direct use for fuel cells and water electrolyzers. *Chem Commun*. 2009;0(43):6589-6591. doi:10.1039/B915014E

48. Ito H, Maeda T, Nakano A, Takenaka H. Properties of Nafion membranes under PEM water electrolysis conditions. *Int J Hydrog Energy*. 2011;36(17):10527-10540. doi:10.1016/j.ijhydene.2011.05.127

49. Ren S, Sun G, Li C, Liang Z, Wu Z, Jin W, Qin X, Yang X. Organic silica/Nafion® composite membrane for direct methanol fuel cells. *J Membr Sci*. 2006;282(1):450-455. doi:10.1016/j.memsci.2006.05.050

50. Tang H, Peikang S, Jiang SP, Wang F, Pan M. A degradation study of Nafion proton exchange membrane of PEM fuel cells. *J Power Sources*. 2007;170(1):85-92. doi:10.1016/j.jpowsour.2007.03.061

51. Steele BCH, Heinzel A. Materials for fuel-cell technologies. In: Dusastre V, ed. *Materials for Sustainable Energy*. World Scientific Nature Publishing Group; 2010:224-231. doi:10.1142/9789814317665_0031

52. Heinzel A, Barragan VM. A review of the state-of-the-art of the methanol crossover in direct methanol fuel cells. *J Power Sources*. 1999;84:70-74. doi:10.1016/S0378-7753(99)00302-X

53. Neburchilov V, Martin J, Wang H, Zhang J. A review of polymer electrolyte membranes for direct methanol fuel cells. *J Power Sources*. 2007;169:221-238. doi:10.1016/j.jpowsour.2007.03.044

54. Mehta V, Cooper JS. Review and analysis of PEM fuel cell design and manufacturing. *J Power Sources*. 2003;114(1):32-53. doi:10.1016/S0378-7753(02)00542-6

55. Deluca NW, Elabd YA. Polymer electrolyte membranes for the direct methanol fuel cell: A review. *J Polym Sci Part B Polym Phys*. 2006;44:2201-2225. doi:10.1002/polb.20861

56. Lim RJ, Xie M, Sk MA, Lee JM, Fisher A, Wang X, Lim KH. A review on the electrochemical reduction of CO2 in fuel cells, metal electrodes and molecular catalysts. *Catal Today*. 2014;233:169-180. doi:10.1016/j.cattod.2013.11.037

57. Peighambardoust SJ, Rowshanzamir S, Amjadi M. Review of the proton exchange membranes for fuel cell applications. *Int J Hydrog Energy*. 2010;35(17):9349-9384. doi:10.1016/j.ijhydene.2010.05.017

58. Beckingham BS, Lynd NA, Miller DJ. Monitoring multicomponent transport using in situ ATR FTIR spectroscopy. *J Membr Sci*. 2018;550:348-356. doi:10.1016/j.memsci.2017.12.072

59. US EPA. *Sources of Global Greenhouse Gas Emissions*.; 2020.

60. P. Kuhl K, R. Cave E, N. Abram D, F. Jaramillo T. New insights into the electrochemical reduction of carbon dioxide on metallic copper surfaces. *Energy Environ Sci*. 2012;5(5):7050-7059. doi:10.1039/C2EE21234J

61. Lefèvre M, Proietti E, Jaouen F, Dodelet J-P. Iron-Based Catalysts with Improved Oxygen Reduction Activity in Polymer Electrolyte Fuel Cells. *Science*. 2009;324(5923):71-74. doi:10.1126/science.1170051

62. Gust D, Moore TA, Moore AL. Solar Fuels via Artificial Photosynthesis. *Acc Chem Res*. 2009;42(12):1890-1898. doi:10.1021/ar900209b

63. Gu WY, Lai WM, Mow VC. A Mixture Theory for Charged-Hydrated Soft Tissues Containing Multi-electrolytes: Passive Transport and Swelling Behaviors. *J Biomech Eng*. 1998;120(2):169-180. doi:10.1115/1.2798299

64. Sten-Knudsen O. Passive Transport Processes. In: Tosteson DC, ed. *Concepts and Models*. Membrane Transport in Biology. Springer; 1978:5-113. doi:10.1007/978-3-642-46370-9_2

65. Wijmans JG, Baker RW. The solution-diffusion model: a review. *J Membr Sci*. 1995;107:1-21.

66. Samco Technologies. *The Essential Guide to Microfiltration and Ultrafiltration Membrane Systems*.; 2018.

67. Helfferich F. *Ion Exchange*. Dover Publications; 1995.

68. Carraher CE, Seymour RB. *Polymer Chemistry*. 6th ed., rev.expanded. M. Dekker; 2003.

69. de Castro MDL, Capote FP, Ávila NS. Is dialysis alive as a membrane-based separation technique? *TrAC Trends Anal Chem*. 2008;27(4):315-326. doi:10.1016/j.trac.2008.01.015

70. Aptel P, Challard N, Cuny J, Neel J. Application of the pervaporation process to separate azeotropic mixtures. *J Membr Sci*. 1976;1:271-287. doi:10.1016/S0376-7388(00)82272-3

71. Shao P, Huang RYM. Polymeric membrane pervaporation. *J Membr Sci*. 2007;287(2):162-179. doi:10.1016/j.memsci.2006.10.043

72. Greenlee LF, Lawler DF, Freeman BD, Marrot B, Moulin P. Reverse osmosis desalination: Water sources, technology, and today's challenges. *Water Res*. 2009;43(9):2317-2348. doi:10.1016/j.watres.2009.03.010

73. Kamcev J, Freeman BD. Charged Polymer Membranes for Environmental/Energy Applications. *Annu Rev Chem Biomol Eng*. 2016;7:111-133. doi:10.1146/annurev-chembioeng-080615-033533

74. Geankoplis CJ. Chapter 6. Principles of Mass Transport. In: *Transport Processes and Separation Process Principles*. 4th ed. Prentice Hall. Professional Technical Reference; 2003.

75. Yasuda H, Lamaze CE, Ikenberry LD. Permeability of Solutes through Hydrated Polymer Membranes. Part I. Diffusion of Sodium Chloride. *Akromolekulare Chem*. 1968;118:19-35.

76. Lin H, Kai T, Freeman BD, Kalakkunnath S, Kalika DS. The Effect of Cross-Linking on Gas Permeability in Cross-Linked Poly(Ethylene Glycol Diacrylate). *Macromolecules*. 2005;38:8381-8393.

77. Carter BM, Dobyns BM, Beckingham BS, Miller DJ. Multicomponent transport of alcohols in an anion exchange membrane measured by in-situ ATR FTIR spectroscopy. *Polymer*. 2017;123:144-152. doi:10.1016/j.polymer.2017.06.070

78. Freeman B, Yampolskii Y, Pinnau I. *Materials Science of Membranes for Gas and Vapor Separation*. John Wiley & Sons; 2006.

79. Lin H, Freeman BD. Gas Permeation and Diffusion in Cross-Linked Poly(ethylene glycol diacrylate). *Macromolecules*. 2006;39(10):3568-3580. doi:10.1021/ma051686o

80. Ju H, Sagle AC, Freeman BD, Mardel JI, Hill AJ. Characterization of sodium chloride and water transport in crosslinked poly(ethylene oxide) hydrogels. *J Membr Sci*. 2010;358(1):131-141. doi:10.1016/j.memsci.2010.04.035

81. van de Vossenberg JLCM, Driessen AJM, da Costa MS, Konings WN. Homeostasis of the membrane proton permeability in Bacillus subtilis grown at different temperatures. *Biochim Biophys Acta BBA - Biomembr*. 1999;1419(1):97-104. doi:10.1016/S0005-2736(99)00063-2

82. Wohnsland F, Faller B. High-Throughput Permeability pH Profile and High-Throughput Alkane/Water log P with Artificial Membranes. *J Med Chem*. 2001;44(6):923-930. doi:10.1021/jm001020e

83. Daniel David E. In Situ Hydraulic Conductivity Tests for Compacted Clay. *J Geotech Eng*. 1989;115(9):1205-1226. doi:10.1061/(ASCE)0733-9410(1989)115:9(1205)

84. Hamilton J, Daniel D, Olson R. Measurement of Hydraulic Conductivity of Partially Saturated Soils. In: Zimmie T, Riggs C, eds. *Permeability and Groundwater Contaminant Transport*. ASTM International; 1981:182-196. doi:10.1520/STP28324S

85. Steudle E, Tyerman SD. Determination of permeability coefficients, reflection coefficients, and hydraulic conductivity ofChara corallina using the pressure probe: Effects of solute concentrations. *J Membr Biol*. 1983;75(1):85-96. doi:10.1007/BF01870802

86. Kuchuk FJ, Onur M. Estimating permeability distribution from 3D interval pressure transient tests. *J Pet Sci Eng*. 2003;39(1):5-27. doi:10.1016/S0920-4105(03)00037-8

87. Dumas F, Aussel C, Pernet P, Martin C, Giboudeau J. Gas chromatography applied to the lactulose—mannitol intestinal permeability test. *J Chromatogr B Biomed Sci App*. 1994;654(2):276-281. doi:10.1016/0378-4347(94)00041-7

88. Farhadi A, Keshavarzian A, Holmes EW, Fields J, Zhang L, Banan A. Gas chromatographic method for detection of urinary sucralose: application to the assessment of intestinal permeability. *J Chromatogr B*. 2003;784(1):145-154. doi:10.1016/S1570-0232(02)00787-0

89. Wang Z, Hop CECA, Leung KH, Pang J. Determination of in vitro permeability of drug candidates through a Caco-2 cell monolayer by liquid chromatography/tandem mass spectrometry. *J Mass Spectrom*. 2000;35(1):71-76. doi:10.1002/(SICI)1096-9888(200001)35:1<71::AID-JMS915>3.0.CO;2-5

90. McAuley WJ, Mader KT, Tetteh J, Lane ME, Hadgraft J. Simultaneous monitoring of drug and solvent diffusion across a model membrane using ATR-FTIR spectroscopy. *Eur J Pharm Sci*. 2009;38(4):378-383. doi:10.1016/j.ejps.2009.09.002

91. Dobyns BM, Kim JM, Beckingham BS. Multicomponent transport of methanol and sodium acetate in poly(ethylene glycol) diacrylate membranes of varied fractional free volume. *Eur Polym J*. 2020;134:109809. doi:10.1016/j.eurpolymj.2020.109809

92. Kim JM, Dobyns BM, Zhao R, Beckingham BS. Multicomponent transport of Methanol and Acetatein a series of crosslinked PEGDA-AMPS cation exchange membranes. *J Membr Sci*. Published online 2020.

93. Waggoner R, Blum F, MacElroy J. Dependence of the Solvent Diffusion Coefficient on Concentration in Polymer Solutions. *Macromolecules*. Published online January 1, 1993. doi:10.1021/ma00077a021

94. Müller-Plathe F. Diffusion of water in swollen poly(vinyl alcohol) membranes studied by molecular dynamics simulation. *J Membr Sci*. 1998;141(2):147-154. doi:10.1016/S0376-7388(97)00289-5

95. Mackie JS, Meares P, Rideal EK. The diffusion of electrolytes in a cation-exchange resin membrane I. Theoretical. *Proc R Soc Lond Ser Math Phys Sci*. 1955;232(1191):498-509. doi:10.1098/rspa.1955.0234

96. van der Sman RGM. Moisture transport during cooking of meat: An analysis based on Flory–Rehner theory. *Meat Sci*. 2007;76(4):730-738. doi:10.1016/j.meatsci.2007.02.014

97. Hoch G, Chauhan A, Radke CJ. Permeability and diffusivity for water transport through hydrogel membranes. *J Membr Sci*. 2003;214(2):199-209. doi:10.1016/S0376-7388(02)00546-X

98. Smith RP. The diffusivity of carbon in iron by the steadystate method. *Acta Metall*. 1953;1(5):578-587. doi:10.1016/0001-6160(53)90088-1

Chapter 3: Experimental Methods

This chapter details the materials and methods used in this work**.** Characterization techniques utilized are described. Several characteristics are critical to understanding material behavior for membrane applications. The membrane fabrication methods are described as are the methods used to characterize membrane transport and equilibrium properties, namely solubility, permeability, water uptake, solute uptake, and dimensional swelling. Characterization methods described include the use of in situ attenuated total reflectance Fourier-transform infrared (ATR FTIR) spectroscopy to characterize membrane permeability, and determination of membrane solubility for solutes of interest using equilibrium sorption/desorption experiments, nuclear magnetic resonance (NMR) spectroscopy, and high-performance liquid chromatography (HPLC).

3.1 Materials

Acetone, methanol, and butanol were purchased from British Drug House (BDH) Chemicals (Poole, UK). Poly(ethylene glycol) diacrylate (M_n = 700 g/mol), deuterium oxide, and 2-Acrylamido-2-methyl-1-propanesulfonic acid (99%) were from Sigma-Aldrich (St. Louis, MO). 1-propanol and benzyl alcohol were from Alfa Aesar (Haverhill, MA). Tetramethylsilane was from Merck (Kenilworth, NJ). 2-phenoxyethyl acrylate were from TCI America (Portland, OR). Ethanol was from EMD Millipore Corporation (Burlington, MA). Sodium acetate was purchased from ACS Chemical Inc. (Point Pleasant, NJ). Nafion™ 117 Lot T06C032 was purchased from Alfa Aesar (Haverhill, MA) and Lot 1709FS5172 was purchased from the Fuel Cell Store (College Station, TX), experimentally similar Lots. All chemicals were used as received unless otherwise stated. Ultrapure water was produced by a WaterPro BT water purification system from Labconco (Kansas City, MO).

3.2 Synthesis of Poly(Ethylene Glycol) Diacrylate (PEGDA) Membranes

Synthesis of PEGDA membranes followed established literature procedures.[1–5] Briefly, PEGDA, 0.1 wt % 1-hydroxycyclohexyl phenyl ketone (HCPK) photo-initiator, and water were combined and sonicated in an FS14 Sonicator from Fisher Scientific (Hampton, NH) for 30 minutes to produce a well-mixed system. Once sonicated, the mixture was poured onto a quartz plate between two spacers, used to control membrane thickness (typically 0.5 mm), and another glass plate was slowly lowered onto the system at an angle to ensure air bubbles were expelled. This entire setup was placed under UV light within a Spectroline Spectrolinker™ XL-1500 UV oven (Westbury, NY) under 254 nm at 3.0 mW/cm^2 for three minutes.

3.3. Synthesis of PEGDA – 2-Phenoxyethyl acrylate – 2-Acrylamido-2-methyl-1-Propanesulfonic Acid (PEGDA-PEA-AMPS) Membranes

The PEGDA-PEA-AMPS membranes were synthesized similarly to the PEGDA membranes. However, the pre-polymerization solutions were comprised of 62 wt % PEGDA, 20 wt % DI water, 0.1 wt% HCPK, and varied in PEA and AMPS content (from 0 – 18 wt % PEA and 18 - 0 wt % AMPS).

3.4. Attenuated Total Reflectance Fourier-Transform Infrared (ATR FTIR) Spectroscopy

Attenuated total reflectance Fourier-transform infrared (ATR FTIR) spectroscopy probe-based systems can be utilized to determine multiple solutes in solution.[6,7] The Beer-Lambert Law[8–10] given in Equation 1 relates measured absorbance, A_i, to solute concentration in solution, C_j, with an effective extinction coefficient, $\varepsilon_{i,j}$.

$$A_i = \sum_{\substack{i=1 \\ j=1}}^{n} \varepsilon_{i,j} C_j \qquad 3.1$$

The effective extinction coefficients for each solute at each wavenumber are determined via calibrations. Once concentrations can be determined from measured absorbances, the Yasuda model, Equation 2.44, is used to calculate a permeability value for the membrane to the solute. Full details on this methodology are given in Chapter 4.

A polymer's permeability is essential for membrane processes, as it quantifies how fast solutes transport through the membrane. Here, we utilize an in situ attenuated total reflectance Fourier-transform infrared (ATR FTIR) spectrometer to determine a membrane's permeability from diffusion-cell experiments. This procedure can be used for multiple component experiments and is much simpler than prior techniques.

For a molecule to absorb infrared radiation, it must have an overall change of dipole moment as it vibrates and/or rotates. There are stretching vibrations (changes in the interatomic distances) and bending vibrations (changes in the angles between bonds). Fourier-transform infrared (FTIR) spectrometers have several advantages to dispersive instruments: they have few optical elements and no slits, so the power that is gathered by the detector is more significant and displays better signal-to-noise ratios, they have wavelength reproducibility, very high resolving power, and minimal time required to obtain measurements.[11]

For each calibration, three to five scans were collected, and each experiment was repeated three times to ensure adequate precision. These experiments were performed on a ReactIR 15 from Mettler Toledo (Columbus, OH) with a 9.5 mm AgX Dicomp probe (Au, diamond, C22).

Solutions at five concentrations of the four alcohols were prepared between 0.025 to 0.25 Molar (M). They were placed in a reaction block on an AREX 3 Digital Pro Heating Magnetic Stirrer from Chemglass (Vineland, NJ) to keep them at 25 °C. Five spectra were measured of each concentration and a deionized water spectrum was collected in between each concentration change to show that temperature and instrument fluctuations were minimal, as shown in Figure 3.2. A pure deionized water spectrum, Type 1 water collected from a WaterPro BT Purification System from Labconco (Kansas City, MO), was obtained initially as the reference to subtract from each spectrum taken thereafter. Every experiment was baselined at 1197 cm^{-1} as there were no solute peaks or decreases in the water spectrum at this wavenumber.

Water was selected as the solvent for the permeability experiments because proton exchange membrane (PEM) fuel cells synthesize water from the released protons, electrons, and hydroxide ions and the membranes need to be hydrolyzed to be conductive.[12–14] The deionized water has the largest concentration in the samples because the solutes are, at most, 4 mole solutes/L solution. Therefore, when running a sample, it looks like the absorption of strictly water, with slight variations. The water spectrum is subtracted to see the absorption peaks of the solutes, as can be seen in the difference between Figures 3.1 (without the water subtraction) and 3.2 (with the water subtraction).

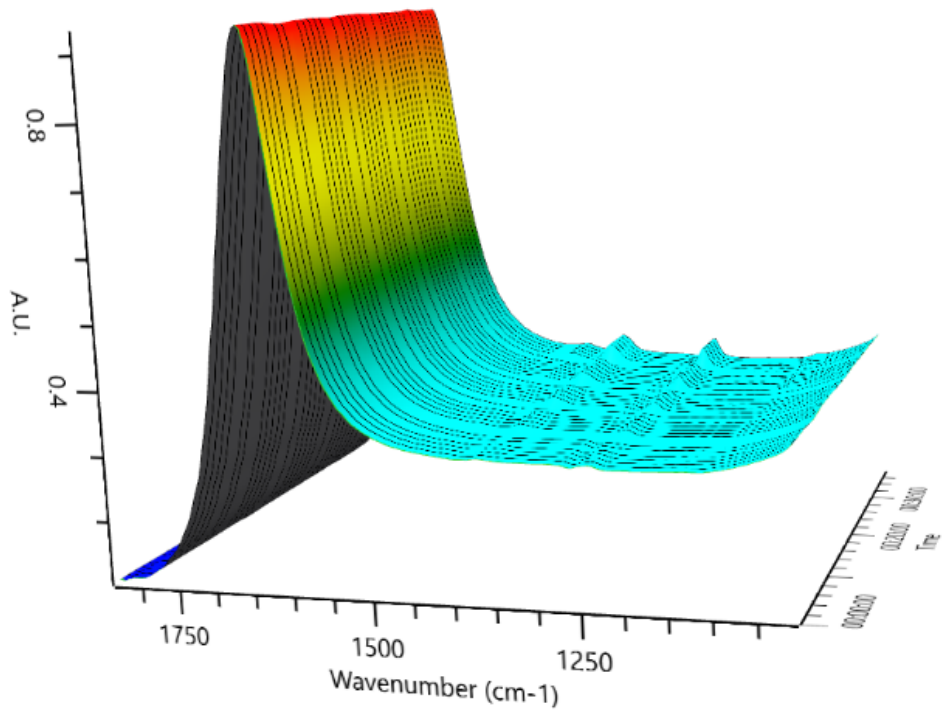

Figure 3.1. Raw ATR FTIR spectrum of an acetone calibration with concentration increasing over time and one deionized water spectrum taken between every change in concentration.

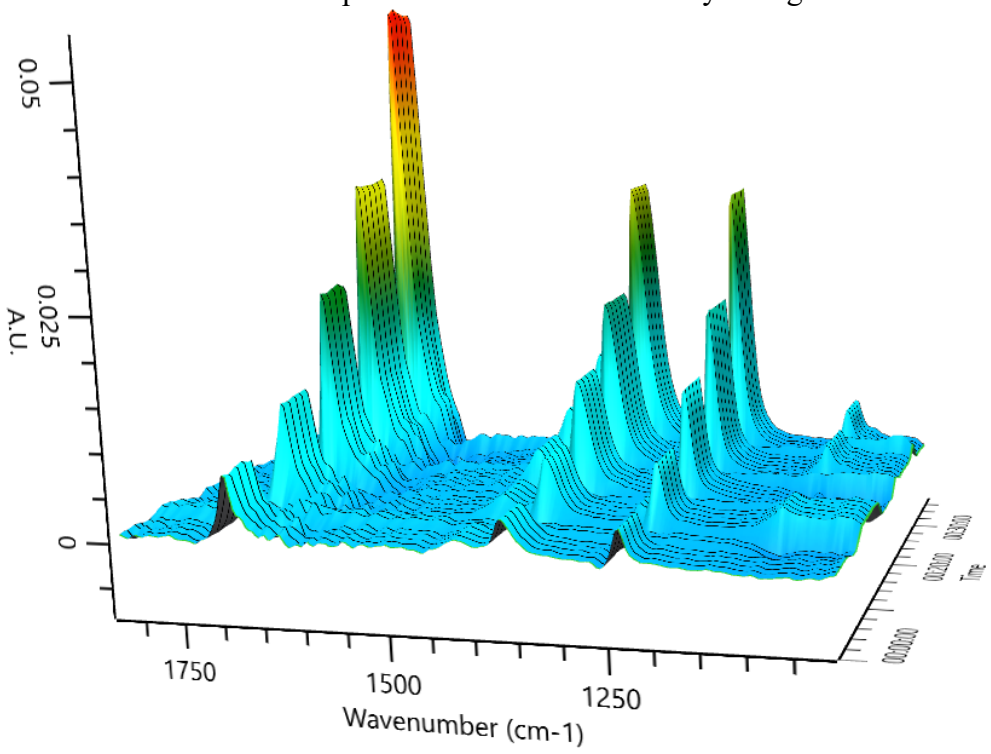

Figure 3.2. Water-subtracted ATR FTIR spectrum of an acetone calibration with concentration increasing over time and one deionized water spectrum taken between every change in concentration.

Baselining is also needed to place all of the spectra at '0' absorption at an elected wavenumber because there are slight differences in each measurement due to small temperature fluctuations and instrument error. The baseline selected was a one-point baseline at 1197 cm^{-1} as none of the solutes peak at this wavenumber, nor is there detraction of water. The one-point baseline was selected because the two-point, three-point, and Pearson's Correction baselines had more significant errors, ensuring any fluctuations were eliminated as much as possible.

To measure permeability, solutions at 1 M concentrations of the alcohol(s) were prepared in 25 mL volumetric flasks and were placed in the donor cell (the cell on the right) of the diffusion-cell apparatus shown in Figure 3.3. The ATR FTIR spectroscopy probe was placed in the receiver cell along with 25 mL of pure DI water. The cells were connected to an Isotemp 3013D chiller from Fisher Scientific (Hampton, NH) and jacketed at 25 °C to ensure that the extinction coefficients found from the calibrations were appropriately employed for the permeability experiments. Small metal stir bars were placed in each cell, and the cells were then placed on an AREX 3 Digital Pro Heating Magnetic Stirrer from Chemglass (Vineland, NJ), to ensure that they were well mixed throughout the experiments. The cells were separated with a membrane (Nafion™ 117 Lot T06C032 from Alfa Aesar (Haverhill, MA) or Lot 1709FS5172 from the Fuel Cell Store (College Station, TX), synthesized PEGDA or synthesized PEGDA-PEA-AMPS) that had been hydrated for at least 24 hours. The cells were covered with parafilm to ensure there was no evaporation.

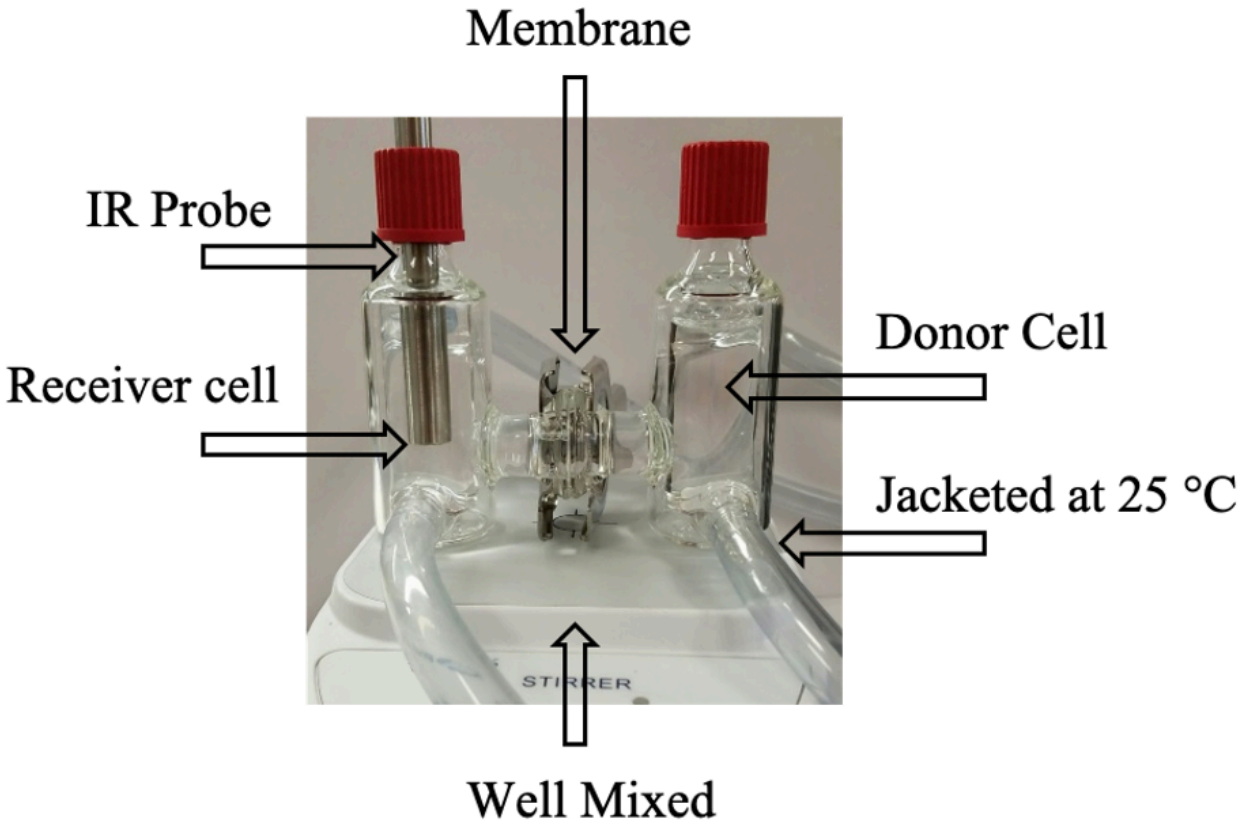

Figure 3.3. The diffusion-cell apparatus used to perform the permeability experiments. The donor cell is on the right, initially containing a 1 M solution of alcohol(s). The receiver cell, including the ATR FTIR probe, is on the left initially containing pure deionized water. The membrane is held between the two cells, which are jacketed at 25 °C and well-mixed with magnetic stir bars.

3.5. Sorption/Desorption Experiments

As will be discussed in greater detail in Chapter 4, the well-known solution diffusion model, Equation 2.34, is used to describe the productivity of the membrane to a solute (permeability) as the product of the thermodynamic solubility and kinetic diffusivity. To determine the solubility of a membrane to solute(s) of interest, a well-known sorption-desorption technique was employed. Fully hydrated membranes were placed in 1 M solute(s) mixtures. The mixtures were prepared analogous to solutions for diffusion-cell experiments; however, only 10 mL of solution was placed in the 25 mL scintillation vials. Fully hydrated films were blotted dry, cut into rounds using a 19 mm hammer-driven sharp metal stamp, and were then weighed, measured for thickness, and measured for diameter. The films were placed in the 1 M solute(s) solutions and allowed to absorb solute(s) to equilibration for three days. After 72 hours, the films were removed from the vials, blotted dry, weighed, measured for thickness, measured for diameter, and then placed in 10 mL of pure DI water. This was repeated until the desorption solution (originally pure DI water) did not contain any solute(s) after 72 hours. Each sorption experiment was performed in triplicate with different membranes and alcohol solutions for replicability.

3.6. Nuclear Magnetic Resonance (NMR) Spectroscopy

NMR spectroscopy uses a strong magnetic field to induce the nuclei of a sample to absorb electromagnetic radiation to split a nucleus's energy levels to +/- 1/2. The electromagnetic radiation that is measured is in the range of 4 to 900 MHz, and this is one of the best tools for determining chemical structures. The magnetic quantum state of a material is neutral without a magnetic field, but, once applied, the nuclei generally position themselves into the lower energy state (m = +1/2). The nuclei in either energy state will absorb radiation. Relaxation of the excited

species should happen as quickly as possible to reduce the chance that the system is saturated (the equalization of the number of nuclei in the low and high energy states producing no absorption).[11] A 600 MHz Bruker NMR spectrometer (Auburn Chemistry Dept., AL) was used to determine the concentrations of the sorption/desorption experiments from Section 3.4. The desorption solutions were transferred into NMR tubes gravimetrically, as was deuterium oxide (the deuterated solvent, in a 90 vol % H_2O/10 vol % D_2O ratio) and benzyl alcohol (as the reference material). Each solution was characterized via a water suppression technique as the concentration(s) of solute(s) are very dilute. The water suppression was by presaturation during relaxation delay and mixing time with four scans. The spectra were recorded using an Avance II Bruker spectrometer running TopSpin version 3.2.

Figure 3.4 shows the raw data file of methanol and ethanol in 90 % water and 10 % D_2O with a known amount of benzyl alcohol. The intense peaks between 4.5 and 5.0 ppm are the large water peaks. The methanol, ethanol, and benzyl alcohol peaks can be seen, however, due to the water suppression technique employed.

The baselined, tuned, and matched spectra with the large water peak(s) excluded are shown in Figure 3.5. The benzyl alcohol peak, 7.2 ppm, was integrated as the reference peak of known concentration. The other integrations are in reference to the known amount of benzyl alcohol added to solution.

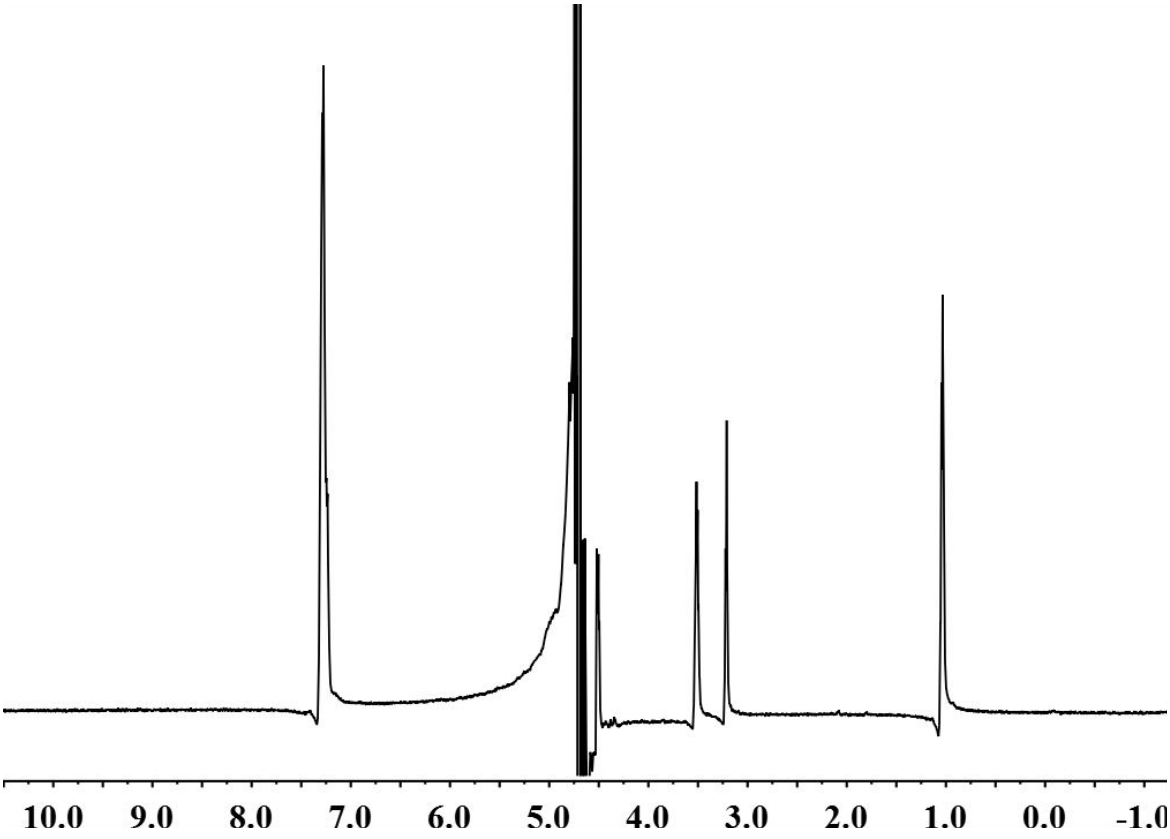

Figure 3.4. Raw methanol, ethanol, and benzyl alcohol NMR spectrum with water suppression.

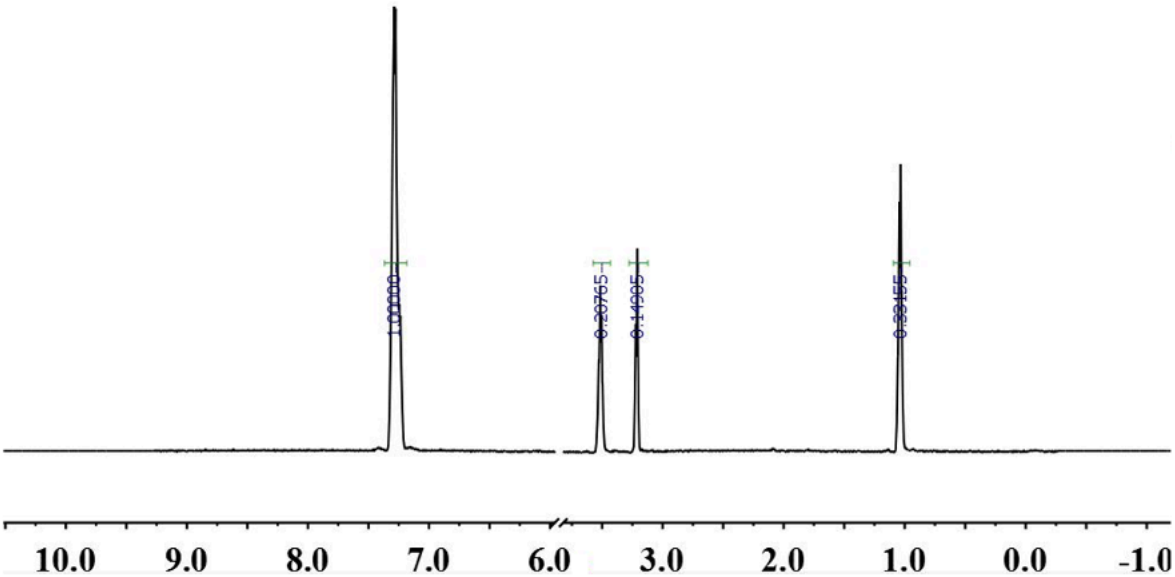

Figure 3.5. Baselined, tuned, and matched methanol, ethanol, and benzyl alcohol NMR spectrum with water suppression.

3.7. High-Performance Liquid Chromatography (HPLC)

To calibrate the HPLC for the desorption solutions, known concentrations of solute(s) were prepared at 0.003, 0.012, and 0.025 M concentrations as the predicted desorption concentrations were within this range. The solutions were prepared analogous to the ATR FTIR calibration solutions; however, a 250 mL volumetric flask was used instead of a 25 mL flask as the concentrations are quite dilute. A representative HPLC chromatograph for a set of calibrations is shown in Figure 3.6.

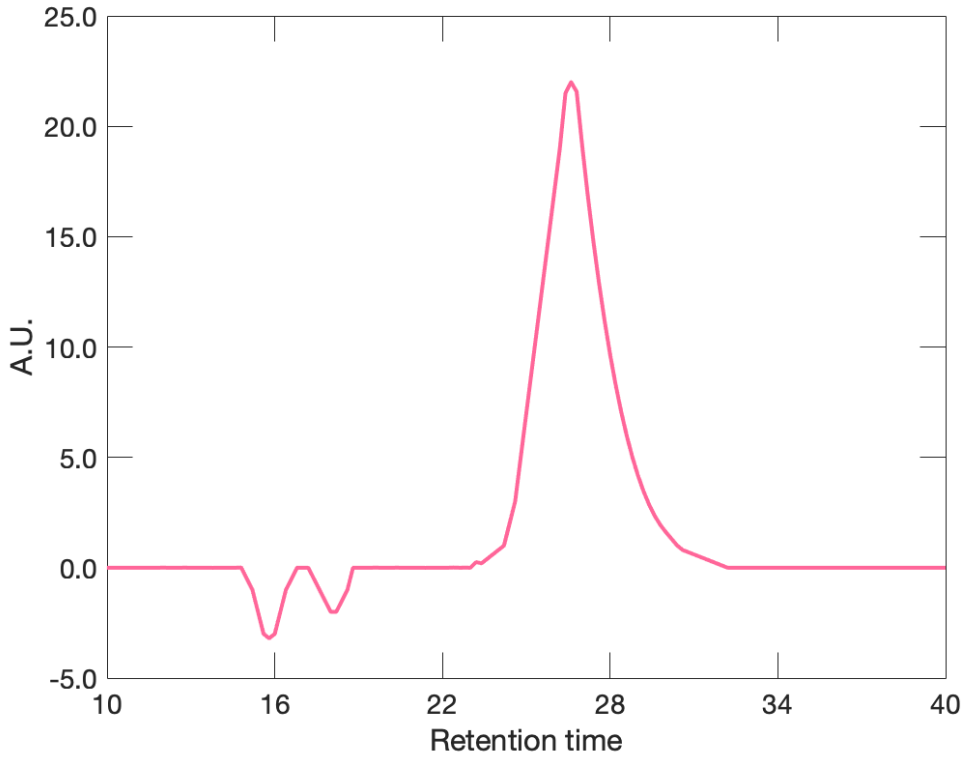

Figure 3.6. Representative chromatograph for 0.02 M acetone.

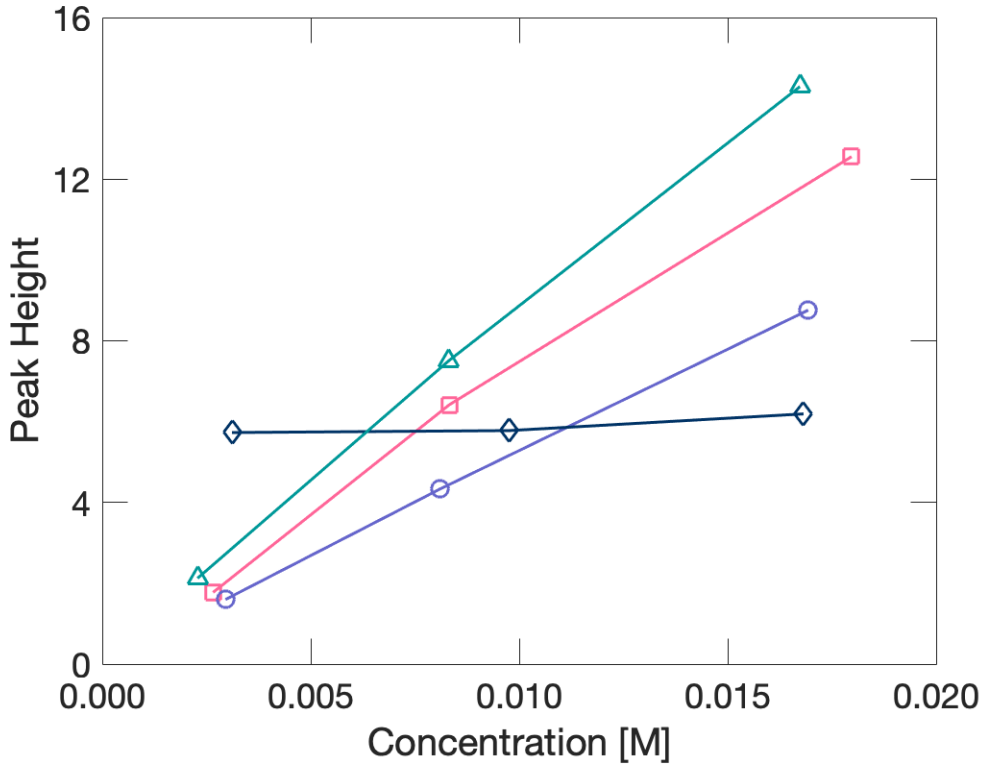

Figure 3.7. HPLC Calibrations. □Acetone, O Ethanol, ◊ Methanol, and Δ n-Propanol.

3.8. Water Uptake Measurements

Membranes were fully hydrated for at least 24 hours. Films were blotted dry and then weighed with a Mettler Toledo (Columbus, OH) ML204T Balance and their thicknesses measured by a Marathon digital caliper (± 1 micron). Films were then air-dried for 24 hours and placed in vacuo for 48 hours at slightly elevated temperatures to achieve fully dried membranes, which were subsequently weighed and measured for thickness. Water uptake, *W*, was calculated utilizing Equation 3.2,

$$W = \frac{m_W - m_D}{m_D} \tag{3.2}$$

where m_W is the mass of the hydrated membrane and m_D is the mass of the dry membrane. Solute uptake, *S*, was also calculated using an analogous process, but in lieu of DI water, membranes were equilibrated in 1 M solutions of the solute(s) of interest and the solute uptake was calculated using Equation 3.3,

$$S = \frac{m_S - m_D}{m_D} \tag{3.3}$$

where m_S is the mass of the solute swollen membrane. Solute uptakes were used in this work as a proxy for relative solubility in cases where solubility studies were unfortunately precluded due to instrumental issues and laboratory shut down for health safety purposes. Once fully hydrated, membranes were placed in 1 M solutions of methanol, sodium acetate, or their mixture and allowed to equilibrate for three days. After 72 hours, films were blotted dry and weighed to obtain the mass of the solute-swollen membrane.

3.9. Dimensional Swelling Measurements

Membranes were fully hydrated for 24 hours, blotted dry, cut into ¾ inch circles via a hammer driven sharp metal stamp, weighed with a Mettler Toledo (Columbus, OH) ML204T Balance and their thicknesses measured by a Marathon digital caliper (± 1 micron). They were dried in open scintillation vials for 24 hours at room temperature and then dried in a vacuum oven at 28 in Hg and room temperature for 48 hours. The completely dried membranes were measured for weight, thickness, and area via images including a ruler using the ImageJ app, which calculates area based upon the included ruler. An example image from this process is shown in Figure 3.8.

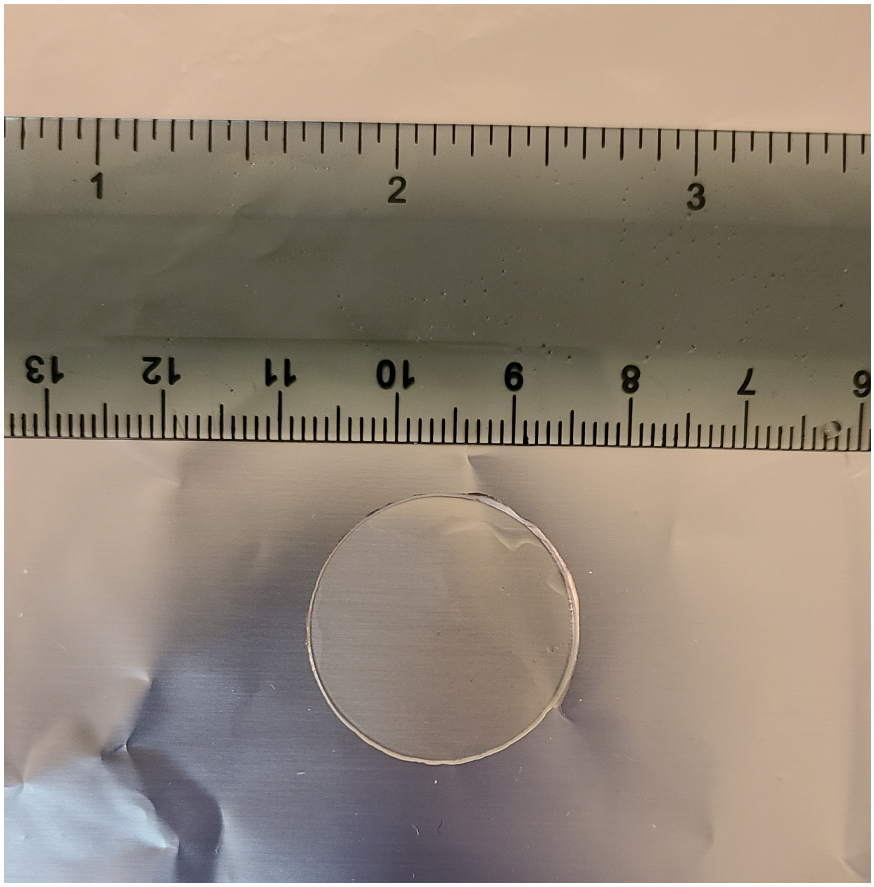

Figure 3.8. Example membrane swelling experiment used in ImageJ application.

3.10. References

1. Galizia M, Paul DR, Freeman BD. Liquid methanol sorption, diffusion and permeation in charged and uncharged polymers. *Polymer*. 2016;102:281-291. doi:10.1016/j.polymer.2016.09.010

2. Yan N, Paul DR, Freeman BD. Water and ion sorption in a series of cross-linked AMPS/PEGDA hydrogel membranes. *Polymer*. 2018;146:196-208. doi:10.1016/j.polymer.2018.05.021

3. Ju H, Sagle AC, Freeman BD, Mardel JI, Hill AJ. Characterization of sodium chloride and water transport in crosslinked poly(ethylene oxide) hydrogels. *J Membr Sci*. 2010;358(1):131-141. doi:10.1016/j.memsci.2010.04.035

4. Ju H, McCloskey BD, Sagle AC, Kusuma VA, Freeman BD. Preparation and characterization of crosslinked poly(ethylene glycol) diacrylate hydrogels as fouling-resistant membrane coating materials. *J Membr Sci*. 2009;330(1):180-188. doi:10.1016/j.memsci.2008.12.054

5. Sagle AC, Van Wagner EM, Ju H, McCloskey BD, Freeman BD, Sharma MM. PEG-coated reverse osmosis membranes: Desalination properties and fouling resistance. *J Membr Sci*. 2009;340(1):92-108. doi:10.1016/j.memsci.2009.05.013

6. Carter BM, Dobyns BM, Beckingham BS, Miller DJ. Multicomponent transport of alcohols in an anion exchange membrane measured by in-situ ATR FTIR spectroscopy. *Polymer*. 2017;123:144-152. doi:10.1016/j.polymer.2017.06.070

7. Beckingham BS, Lynd NA, Miller DJ. Monitoring multicomponent transport using in situ ATR FTIR spectroscopy. *J Membr Sci*. 2018;550:348-356. doi:10.1016/j.memsci.2017.12.072

8. Calloway D. Beer-Lambert Law. *Chem Educ Today*. Published online 1997.

9. Swinehart DF. The Beer-Lambert Law. *J Chem Educ*. 1962;39(7):333-335.

10. BEER A. Bestimmung der Absorption des rothen Lichts in farbigen Flussigkeiten. *Ann Phys*. 1852;162:78-88.

11. Skoog DA, Holler FJ, Crouch SR. *Principles of Instrumental Analysis*. Sixth. Cengage Learning; 2007.

12. Zawodzinski TA, Smith VT, Springer TE. Water Uptake by and TransportThrough Nafion 117 Membranes. *J Electrochem Soc*. 1993;140(4):7. doi:https://doi.org/10.1149/1.2056194

13. Heinzel A, Barragan VM. A review of the state-of-the-art of the methanol crossover in direct methanol fuel cells. *J Power Sources*. 1999;84:70-74. doi:10.1016/S0378-7753(99)00302-X

14. Mehta V, Cooper JS. Review and analysis of PEM fuel cell design and manufacturing. *J Power Sources*. 2003;114(1):32-53. doi:10.1016/S0378-7753(02)00542-6

Chapter 4: Assessment of ATR FTIR Spectroscopy for characterizing complex mixtures in situ

Reproduced in part from: Dobyns BM, Kim JM, Beckingham BS. Multicomponent transport of methanol and sodium acetate in poly(ethylene glycol) diacrylate membranes of varied fractional free volume. *Eur Polym J.* 2020;134:109809. doi:10.1016/j.eurpolymj.2020.109809.with permissions from Jung Min Kim and Bryan S. Beckingham.

As discussed in Chapter 1, experiments measuring solute permeability values for multicomponent mixtures have rarely been performed due to their difficulty. Consequently, single component permeability values are generally utilized to describe transport and to evaluate a membrane for a particular application. However, this route does not account for any specific interactions between multiple solutes, and the complex array of interactions between solutes and the membrane. These various interactions can be significant and considerably impact the permeability and selectivity of a membrane.

Previously, to determine the concentrations of multiple components in solution, the experimenter would need to periodically take aliquots of the receiver cell solution and analyze these aliquots for solute concentrations ex situ with HPLC[1], UV-Vis detector[2,3], mass spectrometer[4], Fourier-transform infrared (FTIR) spectrophotometer[5] or determine the receiver cell solute concentration in situ utilizing a pH[6,7] or conductivity[8–10] probe. Unfortunately, pH and conductivity in situ probe methods only measure differences in the solution properties and cannot distinguish what is causing these differences, e.g., distinguish individual component concentrations for a complex mixture. This chapter describes a methodology that combines the speciation capabilities of the above-mentioned ex situ techniques and with the advantages of non-aliquotic sampling techniques (in situ measurements) via a probe-based attenuated total reflectance (ATR) FTIR spectrophotometer.

4.1. Quantitative aqueous solute concentrations using ATR FTIR spectroscopy and Beer's Law

In this work in situ attenuated total reflectance Fourier-transform infrared (ATR FTIR) spectroscopy is employed for measuring solute concentrations in the receiver-cell solution over time. Absorbance is related to solute concentration by the Beer-Lambert Law,

$$A_i = \sum_{\substack{i=1 \\ j=1}}^{n} \varepsilon_{i,j} C_j \tag{4.1}$$

where A_i is the absorbance at wavenumber i, C_j is the concentration of solute j and $\varepsilon_{i,j}$ is the effective extinction coefficient for solute j at wavenumber i.[11] For single-component transport experiments, this relationship can be used directly; the absorbance at a single wavenumber can be used to determine that solute's concentration. However, for two-component solutions, there are two unknown concentrations, C_A and C_B, requiring the use of two independent expansions of Equation 5 for two distinct wavenumbers (1 and 2), as shown in Equations 4.2 and 4.3.

$$A_1 = \varepsilon_{A1} C_A + \varepsilon_{B1} C_B \tag{4.2}$$

$$A_2 = \varepsilon_{A2} C_A + \varepsilon_{B2} C_B \tag{4.3}$$

These two Beer-Lambert Law expressions can then be solved simultaneously for the concentrations of A and B, yielding Equations 4.4 and 4.5.

$$C_A = \frac{A_1 - \varepsilon_{B1} C_B}{\varepsilon_{A1}} \tag{4.4}$$

$$C_B = \frac{\varepsilon_{A1} A_2 - \varepsilon_{A2} A_1}{\varepsilon_{A1} \varepsilon_{B2} - \varepsilon_{A2} \varepsilon_{B1}} \tag{4.5}$$

To utilize this approach, effective extinction coefficients for methanol and acetate are determined from solutions of known concentration.

Once these effective extinction coefficients were determined, a series of solutions with varied methanol and acetate concentrations were prepared to ensure multicomponent mixture

concentrations could be determined quantitatively. Solute concentrations for these validation mixtures were found to be on or close to the identity line (Figure 4.2), confirming the utility of this approach for determining solute concentrations in mixtures of methanol and acetate.[9]

To determine concentrations in diffusion-cell experiments from absorbance measurements made using ATR FTIR spectroscopy, extinction coefficients for each solute must first be determined. To do so, the Beer-Lambert Law was used to relate the radiant power from a beam of radiation to the path of that beam in an absorbing medium and the concentration of an absorbing species (Equation 4.6)[11–13]

$$A = -log_{10}\frac{P}{P_0} = \epsilon lc \qquad 4.6$$

where A is the measured absorbance, P_0 is the radiant power of an electromagnetic radiation beam, P is the power of that beam within the absorbing medium, ϵ is the extinction coefficient or the molar absorption coefficient, l is the path length of the beam through the solution, and c is the solute concentration. The path length, l, varies negligibly between experiments due to the fact that they are all, generally, water. The path length depends on the refractive index of the solution, and the RI difference between experiments is negligible. Therefore, an effective extinction coefficient, ε, the product of the extinction coefficient and path length, is utilized, as can be seen from Equation 4.7.

$$\varepsilon = \epsilon l \qquad 4.7$$

Therefore, substituting Equation 4.7 into Equation 4.6 gives

$$A = \varepsilon c \qquad 4.8$$

The Beer-Lambert Law is additive, so, at each absorbance, the effect of every solute must be accounted for. Therefore, multiple solute concentrations can be determined from a multiple component solution used in one experiment using Equation 4.9.

$$A_\lambda = \sum_{i=1}^{n} \varepsilon_{i,\lambda} C_i \qquad 4.9$$

The ATR FTIR spectrophotometer measures the absorbance of the solutions, and a plot is produced of measured absorbance versus known concentration. As can be seen from Equation 4.9, from the known concentration of the mixtures and the measured absorbance given by the FTIR spectrometer, $\varepsilon_{i,\lambda}$ is the slope(s) of the line(s). This approach was recently used by Carter, Dobyns, Beckingham, and Miller (2017) and Beckingham, Lynd, and Miller (2018) to measure the downstream concentration of various solutes through Nafion and Selemion. The following sections detail the methodology and procedure of this technique, before validating its use for the multicomponent mixtures of interest.[14,15]

4.2. Methodology

The ATR FTIR spectra of each component exhibit a number of peaks, as shown in Figure 4.1. The boxed peaks are those that were selected for the calculations due to their relatively large effective extinction coefficients and higher R^2 values. The larger the effective extinction coefficient, the more significant the change in absorbance per shift in concentration, meaning that the wavenumbers with more significant extinction coefficients are more sensitive to changes in concentration.

For instance, Carter, Dobyns, Beckingham, and Miller in their 2017 work “Multicomponent transport of alcohols in an anion exchange membrane measured by in situ ATR FTIR

spectroscopy" determined effective extinction coefficients for ethanol, methanol, and n-propanol; values reported here in Table 4.1. The bolded ε and R^2 values are the wavenumbers that were selected for each alcohol in that study based upon their large values and are the wavenumbers that were selected for their work.[15] These wavenumbers were also selected for the work in this dissertation, and calibration curves and effective extinction coefficients were determined independently here (described in Section 4.3) to account for instrumental differences between the ATR FTIR spectrophotometers.

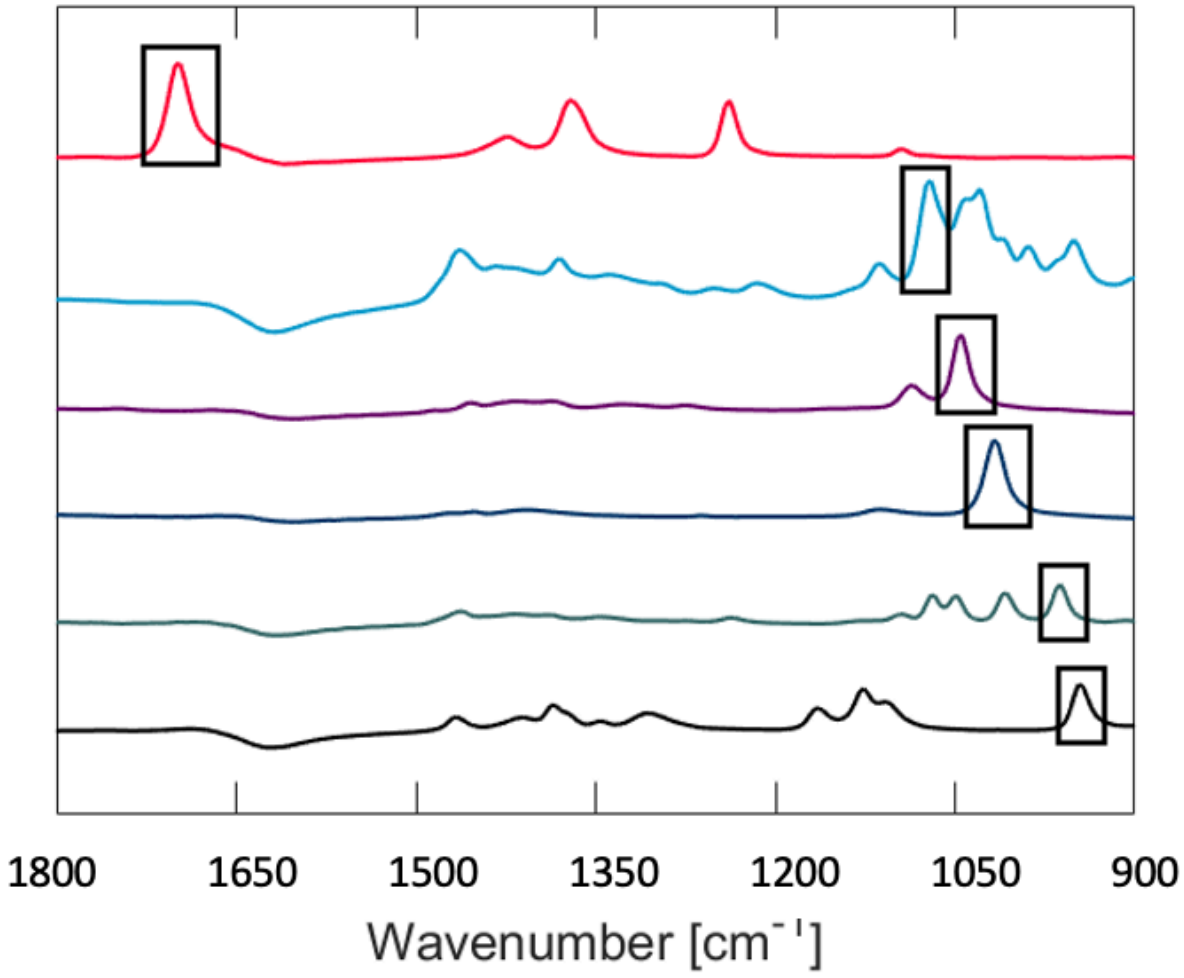

Figure 4.1. The absorption spectra of the six alcohols given by the ATR FTIR. The squared peaks are the ones that were used. From top down acetone, butanol, ethanol, methanol, n-propanol, and isopropanol.

Table 4.1. Effective extinction coefficients of methanol, ethanol, and n-propanol at wavenumbers of interest

	Methanol		**Ethanol**		**Propanol**	
Wavenumber	**ε**	**R^2**	**ε**	**R^2**	**ε**	**R^2**
962	0.000962	0.6851	-0.0023	0.5084	**0.0715**	**0.9987**
1007	0.0721	0.999	0.0023	0.4444	0.049	0.8754
1018	**0.1514**	**0.9987**	0.010029	0.8749	0.0077	-0.552
1044	0.011	0.1871	**0.1568**	**0.9989**	0.0267	-0.63
1070	-0.0045	0.3037	0.0172	0.9343	0.0451	-0.211
1089	-0.0024	-0.243	0.0433	0.9883	0.0019	-0.232
1115	0.0061	0.7826	0.0017	0.7397	-0.0003	0.1875
1126	0.0016	0.4165	0.0015	0.6912	-0.00038	0.2539

Initially, calibrations were performed on the laboratory bench at room temperature using "sterile" BD syringes. Temperature plays a significant role in the absorbance of IR radiation, and therefore must be held constant. Figure 4.2 shows the impact of changes in temperature on the spectra over 12 hours on the laboratory bench. As this variability is unacceptable, a reaction block was purchased from Chemglass (Vineland, NJ), Figure 4.3, to keep the calibration solutions isothermal during measurements. For diffusion cell experiments, this is accomplished with thermally jacketed diffusion cells.

Additionally, a variation in the underlying water spectra was observed, Figure 4.4, resulting in a considerable variation in the spectra at low wavenumbers. The spectra in Figure 4.4 should be generally flat, as they are all water spectra obtained within a single experiment after the first water spectrum was subtracted. This variation was eventually attributed to residual grease, which was held on the "sterile" syringes purchased from BD (Franklin Lakes, NJ) (shown in Figure 4.5a) and could be prevented using gas-tight, glass syringes purchased from Hamilton (shown in Figure 4.5b) which were used for all experiments presented herein.

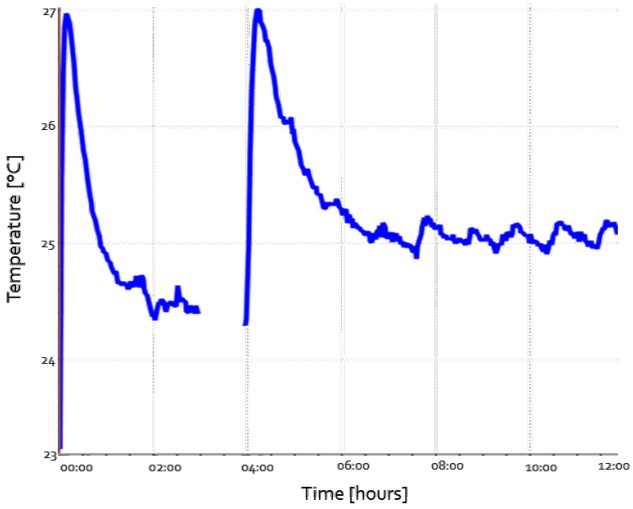

Figure 4.2. ATR FTIR spectra temperature fluctuations within 12 hours.

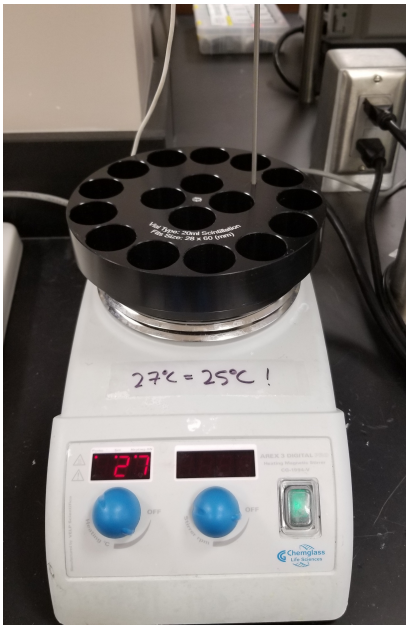

Figure 4.3. Chemglass reaction block to hold calibration temperatures constant.

Figure 4.4. ATR FTIR spectra water fluctuations for one experiment.

a) b)

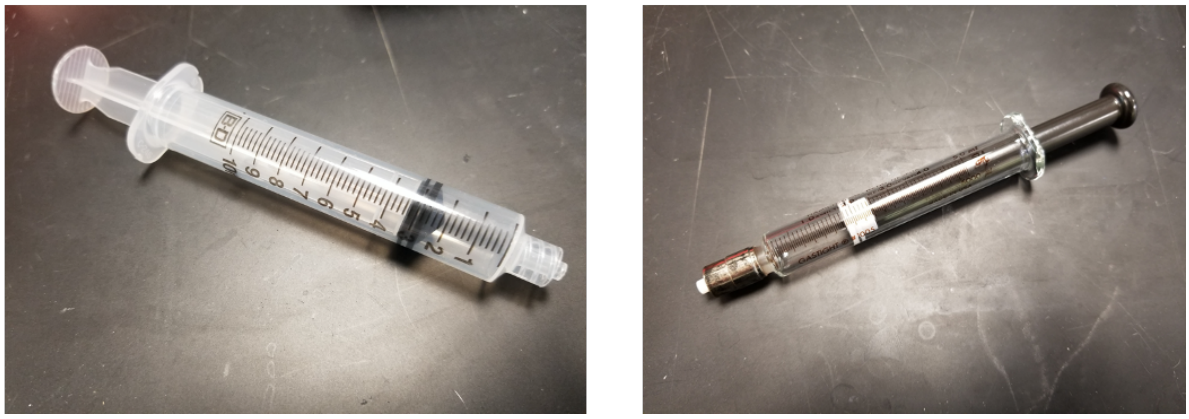

Figure 4.5. Syringes used for experimentation. a) "sterile" BD disposable syringe that contains grease on the plunger and b) Hamilton gas-tight, glass syringe.

4.3. General Calibration Procedure

Solutions of 5 concentrations ranging from 0.025 molar to 0.25 molar of the solute(s) in deionized water were prepared in 25 mL volumetric flasks. These were placed in 20 mL scintillation vials and put in a reaction block and equilibrated at 25 °C to ensure the extinction coefficients were determined at the temperature of interest for subsequent permeability experiments. The probe was placed in the downstream solution, ensuring that the probe tip was thoroughly wetted. At least three measurements were collected at each concentration. Between solution samples, the probe was immersed in DI water to ensure that there was no change in temperature or background spectra and that the probe was clean. Figure 4.6 shows an example of a calibration spectrum. It is methanol from 0.025 to 0.25 M, and as can be seen, as the concentration increases with time, so does the absorbance at 1018 cm^{-1}.

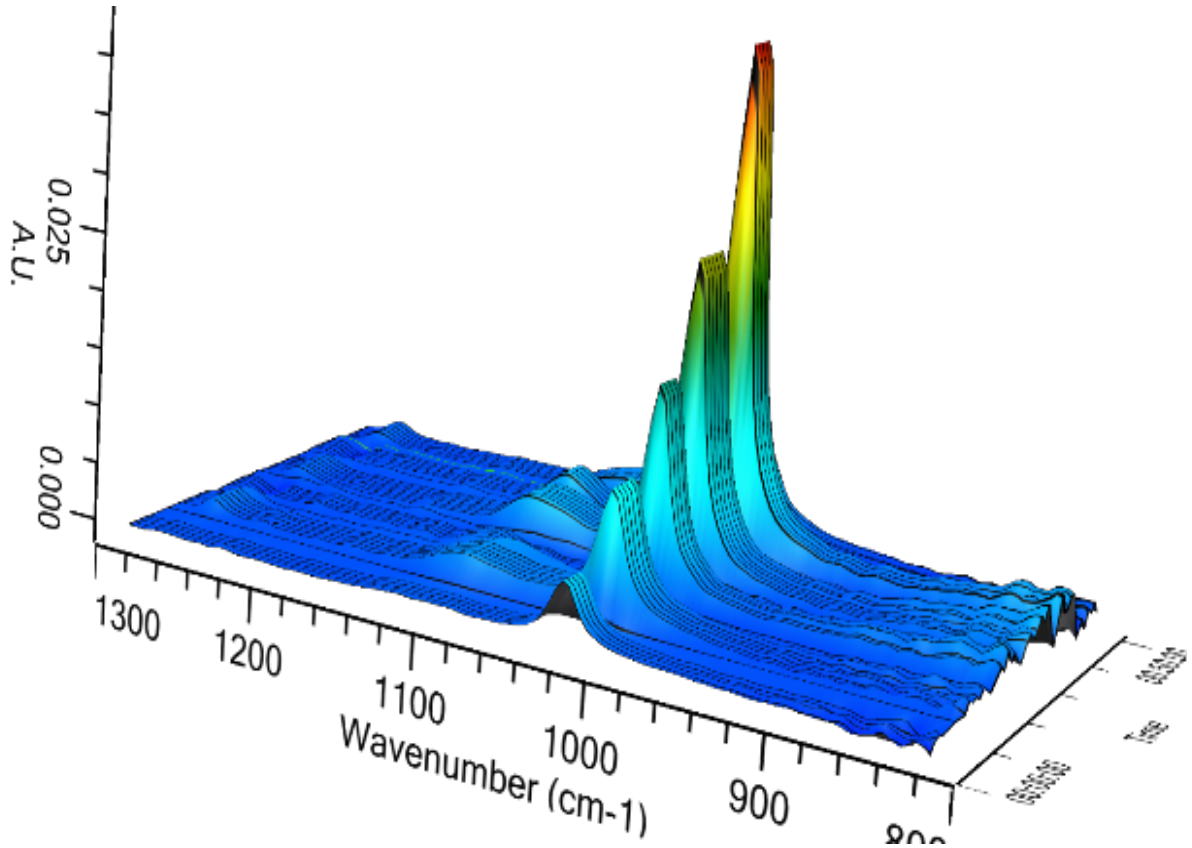

Figure 4.6. Example of an ATR FTIR Calibration for Methanol with 0.025, 0.05, 0.1, 0.15, and 0.25 M solutions. The primary peak is at 1018 cm^{-1}.

4.4 Pure Component Calibrations

The procedure for determining ε was conducted for a series of alcohols and sodium acetate. Based on the spectra shown in Figure 4.1, absorbance values were extracted, and extinction coefficients determined at the wavenumbers of interest, as shown in Table 4.2. Figure 4.7 shows the calibration curve fits for each solute at select wavenumbers.

Table 4.2. Extinction coefficients determined for the alcohols at the wavenumbers of interest

	λ = 1700 cm^{-1}		**λ = 1414 cm^{-1}**		**λ = 1044 cm^{-1}**		**λ = 1018 cm^{-1}**		**λ = 962 cm^{-1}**	
	ε	**R^2**	**ε**	**R^2**	**ε**	**R^2**	**ε**	**R^2**	**ε**	**R^2**
Acetone	0.2064	0.9963			-0.0014	0.067	-0.0008	-0.02	-0.0012	-0.201
Sodium Acetate	-0.0047	0.4986	0.2798	0.9995	-0.0049	0.4748	0.0281	0.9743	-0.0023	-0.461
Ethanol	0.0038	-0.397	0.0086	-0.214	0.131	0.999	-0.0205	0.9448	0.0004	-0.05
Methanol	0.0025	0.2435	0.0059	0.7722	-0.0128	0.993	0.1515	0.9952	-0.0022	0.771
Propanol	-0.0005	0.0245			0.0236	0.9865	0.0173	0.172	0.0801	0.9956

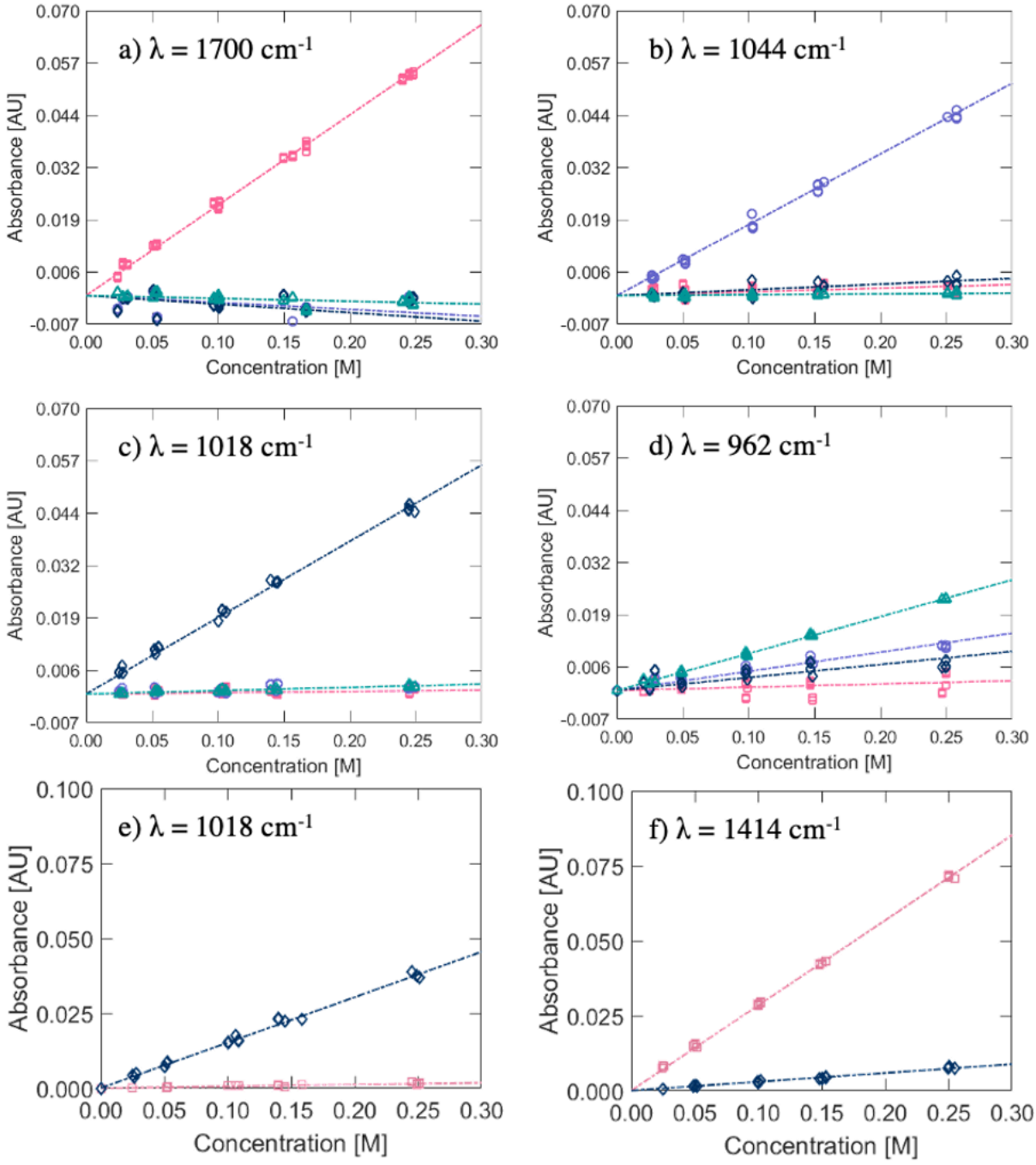

Figure 4.7. Calibration plots for □Acetone, O Ethanol, ◊ Methanol, Δ n-Propanol, and □Sodium Acetate. at (a) 1700 cm^{-1}, (b) 1044 cm^{-1}, (c) 1018 cm^{-1}, (d) 962 cm^{-1}, (e) 1018 cm^{-1}, and (f) 1414 cm^{-1}.

When selecting a particular wavenumber for a solute, multiple factors must be considered: highest extinction coefficient, absorbance of the other solutes, and water suppression. A decrease in absorbance occurs between 1650 and 1500 cm^{-1} with increasing solute concentration due to decreasing water concentration and, therefore, no wavenumbers in this range were selected. Otherwise, the highest extinction coefficient values were used for each solute, as this corresponds to the wavenumber with the most substantial change in absorbance for a given change in concentration. In other words, the higher the effective extinction coefficient, the more sensitive this technique is to small changes in concentration. 962 cm^{-1} was selected for n-propanol, as this wavenumber had the lowest effective extinction coefficients for the other solutes, and the measurement error using this wavenumber proved to be less than using 1070 cm^{-1}, the wavenumber with the largest effective extinction coefficient for n-propanol. Otherwise, the highest extinction coefficient wavenumber was selected (1700 cm^{-1} for acetone, 1414 cm^{-1} for sodium acetate, 1044 cm^{-1} for ethanol, 1018 cm^{-1} for methanol, and 962 cm^{-1} for sodium acetate).

4.5 Verification of Approach for Multicomponent Mixtures

To verify this approach for multicomponent mixtures, a series of two-component, three-component, and four-component mixtures of these alcohols were prepared, and their spectra obtained. The measured concentration of each species is determined using Equation 4.4 and compared to the prepared concentration. Equations 4.4 and 4.5 were used to calculate the 2 component concentrations. Analogous derivations for determining the solute concentrations in three and four-component mixtures equations can be derived, with the three-component derivation presented in Equations 4.10 - 4.14 as an illustration. However, it was found that using these sequential equations to determine multicomponent concentrations resulted in a sizeable

experimental % error, as high as 18%. Instead, a matrix left division MATLAB code was developed to solve the system of linear equations. This generated MATLAB code allows for the calculation of the concentrations via the absorbances, calculated effective extinction coefficients, and time via a square matrix of coefficients and a vector of right sides of equations. This code calculated concentrations that were no larger than 2 % error of the calculated experiment.

$$\phi = 1 - \frac{\varepsilon_{A2}\varepsilon_{B1}}{\varepsilon_{A1}\varepsilon_{B2}} + \frac{\varepsilon_{A3}\varepsilon_{B1}\varepsilon_{C2}}{\varepsilon_{A1}\varepsilon_{B2}\varepsilon_{C3}} - \frac{\varepsilon_{A3}\varepsilon_{C1}}{\varepsilon_{A1}\varepsilon_{C3}} \tag{4.10}$$

$$\varphi = 1 - \frac{\varepsilon_{A2}\varepsilon_{B1}\varepsilon_{B3}\varepsilon_{C2}}{\varepsilon_{A1}\varepsilon_{B2}^2\varepsilon_{C3}\phi} + \frac{\varepsilon_{A2}\varepsilon_{B3}\varepsilon_{C1}}{\varepsilon_{A1}\varepsilon_{B2}\varepsilon_{C3}\phi} \tag{4.11}$$

$$C_A = \frac{\frac{A_1}{\varepsilon_{A1}} - \frac{A_2\varepsilon_{B1}}{\varepsilon_{A1}\varepsilon_{B2}} + \frac{A_3\varepsilon_{B1}\varepsilon_{C2}}{\varepsilon_{A1}\varepsilon_{B2}\varepsilon_{C3}} - \frac{A_3\varepsilon_{C1}}{\varepsilon_{A1}\varepsilon_{C3}} - \frac{C_B\varepsilon_{B1}\varepsilon_{B3}\varepsilon_{C2}}{\varepsilon_{A1}\varepsilon_{B2}\varepsilon_{C3}} + \frac{C_B\varepsilon_{B3}\varepsilon_{C1}}{\varepsilon_{A1}\varepsilon_{C3}}}{\phi} \tag{4.12}$$

$$C_B = \frac{\frac{A_2}{\varepsilon_{B2}} - \frac{A_1\varepsilon_{A2}}{\varepsilon_{A1}\varepsilon_{B2}\phi} + \frac{A_2\varepsilon_{A2}\varepsilon_{B1}}{\varepsilon_{A1}\varepsilon_{B2}^2\phi} - \frac{A_3\varepsilon_{A2}\varepsilon_{B1}\varepsilon_{C2}}{\varepsilon_{A1}\varepsilon_{B2}^2\varepsilon_{C3}\phi} + \frac{A_3\varepsilon_{A3}\varepsilon_{C1}}{\varepsilon_{A1}\varepsilon_{B2}\varepsilon_{C3}\phi} + \frac{C_C\varepsilon_{C2}}{\varepsilon_{B2}}}{1 - \frac{\varepsilon_{A2}\varepsilon_{B1}\varepsilon_{B3}\varepsilon_{C2}}{\varepsilon_{A1}\varepsilon_{B2}^2\varepsilon_{C3}\phi} - \frac{\varepsilon_{A2}\varepsilon_{B3}\varepsilon_{C1}}{\varepsilon_{A1}\varepsilon_{B2}\varepsilon_{C3}\phi}} \tag{4.13}$$

$$C_c = \frac{\frac{A_3}{\varepsilon_{C3}} - \frac{A_1\varepsilon_{A3}}{\varepsilon_{A1}\varepsilon_{C3}\phi} + \frac{A_2\varepsilon_{A3}\varepsilon_{B1}}{\varepsilon_{A1}\varepsilon_{B2}\varepsilon_{C3}\phi} - \frac{A_3\varepsilon_{A3}\varepsilon_{B1}\varepsilon_{C2}}{\varepsilon_{A1}\varepsilon_{B2}\varepsilon_{C3}^2\phi} + \frac{A_3\varepsilon_{A3}\varepsilon_{C2}}{\varepsilon_{A1}\varepsilon_{C3}^2\phi} + \cdots}{1 + \frac{\varepsilon_{A3}\varepsilon_{B1}\varepsilon_{B3}\varepsilon_{C2}^2}{\varepsilon_{A1}\varepsilon_{B2}^2\varepsilon_{C3}\phi\varphi} - \frac{\varepsilon_{A3}\varepsilon_{B3}\varepsilon_{C1}\varepsilon_{C2}}{\varepsilon_{A1}\varepsilon_{B2}\varepsilon_{C3}^2\phi\varphi} - \frac{\varepsilon_{B3}\varepsilon_{C2}}{\varepsilon_{B2}\varepsilon_{C3}\varphi}}$$

$$\cdots \frac{\left[\frac{A_2}{\varepsilon_{B2}\varphi} - \frac{A_1\varepsilon_{A2}}{\varepsilon_{A1}\varepsilon_{B2}\phi\varphi} + \frac{A_2\varepsilon_{A2}\varepsilon_{B1}}{\varepsilon_{A1}\varepsilon_{B2}^2\phi\varphi} - \frac{A_3\varepsilon_{A2}\varepsilon_{B1}\varepsilon_{C2}}{\varepsilon_{A1}\varepsilon_{B2}^2\varepsilon_{C3}\phi\varphi} + \frac{A_3\varepsilon_{A2}\varepsilon_{C1}}{\varepsilon_{A1}\varepsilon_{B2}\varepsilon_{C3}\phi\varphi}\right]\left[\frac{\varepsilon_{A3}\varepsilon_{B1}\varepsilon_{B3}\varepsilon_{C2}}{\varepsilon_{A1}\varepsilon_{B2}\varepsilon_{C3}^2\phi} - \frac{\varepsilon_{A3}\varepsilon_{B3}\varepsilon_{C1}}{\varepsilon_{A1}\varepsilon_{C3}^2\phi} - \frac{\varepsilon_{B3}}{\varepsilon_{C3}}\right]}{1 + \frac{\varepsilon_{A3}\varepsilon_{B1}\varepsilon_{B3}\varepsilon_{C2}^2}{\varepsilon_{A1}\varepsilon_{B2}^2\varepsilon_{C3}\phi\varphi} - \frac{\varepsilon_{A3}\varepsilon_{B3}\varepsilon_{C1}\varepsilon_{C2}}{\varepsilon_{A1}\varepsilon_{B2}\varepsilon_{C3}^2\phi\varphi} - \frac{\varepsilon_{B3}\varepsilon_{C2}}{\varepsilon_{B2}\varepsilon_{C3}\varphi}} \tag{4.14}$$

Carter, Dobyns, Beckingham, and Miller investigated two- and three-component mixtures of methanol, ethanol, and n-propanol and found excellent agreement (typically, of 5% error or less).[15] Beckingham, Miller, and Lynd similarly found good agreement for two-and three-component mixtures of methanol, sodium formate, and sodium acetate.[14] Here we assess the effectiveness of this methodology for multicomponent mixtures of acetone, butanol, ethanol, methanol, n-propanol, isopropanol, and sodium acetate.

Figures 4.8 and 4.9 show excellent agreement with the pure component calculated effective extinction coefficients and the two-component mixtures of acetone, ethanol, methanol, and/or n-propanol as well as methanol and sodium acetate. The experimental points are within 0.02 M of the identity line (dotted and solid lines in Figure 4.8 and 4.9, respectively). Therefore, these epsilon values are constant quantities and can be used for any concentration and mixture of solutes. Figure 4.10 shows the four triple-component validation mixtures of the neutral alcohols. The solutes, however, must absorb infrared radiation via covalent bond's dipole moments. In other words, pure ionic species (such as Na^+ and Cl^-) will not work with this particular methodology. Figure 4.11, however, shows that butanol does not show good agreement with two- and three-component calibration mixtures. Butanol is only partially miscible in water; they will not mix above 0.98 M butanol at 25 °C. Therefore, butanol was not used for the permeability experiments, nor was isopropanol as the transport of methanol, ethanol, 1-propanol (isopropanol), and 2-propanol was already characterized through Nafion™ 117 membranes by Godino et al.[16] Figure 4.10 shows the two-component validation mixture for methanol and sodium acetate. Again, this combination shows excellent agreement with the calculated effective extinction coefficients.

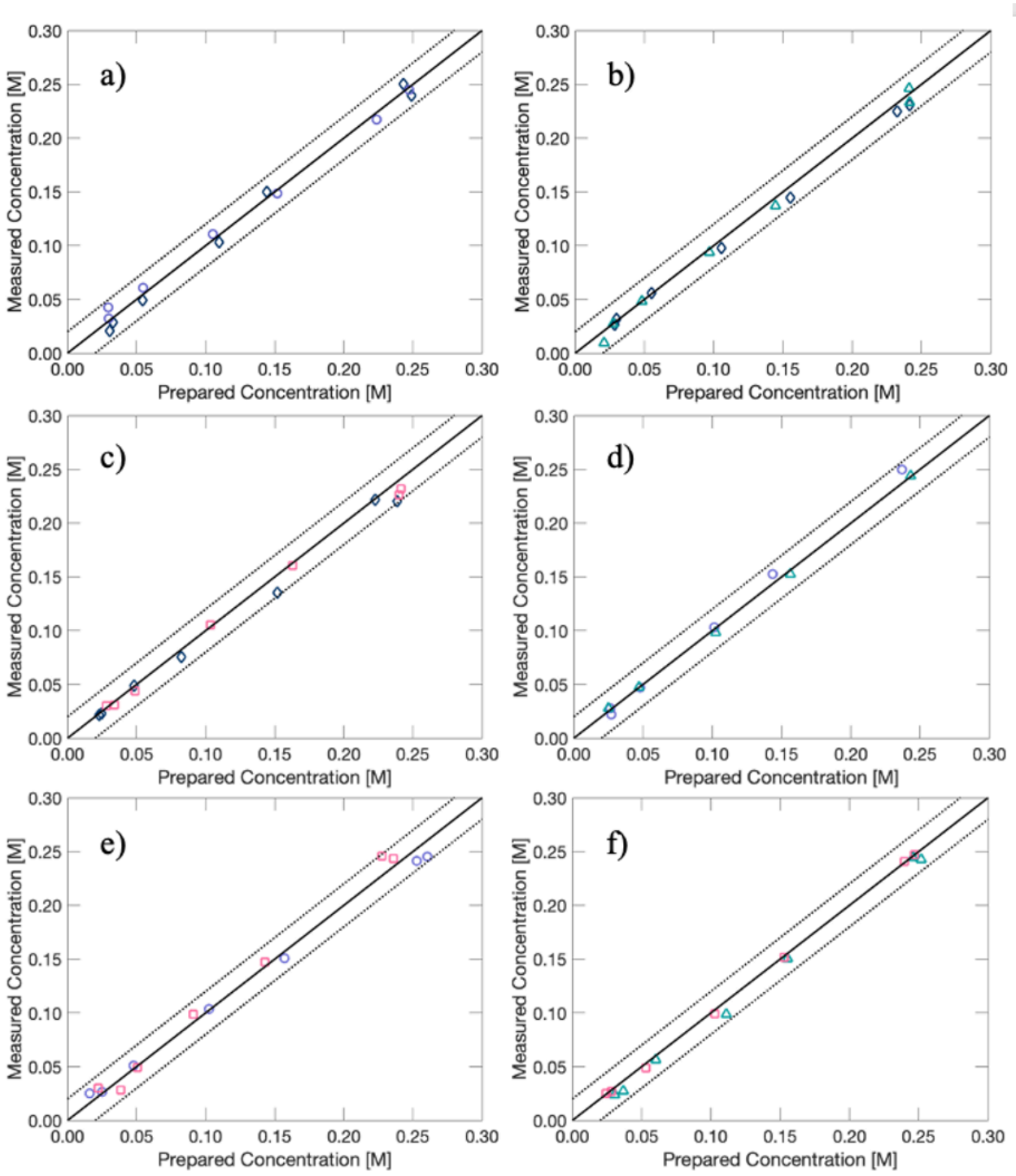

Figure 4.8. Binary component validation mixtures. □ Acetone, O Ethanol, ◊ Methanol, and Δ n-Propanol. A) methanol and ethanol, b) methanol and n-propanol, c) methanol and acetone, d) ethanol and n-propanol, e) ethanol and acetone, and f) n-propanol and acetone. The solid lines are the identity lines and the dotted lines are 0.02 M from the identity lines.

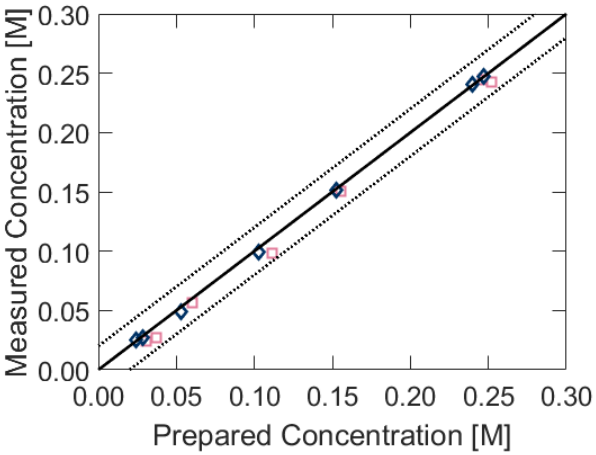

Figure 4.9. Methanol and acetate measured concentration vs. prepared concentration. The measured concentration was calculated from the measured absorbance and the calculated effective extinction coefficients. ◊ are the methanol experimental points and □ are the acetate experimental points for various mixtures. The solid line is the identity line and the dotted lines are ± 0.02 M corresponding to the maximum compound instrumental error for solution preparation and characterization.

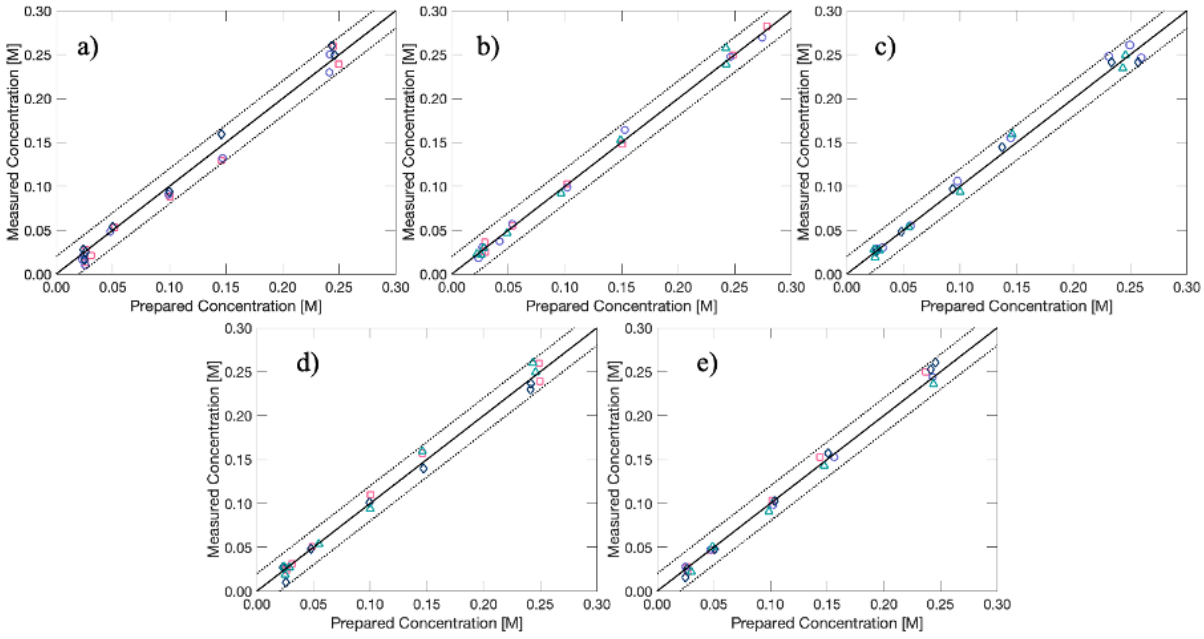

Figure 4.10. Measured solution concentration extracted from ATR FTIR spectra data plotted against prepared solution concentration for three-component solutions of a). acetone, ethanol and methanol b) acetone, ethanol and n-propanol c) acetone, methanol and n-propanol and d) ethanol, methanol and n-propanol., and e) four-component solution of acetone, ethanol, methanol, and n-propanol. □ Acetone, O Ethanol, ◊ Methanol, and Δ n-Propanol. The solid black line is y = x and the dotted lines are ± 0.02 M (instrumental error).

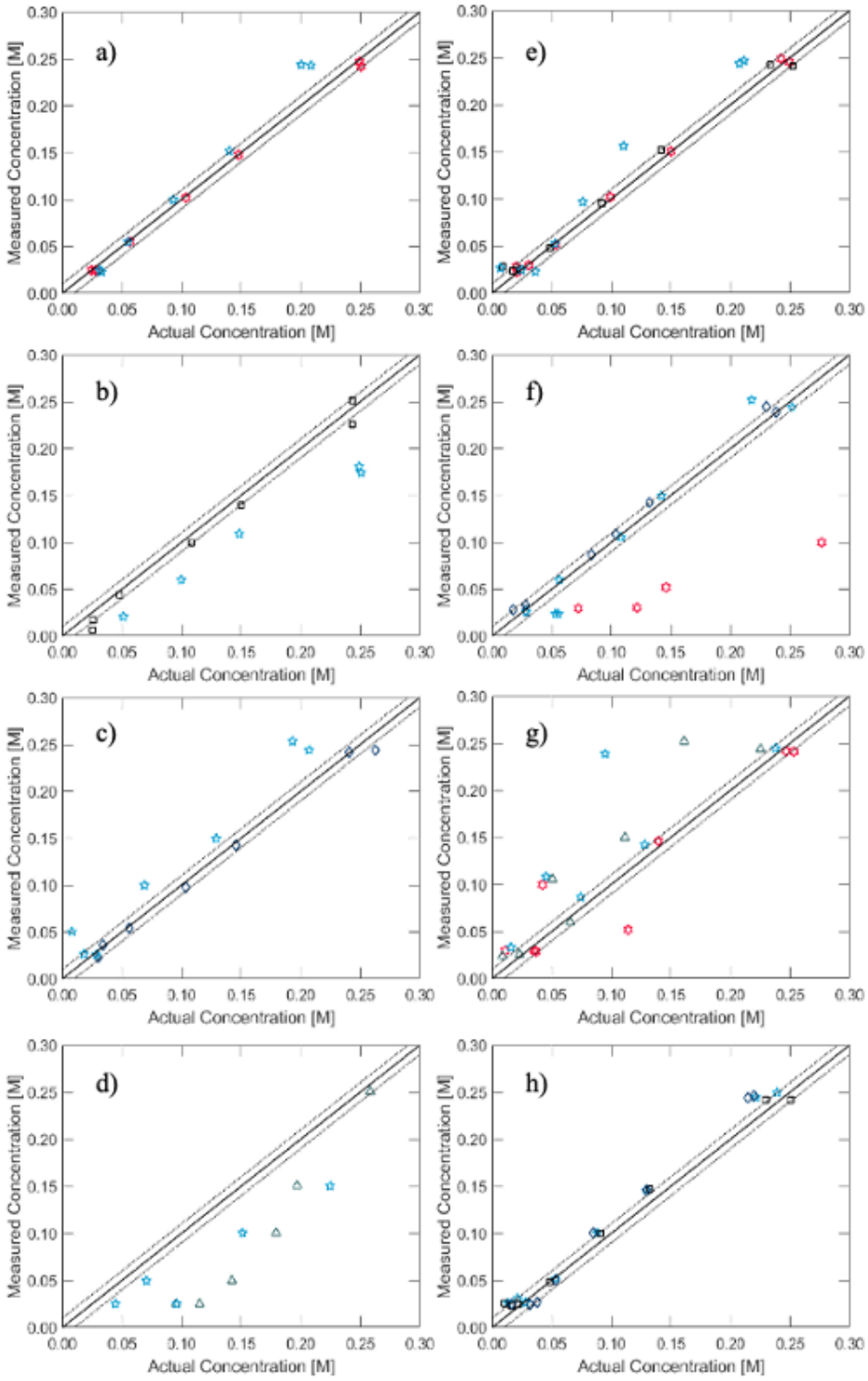

Figure 4.11. Two-component calibrations utilizing the effective extinction coefficients found, all with butanol. ✡Acetone, ☆butanol, □isopropanol, ◇methanol, and △n-propanol. a) acetone and butanol, b) butanol and isopropanol, c) butanol and methanol, d) butanol and n-propanol, e) acetone, butanol, and isopropanol, f) acetone, butanol, and methanol, g) acetone, butanol, and n-propanol, and h) butanol, isopropanol, and methanol.

4.6 Conclusions

This chapter detailed the underlying work necessary to validate the use of in situ ATR FTIR spectroscopy for monitoring receiver cell concentrations for multicomponent diffusion cell experiments. Experimental issues surrounding the water background and ambient temperature variation were identified and remedied via a reaction block and glass syringes. Effective extinction coefficients were determined for a series of alcohols from triplicate calibration experiments and the Beer-Lambert Law. These effective extinction coefficients were then used to assess solute concentrations from ATR FTIR absorbance spectra collected for a series of multicomponent solutions, and extracted solute concentrations were found to be within 0.02 M of the target prepared solute concentrations. Two-, three-, and four-component effective extinction coefficients are found to be constant and accurate in the concentration regime of interest and were found to be valid for multicomponent mixtures except for solute mixtures including butanol as a component. Overall, this validated the use of this methodology for the species investigated in the remainder of this dissertation: methanol, ethanol, n-propanol, acetone, and sodium acetate, and their complex mixtures.

4.7 References

1. Voegelin A, Vulava VM, Kuhnen F, Kretzschmar R. Multicomponent transport of major cations predicted from binary adsorption experiments. *J Contam Hydrol*. 2000;46(3):319-338. doi:10.1016/S0169-7722(00)00132-7
2. Ghoreyshi SAA, Farhadpour FA, Soltanieh M. Multicomponent transport across nonporous polymeric membranes. *Desalination*. 2002;144(1):93-101. doi:10.1016/S0011-9164(02)00295-3
3. Katz GE, Berkowitz B, Guadagnini A, Saaltink MW. Experimental and modeling investigation of multicomponent reactive transport in porous media. *J Contam Hydrol*. 2011;120-121:27-44. doi:10.1016/j.jconhyd.2009.11.002
4. Arnošt D, Schneider P. Dynamic transport of multicomponent mixtures of gases in porous solids. *Chem Eng J Biochem Eng J*. 1995;57(2):91-99. doi:10.1016/0923-0467(94)02900-8
5. Ern A, Giovangigli V. Fast and Accurate Multicomponent Transport Property Evaluation. *J Comput Phys*. 1995;120(1):105-116. doi:10.1006/jcph.1995.1151
6. Lee HC, Forte JG. A study of H+ transport in gastric microsomal vesicles using fluorescent probes. *Biochim Biophys Acta BBA - Biomembr*. 1978;508(2):339-356. doi:10.1016/0005-2736(78)90336-X
7. Wylie Nichols J, Hill MW, Bangham AD, Deamer DW. Measurement of net proton-hydroxyl permeability of large unilamellar liposomes with the fluorescent pH probe, 9-aminoacridine. *Biochim Biophys Acta BBA - Biomembr*. 1980;596(3):393-403. doi:10.1016/0005-2736(80)90126-1
8. Steudle E, Oren R, Schulze E-D. Water Transport in Maize Roots: Measurement of Hydraulic Conductivity, Solute Permeability, and of Reflection Coefficients of Excised Roots Using the Root Pressure Probe. *Plant Physiol*. 1987;84(4):1220-1232. doi:10.1104/pp.84.4.1220
9. Teraoka Y, Nobunaga T, Okamoto K, Miura N, Yamazoe N. Influence of constituent metal cations in substituted LaCoO3 on mixed conductivity and oxygen permeability. *Solid State Ion*. 1991;48(3):207-212. doi:10.1016/0167-2738(91)90034-9
10. Avellaneda M, Torquato S. Rigorous link between fluid permeability, electrical conductivity, and relaxation times for transport in porous media. *Phys Fluids Fluid Dyn*. 1991;3(11):2529-2540. doi:10.1063/1.858194
11. Paynter RW. Modification of the Beer–Lambert equation for application to concentration gradients. *Surf Interface Anal*. 1981;3(4):186-187. doi:10.1002/sia.740030410
12. Liebhafsky HA, Pfeiffer HG. Beer's law in analytical chemistry. *J Chem Educ*. 1953;30(9):450. doi:10.1021/ed030p450
13. Glaister P. Titration Curve Analysis: Some Observations. *J Chem Educ*. 1997;74(7):744. doi:10.1021/ed074p744.6
14. Beckingham BS, Lynd NA, Miller DJ. Monitoring multicomponent transport using in situ ATR FTIR spectroscopy. *J Membr Sci*. 2018;550:348-356. doi:10.1016/j.memsci.2017.12.072

15. Carter BM, Dobyns BM, Beckingham BS, Miller DJ. Multicomponent transport of alcohols in an anion exchange membrane measured by in-situ ATR FTIR spectroscopy. *Polymer*. 2017;123:144-152. doi:10.1016/j.polymer.2017.06.070
16. Godino MP, Barragán VM, Villaluenga JPG, Izquierdo-Gil MA, Ruiz-Bauzá C, Seoane B. Liquid transport through sulfonated cation-exchange membranes for different water–alcohol solutions. *Chem Eng J*. 2010;162(2):643-648. doi:10.1016/j.cej.2010.06.013

Chapter 5: Multicomponent transport of alcohols in Nafion™ 117 measured by in situ ATR FTIR spectroscopy

Reproduced in part from Multicomponent transport of alcohols in NafionTM 117 measured by in situ ATR FTIR spectroscopy with permission from Jung M. Kim, Jing Li, Zhihua Jiang, and Bryan S. Beckingham. Submitted to European Polymer Journal, In Review

5.1. Introduction

Synthetic polymeric membranes are of great interest in research and industry for a broad range of applications (biomedical applications, water purification, fuel cells, electrolyzers, etc.) due to their ability to selectively transport species with comparably low carbon footprint and energy requirements.[1] In energy production applications such as fuel cells and electrolyzers, polymer electrolyte membranes (PEMs) are used to transport ions between the two electrodes to maintain charge neutrality, while limiting the transport of oxidation and reduction products which may degrade the opposing electrolytic catalysts.[12–4] There has been extensive research on both cation (such as Nafion™ 117[5–12]) and anion (such as Selemion AMV[13–21]) exchange membranes as both of these commercially available membranes are used heavily in electrochemical systems including direct methanol fuel cells for Nafion™ and vanadium redox fuel cells for Selemion AMV. Artificial photosynthesis devices are one class of electrochemical cell which splits water into hydrogen and oxygen[22], and also converts carbon dioxide into high-end products such as alcohols.[23] The polyelectrolyte membrane (PEM) in these devices plays a critical role in allowing the transport of ions (protons or hydroxyls depending on the device architecture) while hindering the transport of the many products produced due to a lack of selectivity by the metallic catalysts. Thus, it is critical to understand the transport and co-transport behavior (permeability) of these membranes to solutes (such as the alcohols examined herein), which can impact device performance.

The permeability of a solute is dependent on its diffusion through and solubility within that polymer membrane, as can be seen from Equation 5.1, known as the solution-diffusion model[24]

$$P_i = D_i \cdot K_i \quad 5.1$$

where P_i is the permeability coefficient, D_i is the diffusivity coefficient, and K_i is the solubility coefficient. The solution-diffusion model is commonly used for dense polymeric films (such as Nafion™ and Selemion AMV) as it can be used to quantify a solute's sorption into, diffusion through, and desorption from the membrane. Recently, we have adopted an in situ attenuated total reflectance Fourier-transform infrared (ATR FTIR) spectroscopy technique to probe the permeability of polymer membranes to complex mixtures as it allows for facile determine of solution concentrations without the need for ex situ analyses[5,13,25,26] which require offline evaluation. This technique has distinct advantages over other in situ techniques such as pH[31,32] and conductivity[33,34] probes, which have been used to quantify permeability without the need for aliquotic sampling, as those techniques can only quantify the permeability of a single solute through overall changes in solution character. Using this methodology, the transport and co-transport behavior of the CO_2 reduction products methanol, acetate, and formate were investigated in the cation exchange membrane Nafion™ 117.[5] Interestingly, emergent transport behavior was observed where the permeability to acetate and formate generally increased in co-transport experiments while the permeability to methanol decreased.[5] These changes were found to be correlated with solute sorption, whereas diffusion coefficients were similar, suggesting modifications in solute solubility were driving the co-transport behavior. This type of co-transport behavior was also studied for the anion exchange membrane Selemion AMV for a different series of alcohol CO_2 reduction products, namely methanol, ethanol, and n-propanol.[13] In that case, a combination of changes in solubility and diffusivity across the binary pairs and ternary mixture

were found to impact the membrane permeability to each solute. For instance, permeability to methanol increased in co-permeation with ethanol and/or n-propanol, while permeability to n-propanol increased in co-permeation with methanol and/or ethanol. Such changes were found to be a consequence of both solubility and diffusivity changes through competitive sorption and flux coupling.[13,35]

Here, we employ in situ ATR FTIR spectroscopy to again monitor the permeation of a series of CO_2 reduction product alcohols; however, here we investigate transport behavior for the cation exchange membrane Nafion™ 117. Permeability experiments were conducted for unary, binary, ternary, and quaternary mixtures (15 total permeation feed solutions) using our custom-built diffusion cell apparatus outfitted with in situ ATR FTIR spectroscopy to monitor the temporal receiver cell solution concentrations of methanol, ethanol, n-propanol, and acetone. Solute sorption/desorption experiments are also performed to evaluate solute solubility for each of the 15 solute feed combinations and used to calculate solute diffusivities using the solution-diffusion model (Equation 5.1). The relative changes in alcohol permeability and permselectivity is discussed, as are the underlying changes in solubility and diffusivity across this broad array of solute combinations in transport and co-transport experiments.

5.2. Results and Discussion

5.2.1. Quantitative multicomponent aqueous solute concentrations using in situ ATR FTIR spectroscopy

To monitor receiver-cell solute concentrations for multicomponent transport experiments, we deploy in situ ATR FTIR spectroscopy and first validate our capability to do so quantitatively for

mixtures of our solutes of interest. The Beer-Lambert Law describes the absorption of light as it passes through an analyte. As described previously, due to pathlength equivalence at each wavenumber, we utilize an effective molar absorptivity, ε_λ, such that $A_\lambda = \varepsilon_\lambda C$, where A_λ is the absorbance at wavenumber λ and C is the solute concentration.[5,13] The concentration of a single solute can be determined from the ATR FTIR spectra's measured absorbance given these effective extinction coefficients are known. Spectra were obtained for methanol, ethanol, n-propanol, and acetone in 1.0 M aqueous solutions with the ATR FTIR spectrophotometer to assess spectral overlap and potential wavenumbers of interest. In each spectrum, the absorbance of pure DI water is subtracted, such that the spectra shown in Figure 5.1a correspond solely to the absorbance contributions from methanol, ethanol, n-propanol, and acetone, respectively. Each solute displays distinct absorption peaks at various wavenumbers due to their dissimilar dipole moments when absorbing IR radiation.[27]

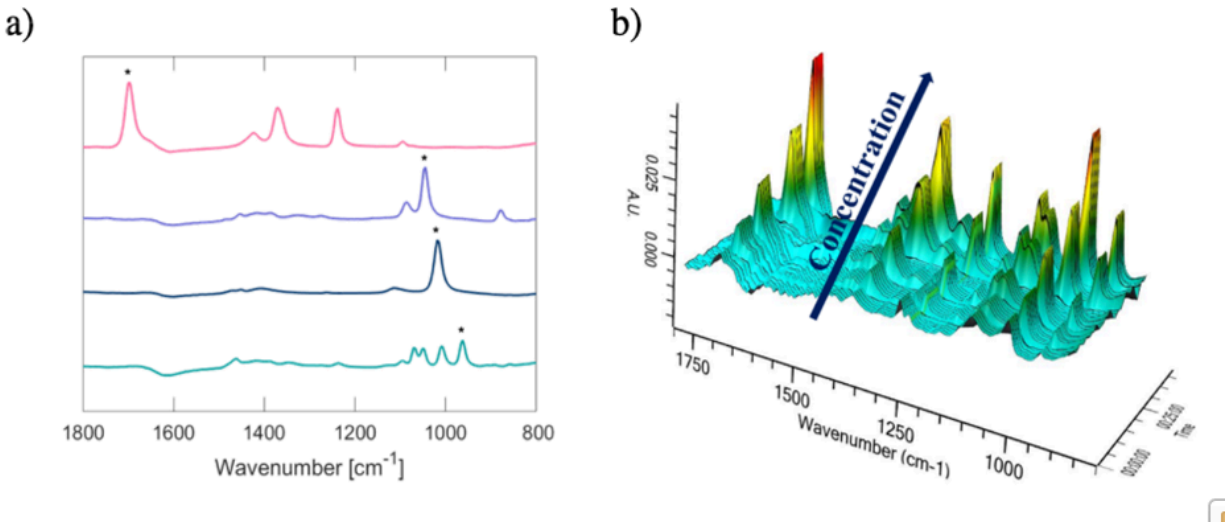

Figure 5.1. a) The absorption spectra of the solutes. These spectra were baselined at 1197 cm^{-1} and the water spectrum subtracted. — Acetone, — Ethanol, — Methanol, and — n-Propanol. The * indicates which wavenumbers were selected for each solute. B) Acetone, ethanol, methanol, and n-propanol calibration spectra of absorbance units (A.U.) versus wavenumber (cm^{-1}) and time.

To determine effective molar absorptivities of each solute, a series of standard aqueous solutions of methanol, ethanol, n-propanol, and acetone at known concentrations from 0.025 to 0.25 M were prepared and their ATR FTIR spectra acquired (Figure 5.1b for the four-component mixture). This concentration range was elected to be consistent with the concentration range of interest for subsequent diffusion-cell experiments and analysis via the Yasuda model.[28] The wavenumbers were selected, noted via asterisks in Figure 5.1a, to minimize overlap between solutes and maximize sensitivity to changes in concentration; i.e., more significant effective extinction coefficients are preferred as $\varepsilon_\lambda = dA/dC$. Each calibration was performed three separate times using newly prepared solutions. The effective molar absorptivity at each wavenumber of interest for each solute was determined from a linear least-squares regression fit of the acquired absorbances from all three calibration experiments (Figure 5.3). Overall, excellent linear fits to the acquired absorbance data and typical squared correlation coefficients (R^2) values greater than 0.98 were obtained (see Table 5.1).

For multicomponent solutions, the absorbance, A_i, at each wavenumber i is a summation of the absorbance contributions from each solute j:

$$A_i = \sum_{\substack{i=1 \\ j=1}}^{n} \varepsilon_{i,j} C_j \qquad 5.2$$

The concentration of n aqueous solutes using water-subtracted FTIR spectra can thereby be calculated using a system of n equations. For two solutes (A & B), Equation 5.2 can be written to describe the absorbance at two wavenumbers (A_1 & A_2) for two unknown concentrations (C_A and C_B).

$$A_1 = \varepsilon_{A1} C_A + \varepsilon_{B1} C_B \qquad 5.3$$

$$A_2 = \varepsilon_{A2} C_A + \varepsilon_{B2} C_B \qquad 5.4$$

These equations can be solved simultaneously through rearrangement and substitution, as shown in Equations 5.5 and 5.6, where C_B can first be obtained directly from the absorbance data (Equation 5.6), followed by C_A (Equation 5.5).

$$C_A = \frac{A_1 - \varepsilon_{B1} C_B}{\varepsilon_{A1}} \quad 5.5$$

$$C_B = \frac{\varepsilon_{A1} A_2 - \varepsilon_{A2} A_1}{\varepsilon_{A1} \varepsilon_{B2} - \varepsilon_{A2} \varepsilon_{B1}} \quad 5.6$$

Equation 5.2 can also be expanded for three solutes (A, B and C) utilizing the absorbances at three wavenumbers (A_1, A_2, and A_3) to calculate three unknown concentrations (C_A, C_B, and C_C) (Equations 5.7-5.9)

$$A_1 = \varepsilon_{A1} C_A + \varepsilon_{B1} C_B + \varepsilon_{C1} C_C \quad 5.7$$

$$A_2 = \varepsilon_{A2} C_A + \varepsilon_{B2} C_B + \varepsilon_{C2} C_C \quad 5.8$$

$$A_3 = \varepsilon_{A3} C_A + \varepsilon_{B3} C_B + \varepsilon_{C3} C_C \quad 5.9$$

Similarly, this expansion for four solutes using the absorbances at four distinct wavenumbers is used to determine the four unknown concentrations (Equations 5.10-5.13).

$$A_1 = \varepsilon_{A1} C_A + \varepsilon_{B1} C_B + \varepsilon_{C1} C_C + \varepsilon_{D1} C_D \quad 5.10$$

$$A_2 = \varepsilon_{A2} C_A + \varepsilon_{B2} C_B + \varepsilon_{C2} C_C + \varepsilon_{D2} C_D \quad 5.11$$

$$A_3 = \varepsilon_{A3} C_A + \varepsilon_{B3} C_B + \varepsilon_{C3} C_C + \varepsilon_{D3} C_D \quad 5.12$$

$$A_4 = \varepsilon_{A4} C_A + \varepsilon_{B4} C_B + \varepsilon_{C4} C_C + \varepsilon_{D4} C_D \quad 5.13$$

Table 5.1: Effective molar absorptivities and their correlation coefficients

	$\lambda = 1018\ cm^{-1}$		$\lambda = 1044\ cm^{-1}$		$\lambda = 962\ cm^{-1}$		$\lambda = 1700\ cm^{-1}$	
	ε	**R^2**	**ε**	**R^2**	**ε**	**R^2**	**ε**	**R^2**
Methanol	0.1515	0.9952	-0.0128	0.9930	-0.0002	0.0345	0.0025	0.2435
Ethanol	-0.0205	0.9448	0.1310	0.9990	-0.0124	0.9966	0.0038	-0.3970
n-Propanol	0.0173	0.1720	0.0236	0.9865	0.0370	0.9956	-0.0005	0.0245
Acetone	-0.0008	-2.0000	-0.0014	0.0670	0.0007	0.2346	0.2064	0.9963

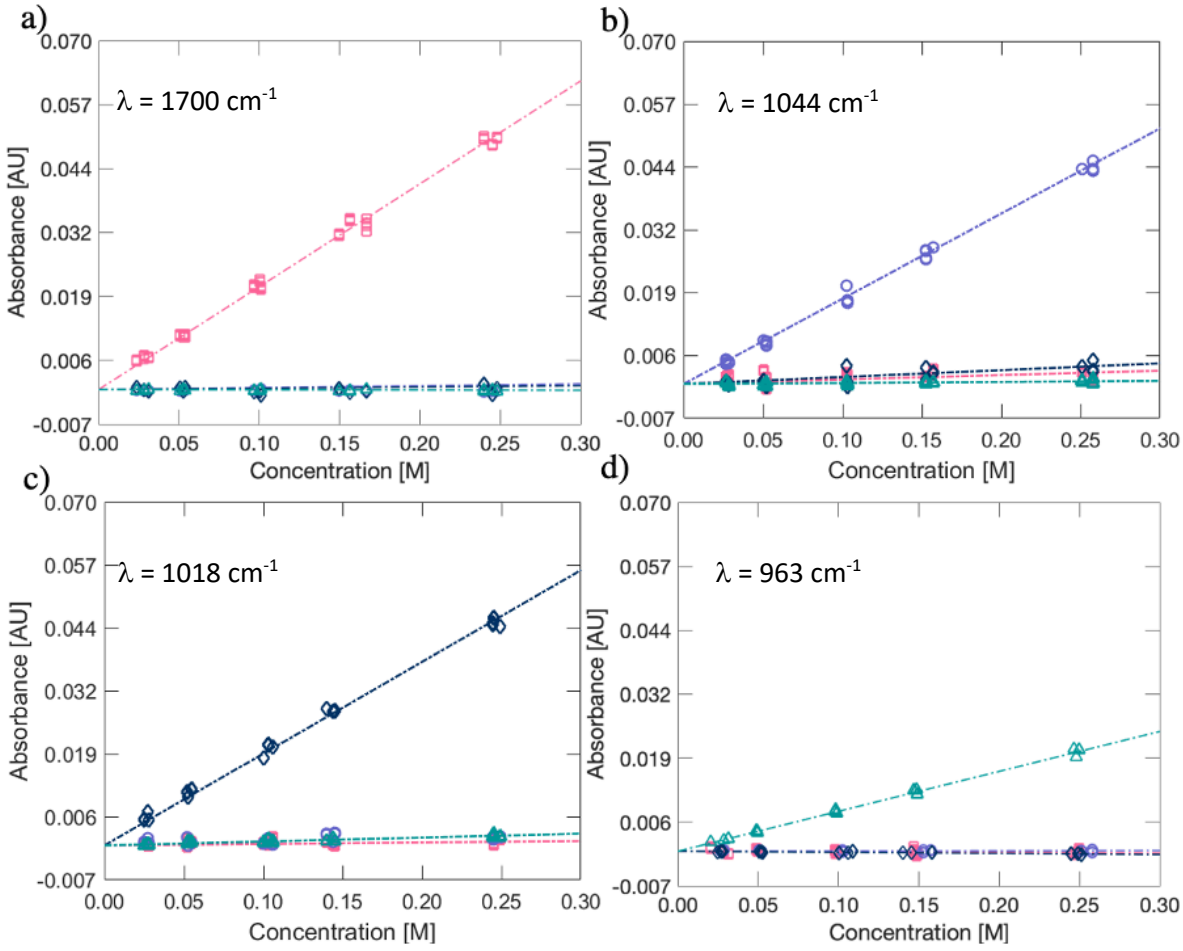

Figure 5.2. Absorbance vs. concentration graphs of calibration solutions at a) 1700 cm^{-1}, b) 1044 cm^{-1}, c) 1018 cm^{-1}, and d) 1070 cm^{-1}. □ Acetone, O Ethanol, ◊ Methanol, and Δ n-Propanol. The points are experimental data and the dotted lines are the Beer's Law fits utilizing the determined effective extinction coefficients.

To validate this methodology for determining the concentrations of the multiple solutes of interest, a series of two-component solutions were prepared with solute concentrations of 0.025 M, 0.05 M, 0.10 M, 0.15 M, and 0.25 M. Each set of experiments contained five equal solute concentrations and two opposing concentrations (0.025 M of solute A and 0.25 M of solute B and vice versa) to ensure that the equations and effective molar absorptivities held, even if there was overlap or differing solute concentrations. Each of the solute concentrations was determined from the solution absorbance, the above described effective extinction coefficients, and the systems of concentration equations. Figure 4.10 shows a comparison between the measured and actual concentrations of each solute for the three solute combinations (Figure 4.10a-d) and the four solute (methanol, ethanol, n-propanol, and acetone) mixture (Figure 4.10e). Analogous plots for each of the binary component mixtures are shown in Figure 4.8. The identity line (y = x) is provided as a guide as this corresponds to complete agreement between the actual and measured solution concentrations. As is clear from Figures 4.8 and 4.10, the concentrations calculated from the infrared absorbances and effective molar absorptivities are very close to the identity line, with nearly all lying within 0.02 M, signifying excellent agreement. Comparable results have been previously reported for methanol, ethanol, propanol, and their binary and ternary mixtures.[13] The results here confirm these prior results and expand upon these validations to additional binary, ternary, and even quaternary. Overall, we find this facile technique can be used to determine unknown concentrations of these four solutes in their various complex mixtures, and as demonstrated in the following sections, the in situ monitoring of solute concentrations in these complex mixtures.

5.2.2. Permeability of Nafion™ 117 to methanol, ethanol, n-propanol, and acetone

Nafion™ 117 is a dense, non-porous membrane, and the solution-diffusion model describes its permeability to solutes.[24] Permeation of a solute from the donor chamber, through a dense and hydrated polymer membrane, to the receiver chamber is a consequence of the chemical potential difference. Permeability of the membrane to the solute is extracted from measuring the time-resolved receiver cell concentration. Utilizing our custom-built diffusion cell with in situ ATR FTIR spectroscopy, the permeabilities of Nafion™ 117 to methanol, ethanol, n-propanol, and acetone in one, two, three and four-component mixtures were determined using the Yasuda model to extract permeability from concentration versus time data for hydrated polymeric membranes.[28] The Yasuda model (Equation 5.14) describes the transport of ions and small molecules through hydrated, dense polymeric membranes[28,29] to calculate the diffusive permeability of the solute i, P_i,

$$ln\left(1-\frac{2C_{i_t}}{C_{i_0}}\right)=P_i\left(-\frac{2At}{V\ell}\right) \tag{5.14}$$

where C_{it} is calculated from the measured absorbance in the receiver cell with in situ ATR FTIR spectroscopy, C_{i0} is the initial feed concentration of solute i in the donor cell (1.0 M), and the membrane thickness, l, is measured using a digital caliper (± 1 μm) after the permeation experiment to account for osmotic de-swelling[5,30] effects. This model is commonly used for measuring permeability in hydrated, dense, polymer membranes such as hydrogels, dialysis membranes, and ion exchange membranes such as Nafion™ 117 and Selemion AMV.[5,13,29,30,36] The diffusion cells were jacketed at 25 °C, well mixed with magnetic stir bars, and covered with parafilm to diminish evaporation effects. Each permeability experiment was performed in triplicate. The 3D ATR FTIR spectra and extracted concentration versus time data for the single component permeability of

Nafion™ 117 to methanol are shown in Figure 5.4. In Figure 5.4, data from each of the three permeation experiments is fitted to the Yasuda model (dotted lines), and those permeabilities are used to calculate an average extracted permeability using the Yasuda model (solid line), shown in Figure 5.3. This average permeability is obtained from each set of diffusion cell experiments for each solute and is the value used for calculations and comparisons herein. Analogous single component concentration versus time plots for all other solutes are provided in Figure 5.3, and the permeabilities of Nafion™ 117 to each species are given in Table 5.2.

The permeability to methanol is within the reported literature range[5,37–43], as a validating check that this technique is adequate for quantifying membrane permeability. Compared to methanol, the permeabilities to ethanol and n-propanol decrease 12 % and 19 % respectively, consistent with their larger molecular size; kinetic diameters for methanol, ethanol, and n-propanol are 0.38 nm, 0.43 nm, and 0.47 nm, respectively.[44] In that respect, acetone is an outlier as it is a large solute (kinetic diameter of 0.47 nm[44]), yet displays the highest permeability. Acetone enolizes in water, resulting in a more positive hydroxyl carbon and behaving as a diol in these solutions.[45] Acetone's behavior here is anticipated as it has previously been found to exhibit a higher diffusivity in polymer thin films than both methanol and ethanol[46], and is known for exhibiting a similarly higher permeability[47] in polymer membranes attributed to a combination of lower solute viscosity and differences in swelling behavior.[48]

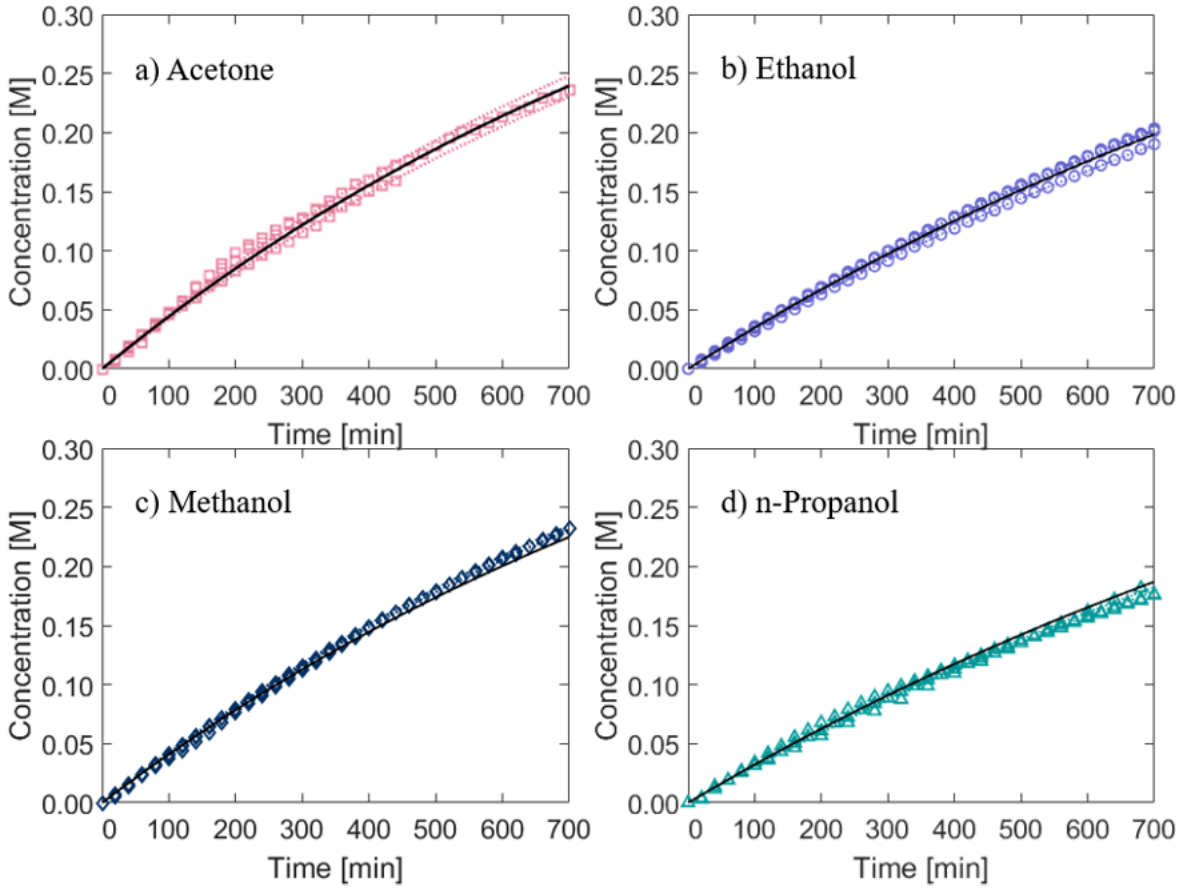

Figure 5.3. Single component permeability plots as concentration in molarity versus time in minutes. a) □ Acetone, b) O Ethanol, c) ◊ Methanol, and d) Δ n-Propanol. Dotted colored lines are the individual Yasuda model permeability fits to each particular experiment, and the solid black lines are the averaged Yasuda model permeability fits.

Table 5.2. Apparent diffusive permeabilities of methanol, ethanol, n-propanol, and acetone in Nafion™ 117. Uncertainties, where given, are standard deviations on triplicate replicate measurements.

	P_i [=] cm^2/s *10^6
Methanol	3.09 ± 0.1
Ethanol	2.71 ± 0.2
n-Propanol	2.51 ± 0.1
Acetone	3.54 ± 0.3

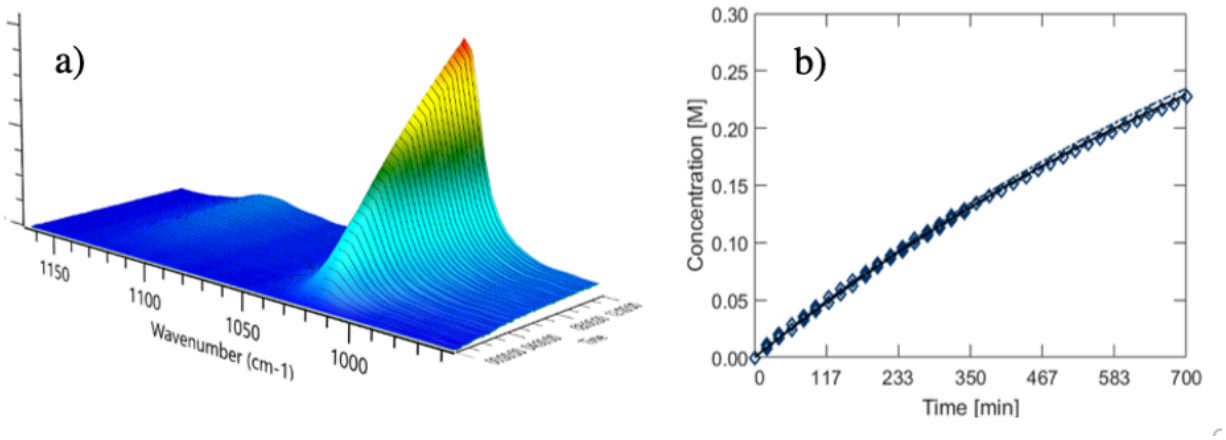

Figure 5.4. Methanol permeability through Nafion™ 117. a) Methanol 3D plot from ic IR 7.0 software of A.U. vs. wavenumber vs. time and b) Methanol molar concentration vs. time in minutes

5.2.3 Multicomponent permeability of Nafion™ 117 to methanol, ethanol, n-propanol, and acetone

Multicomponent permeability experiments were performed to calculate true selectivity for all six binary pairs, all four three-component sets, and the complex mixture of all four solutes investigated herein. These experiments thereby incorporate any solute-solute interactions or multiple solute-membrane interactions that impact transport behavior in these more complex mixtures. To begin, a representative concentration versus time plot for all six of the binary pairs of solutes is shown in Figure 5.5; see Figure 5.6a-f for smaller, analogous plots for other multicomponent experiments. The concentration versus time data for each solute in each experiment was fitted using the Yasuda model to extract the permeability for each solute in each case (Table 5.3). From a cursory glance at Table 5.3, it is clear that the multicomponent permeabilities for some solutes in mixtures deviate from their single solute permeability, while others do not. As multiple solutes transport through the same membrane fractional free volume, an overall decrease in permeability of individual solutes could be expected. However, the two-component permeabilities increased in 21 % of the

cases when compared to the single component permeabilities. Permeability to methanol was found to increase in binary permeation experiments with all three co-solutes. In a binary mixture with ethanol, the methanol permeability increases but is within the standard deviation of the data. Meanwhile, the largest and most significant increase (17 %) is observed for co-permeation with acetone. Alternatively, the permeability to n-propanol both increased and decreased depending on the co-solute in the binary mixture. For instance, the permeability to n-propanol decreased 25 % in co-permeation with ethanol, while in co-permeation with acetone, it increased 5 %. Similar behavior is observed for ethanol, where the permeability to ethanol rose 20 % in co-permeation with n-propanol and decreased 6 % in co-permeation with acetone. As the permeability for methanol, ethanol, and n-propanol in Nafion™ 117 is an order of magnitude higher than that measured for their transport in Selemion AMV, we make no attempt at a direct comparison of their transport and co-transport behavior here other to note this difference, and that it is a consequence of both higher solubility and diffusivity for these solutes (as described below[13]).

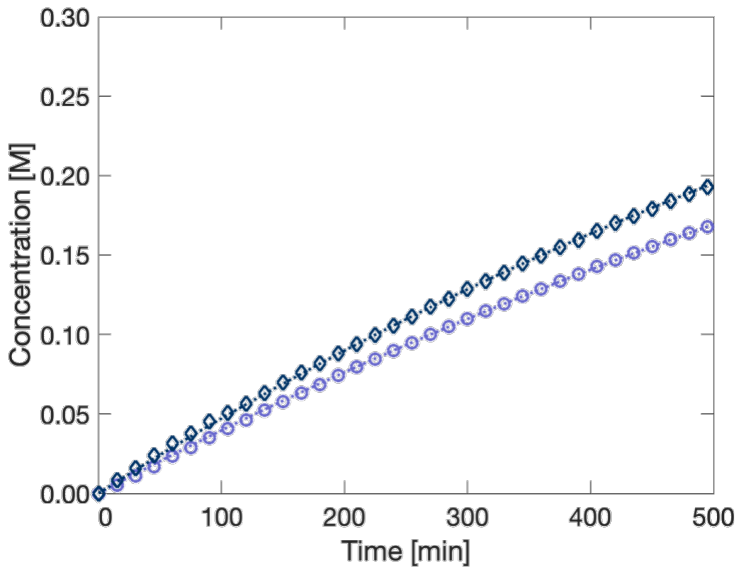

Figure 5.5. Methanol and ethanol concentration versus time plot depicting multicomponent permeability through Nafion™ 117. ◊ Methanol and O Ethanol.

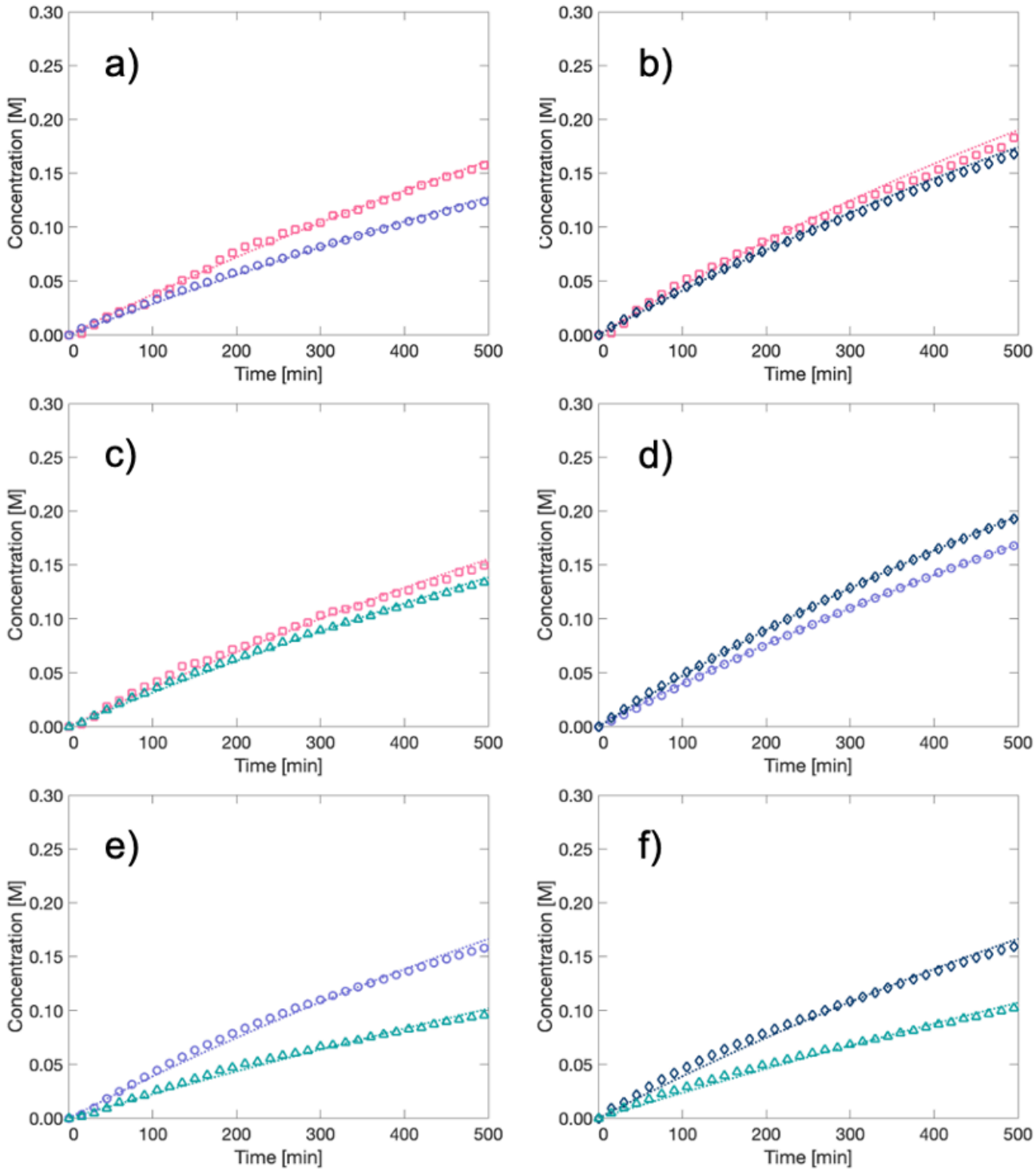

Figure 5.6. Double component concentration versus time plots depicting multicomponent permeability through Nafion^{TM} 117. □□Acetone, O Ethanol, ◊ Methanol, and Δ n-Propanol. a) acetone and ethanol, b) acetone and methanol, c) acetone and n-propanol, d) ethanol and methanol, e) ethanol and n-propanol, and f) methanol and n-propanol.

Table 5.3. Apparent diffusive permeabilities of methanol, ethanol, n-propanol, acetone, and mixtures thereof in Nafion™ 117. Uncertainties, where given, are standard deviations on triplicate replicate measurements.

Apparent solute diffusive permeabilities ($cm^2/s * 10^6$) in Nafion™ 117				
	Methanol	**Ethanol**	**n-Propanol**	**Acetone**
Single solute	3.09 ± 0.1	2.71 ± 0.2	2.51 ± 0.1	3.54 ± 0.3
Two-Component Mixture with Methanol	-	2.71 ± 0.2	2.18 ± 0.04	3.55 ± 0.2
Two-Component Mixture with Ethanol	3.20 ± 0.3	-	1.88 ± 0.05	3.34 ± 0.2
Two-Component Mixture with Propanol	3.63 ± 0.3	3.25 ± 0.05	-	3.09 ± 0.1
Two-Component Mixture with Acetone	3.38 ± 0.2	2.55 ± 0.2	2.63 ± 0.1	-
Three-Component Mixture of Methanol, Ethanol, and Propanol	2.75 ± 0.2	2.22 ± 0.08	1.02 ± 0.08	-
Three-Component Mixture of Methanol, Ethanol, and Acetone	2.65 ± 0.1	2.28 ± 0.1	-	3.29 ± 0.3
Three-Component Mixture of Methanol, Propanol, and Acetone	2.78 ± 0.1	-	1.90 ± 0.1	3.41 ± 0.3
Three-Component Mixture of Ethanol, Propanol, and Acetone	-	2.71 ± 0.1	1.74 ± 0.05	3.23 ± 0.2
Four-Component Mixture	2.82 ± 0.1	2.90 ± 0.1	2.49 ± 0.2	3.55 ± 0.3

Table 5.4. Ideal and true selectivity and the percent change between these values.

	Ideal	**True**	**% Dif.**
Methanol/Ethanol	1.14	1.18	4
Methanol/n-Propanol	1.23	1.67	35
Methanol/Acetone	0.87	0.95	9
Ethanol/n-Propanol	1.08	1.73	60
Ethanol/Acetone	0.77	0.76	0
n-Propanol/Acetone	0.71	0.85	20

These changes in solute permeability can also be assessed through the lens of permselectivity to examine changes in relative permeability, and how these permeability changes would impact membrane separations. Membrane selectivity ($\alpha_{i/j}$), calculated using Equation 5.15, quantifies a membrane's preference for transporting one molecule compared to another based upon their relative permeability values (P_i and P_j for components i and j, respectively).

$$\alpha_{i/j} = \frac{P_i}{P_j} \tag{5.15}$$

Here, selectivity is calculated using the traditional single-solute diffusion cell experiment permeabilities and denoted as the 'ideal' selectivity. As this ideal selectivity is based on the single-solute permeability values, it does not consider the specific interactions between solutes and the membrane, which may impact solute transport behavior. The selectivity from the binary pair diffusion cell experiments is also calculated and denoted as the 'true' selectivity. Obtained values for both ideal and true selectivities for each binary pair of solutes are shown in Table 5.4. For consistency, the order of preference for the numerator permeability in calculating the permeability was methanol, ethanol, n-propanol, acetone, which results in selectivity values less than one in some cases.

The 'ideal' selectivity is the traditional selectivity determined from diffusion cell experiments and generally used for membrane selection. As shown in Table 5.4, significant differences are observed between these two selectivity values, illustrating the importance of investigating multicomponent transport behavior to account for the complex array of solute-solute and multiple solute-membranes interactions that can occur. For instance, for ethanol and n-propanol, the true selectivity was 60 % greater than the ideal selectivity due to an increasing ethanol permeability in the presence of n-propanol, and a decreasing n-propanol permeability in the presence of ethanol.

Alternatively, for methanol and acetone, the permeability to acetone is unchanged, and permeability to methanol increases in the binary case resulting in a higher selectivity for methanol. Overall, these differences between ideal and true selectivity values ranged from insignificant (e.g., for ethanol and acetone) to quite large (60 % for ethanol and n-propanol) depending upon the solute pair. These types of effects have been previously attributed to complementary and competitive sorption within the membrane[49–51] as well as coupled fluxes.[52,53]

Next, we consider the permeability values for the three- and four-component diffusion cell experiments. As with the binary pairs, evaluation of the changes in permeability for three and four solute mixtures also displays complex behavior depending on the solutes. In the three solute permeabilities, decreased permeability is observed for methanol and n-propanol in all cases compared to both the single-solute and binary pair permeabilities. Alternatively, the permeability to acetone is slightly decreased but within the standard deviation of its single solute permeability. Meanwhile, the change in permeability to ethanol in two three-component mixtures with methanol, namely methanol-ethanol-n-propanol and methanol-ethanol-acetone, exhibit lower ethanol permeabilities. In contrast, permeability to ethanol, n-propanol, and acetone is unchanged compared to the single solute permeabilities. In the four-component mixture, permeabilities to n-propanol and acetone were close to those from single solute experiments, while permeabilities to methanol and ethanol increased. This last mixture is quite interesting as one expects the permeability to generally decrease with these additional solutes co-permeating and thereby occupying the limited membrane fractional free volume. As Nafion^{TM} 117 is not a crosslinked membrane, the presence of different solutes can influence the size and arrangement of both hydrophobic regions and ionic clusters and lead to differences in solute uptake, diffusivity and

ultimately permeability. Overall, the variation in permeability in direction and magnitude for different co-solute mixtures highlights the complexity in predicting multi-solute transport behavior from single-solute permeability experiments.

5.2.4. Solubility and Diffusivity of methanol, ethanol, n-propanol, and acetone in Nafion™ 117

The well-known solution diffusion model (Equation 5.1) describes the permeability of a membrane to a solute as the product of the thermodynamic solubility and the kinetic diffusivity.[5,43,54,55] The solubility of a membrane to a solute describes the thermodynamic partitioning, or the membrane's affinity, of a solute to the membrane, and the diffusivity describes the solute movement through the polymer membrane. Characterization of these quantities can thereby provide insight into the essential properties that govern the observed permeabilities. The solubilities of methanol, ethanol, n-propanol, acetone, and their binary mixtures in Nafion™ 117 are shown in Table 5.5. First, we examine the solubilities from single-component solutions. A range of values from 0.4 – 1.0 have been reported for the solubility of methanol in Nafion™ 117 with measurements from a variety of techniques and different membrane pretreatments.[5,7,56] The solubility found here is in the middle of this reported range. Interestingly, the solubility to ethanol and n-propanol are increasingly greater than that of methanol in contrast to the observed decreasing solute permeabilities for these larger solutes. This is a confirmation of our description above from the solute permeabilities that the solute size is the primary contributor to the observed differences in permeability. The solubility to acetone again does not follow this trend as its solubility falls between that of methanol and ethanol, indicating a higher membrane affinity to acetone than methanol. However, this higher solubility alone would not account for acetone exhibiting the highest permeability.

The solubilities extracted from binary solution sorption measurements are more complex and are found to increase, decrease, or remain unchanged depending on the co-solute. The solubility of methanol increases significantly (86 %) in the presence of ethanol but decreases with n-propanol (9 %) or acetone (35 %) as the co-solute. The solubility of ethanol increases with methanol as the co-solute (20 %) yet is essentially unchanged with either n-propanol or acetone as the co-solute. For methanol, ethanol, and n-propanol, the solubility increases in the binary mixture case if the co-solute is methanol or ethanol, and decreases or remains unchanged if the co-solute is n-propanol or acetone. Acetone, again, is an outlier in this respect as, while its solubility does decrease with n-propanol as the co-solute, its solubility decreases with methanol and remains unchanged with ethanol as the co-solute.

Relating these changes in solute solubility to the observed changes in solute permeability also does not follow a single trend (e.g., decreasing solubility and decreasing permeability are not universally linked across the binary pairs). For instance, while the permeability and solubility to methanol both increase with ethanol as the co-solute, the permeability to methanol increases, and the solubility decreases with acetone as the co-solute. Interestingly, for n-propanol, the changes in permeability and solubility are inversely correlated. The permeability to n-propanol decreases and the solubility increases with methanol and ethanol as the co-solutes. In contrast, the permeability increases and solubility decreases with acetone as the co-solute.

Table 5.5. Solubilities of methanol, ethanol, n-propanol, acetone, and mixtures thereof in Nafion™ 117. Uncertainties, where given, are standard deviations on triplicate replicate measurements.

Solute solubilities in Nafion™ 117				
	Methanol	**Ethanol**	**n-Propanol**	**Acetone**
Single-solute	0.80 ± 0.05	1.22 ± 0.04	2.06 ± 0.3	1.11 ± 0.2
Two-Component Mixture with Methanol	-	1.46	2.80	0.94
Two-Component Mixture with Ethanol	1.49	-	2.62	1.11
Two-Component Mixture with n-Propanol	0.73	1.21	-	0.64
Two-Component Mixture with Acetone	0.52	1.18	1.64	-

Table 5.6. Diffusivities of methanol, ethanol, n-propanol, acetone, and mixtures thereof in Nafion™ 117 where uncertainties are standard deviations.

Solute diffusivities ($cm^2/s * 10^6$) in Nafion™ 117				
	Methanol	**Ethanol**	**n-Propanol**	**Acetone**
Single-solute	3.86 ± 0.08	2.22 ± 0.10	1.22 ± 0.20	3.19 ± 0.2
Two-Component Mixture with Methanol	-	1.86 ± 0.2	0.78 ± 0.04	3.78 ± 0.2
Two-Component Mixture with Ethanol	2.15 ± 0.3	-	0.72 ± 0.05	3.01 ± 0.2
Two-Component Mixture with n-Propanol	4.97 ± 0.3	2.69 ± 0.05	-	4.83 ± 0.1
Two-Component Mixture with Acetone	6.50 ± 0.2	2.16 ± 0.2	1.60 ± 0.1	-

The solute diffusivities, shown in Table 5.6, are calculated from the measured permeability and solubility for each solute using the solution-diffusion model (Equation 5.1). Changes in solute diffusivity are thereby also dependent on co-solute(s) and are directly linked (inversely) to the relative changes in solubility, discussed above. Each solute's diffusivity increases from single to multicomponent experiments when co-transporting with n-propanol, and nearly all increase when co-transporting with acetone (either increased or relatively unchanged). For co-transporting with methanol, both ethanol and n-propanol diffusivities decrease while acetone increases. Meanwhile, the diffusivity of each solute co-transporting with ethanol decreases from single to multicomponent experiments. Again, these diffusivity changes do not directly correlate to changes in solute permeability, just as the solute solubilities do not correlate. In other words, the transport of these four charge-neutral solutes through charged Nafion is driven by changes in both solubility and diffusivity.

A final lens through which to view these changes is through changes in the solubility-selectivity and diffusivity-selectivity (ratios of solubility and diffusivity, selectively). This analysis gives an excellent visual representation of how the relative differences in permeability, solubility, and diffusivity between the single and binary component experiments are impacting transport behavior. Solubility selectivity and diffusivity selectivity are calculated for each binary pair using the single component data (ideal selectivity, solid bars) and binary data (true selectivity, outlined bars) and presented in Figure 5.7. For instance, binary pairs with the most significant differences in permselectivity—methanol/n-propanol and ethanol/n-propanol)—both show substantial differences in diffusivity selectivity. In the case of ethanol and acetone, all three of the selectivities (permselectivity, solubility-selectivity, and diffusivity-selectivity) are essentially unchanged.

Alternatively, for methanol and ethanol, the essentially constant permselectivity due to an increasing solubility-selectivity and decreasing diffusivity-selectivity offsetting one another. Meanwhile, for n-propanol and acetone, a 20 % increase in permselectivity is observed, which results in a significant increase in solubility-selectivity (38 %) and a smaller decrease in diffusivity-selectivity (13 %).

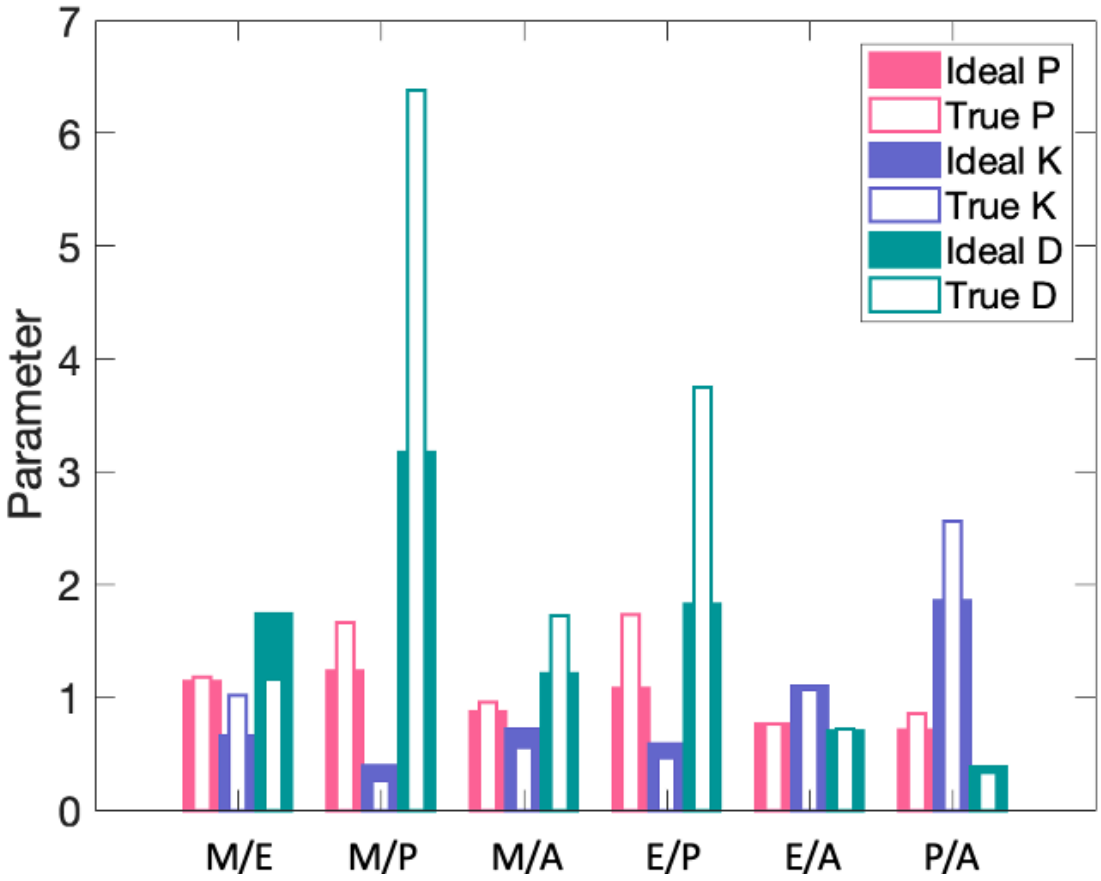

Figure 5.7. Permeability selectivity, solubility selectivity, and diffusivity selectivity for ideal (one component) and true (two-component) ratios.

5.3. Conclusions

An in situ ATR FTIR spectrometer probe was used to accurately characterize multiple components in solution, following calibrations for each solute at each wavenumber of interest. Exploiting the measured effective extinction coefficients, the permeabilities to methanol, ethanol, n-propanol, and acetone were determined in single, double, triple, and quadruple component experiments. The observed changes in permeability are complex and, in some cases, significant. This was exemplified by comparison of 'ideal' and 'true' permselectivity determined from single solute and two-solute diffusion cell experiments, respectively, and were found to vary by as much as 60 % (for ethanol/n-propanol). The cause of these changes was probed using a well-known sorption-desorption technique to measure membrane solubility for each solute. Changes in solute solubility and diffusivity are inversely correlated (as expected) through the solution-diffusion model, and changes in solubility and diffusivity were found to impact the observed permeability. Understanding the transport behavior for solutes in complex mixtures is a challenge, requiring significantly more experimentation to elucidate governing trends in behavior based on solute and membrane characteristics. For the series of solutes here, changes in their permeation behavior in Nafion^{TM} 117 are a result of changes in solubility and diffusivity and can have a tremendous impact on the resulting permselectivity.

5.4. References

1. Baker RW. *Membrane Technology and Applications*. John Wiley & Sons, Ltd; 2012. doi:10.1002/9781118359686

2. Baschuk JJ, Li X. Modeling of ion and water transport in the polymer electrolyte membrane of PEM fuel cells. *Int J Hydrog Energy*. 2010;35(10):5095-5103. doi:10.1016/j.ijhydene.2009.10.032

3. Bi W, Fuller TF. Modeling of PEM fuel cell Pt/C catalyst degradation. *J Power Sources*. 2008;178(1):188-196. doi:10.1016/j.jpowsour.2007.12.007

4. Bi W, Gray GE, Fuller TF. PEM Fuel Cell Pt/C Dissolution and Deposition in Nafion Electrolyte. *Electrochem Solid-State Lett*. 2007;10(5):101-104. doi:10.1149/1.2712796

5. Beckingham BS, Lynd NA, Miller DJ. Monitoring multicomponent transport using in situ ATR FTIR spectroscopy. *J Membr Sci*. 2018;550:348-356. doi:10.1016/j.memsci.2017.12.072

6. Chiou JS, Paul DR. Gas permeation in a dry Nafion membrane. *Ind Eng Chem Res*. 1988;27(11):2161-2164. doi:10.1021/ie00083a034

7. Hallinan DT, Elabd YA. Diffusion and Sorption of Methanol and Water in Nafion Using Time-Resolved Fourier Transform Infrared−Attenuated Total Reflectance Spectroscopy. *J Phys Chem B*. 2007;111(46):13221-13230. doi:10.1021/jp075178n

8. Hobson LJ, Ozu H, Yamaguchi M, Hayase S. Modified Nafion 117 as an Improved Polymer Electrolyte Membrane for Direct Methanol Fuel Cells. *J Electrochem Soc*. 2001;148(10):A1185-A1190. doi:10.1149/1.1402980

9. Liang Z, Chen W, Liu J, et al. FT-IR study of the microstructure of Nafion® membrane. *J Membr Sci*. 2004;233(1):39-44. doi:10.1016/j.memsci.2003.12.008

10. Mauritz KA, Moore RB. State of Understanding of Nafion. *Chem Rev*. 2004;104(10):4535-4586. doi:10.1021/cr0207123

11. Rivin D, Kendrick CE, Gibson PW, Schneider NS. Solubility and transport behavior of water and alcohols in Nafion™. *Polymer*. 2001;42(2):623-635. doi:10.1016/S0032-3861(00)00350-5

12. Tang H, Peikang S, Jiang SP, Wang F, Pan M. A degradation study of Nafion proton exchange membrane of PEM fuel cells. *J Power Sources*. 2007;170(1):85-92. doi:10.1016/j.jpowsour.2007.03.061

13. Carter BM, Dobyns BM, Beckingham BS, Miller DJ. Multicomponent transport of alcohols in an anion exchange membrane measured by in-situ ATR FTIR spectroscopy. *Polymer*. 2017;123:144-152. doi:10.1016/j.polymer.2017.06.070

14. Giffin GA, Lavina S, Pace G, Di Noto V. Interplay between the Structure and Relaxations in Selemion AMV Hydroxide Conducting Membranes for AEMFC Applications. *J Phys Chem C*. 2012;116(45):23965-23973. doi:10.1021/jp3094879

15. Le XT. Contribution to the study of properties of Selemion AMV anion exchange membranes in acidic media. *Electrochimica Acta*. 2013;108:232-240. doi:10.1016/j.electacta.2013.07.011

16. Mohammadi T, Kazacos MS. Evaluation of the chemical stability of some membranes in vanadium solution. *J Appl Electrochem*. 1997;27(2):153-160. doi:10.1023/A:1018495722379

17. Le XT, Bui TH, Viel P, Berthelot T, Palacin S. On the structure–properties relationship of the AMV anion exchange membrane. *J Membr Sci*. 2009;340(1):133-140. doi:10.1016/j.memsci.2009.05.025

18. Kim S, Tighe TB, Schwenzer B, et al. Chemical and mechanical degradation of sulfonated poly(sulfone) membranes in vanadium redox flow batteries. *J Appl Electrochem*. 2011;41(10):1201-1213. doi:10.1007/s10800-011-0313-0

19. Lindstrand V, Sundström G, Jönsson A-S. Fouling of electrodialysis membranes by organic substances. *Desalination*. 2000;128(1):91-102. doi:10.1016/S0011-9164(00)00026-6

20. Mohammadi T, Kazacos MS. Modification of anion-exchange membranes for vanadium redox flow battery applications. *J Power Sources*. 1996;63(2):179-186. doi:10.1016/S0378-7753(96)02463-9

21. Wiśniewski J, Różańska A, Winnicki T. Removal of troublesome anions from water by means of Donnan dialysis. *Desalination*. 2005;182(1):339-346. doi:10.1016/j.desal.2005.02.032

22. Bard AJ, Fox MA. Artificial photosynthesis: Solar splitting of water to hydrogen and oxygen. *Acc Chem Res*. 1995;28(3). doi:10.1021/ar00051a007

23. Kim D, Sakimoto KK, Hong D, Yang P. Artificial Photosynthesis for Sustainable Fuel and Chemical Production. *Angew Chem Int Ed*. 2015;54(11):3259-3266. doi:10.1002/anie.201409116

24. Wijmans JG, Baker RW. The solution-diffusion model: a review. *J Membr Sci*. 1995;107:1-21.

25. Kim JM, Dobyns BM, Zhao R, Beckingham BS. Multicomponent transport of Methanol and Acetatein a series of crosslinked PEGDA-AMPS cation exchange membranes. *J Membr Sci*. In review.

26. Dobyns BM, Kim JM, Beckingham BS. Multicomponent transport of methanol and sodium acetate in poly(ethylene glycol) diacrylate membranes of varied fractional free volume. *Eur Polym J*. 2020;134:109809. doi:10.1016/j.eurpolymj.2020.109809

27. Larkin P. *Infrared and Raman Spectroscopy: Principles and Spectral Interpretation*. Elsevier; 2017.

28. Yasuda H, Lamaze CE, Ikenberry LD. Permeability of solutes through hydrated polymer membranes. Part I. Diffusion of sodium chloride. *Macromol Chem Phys*. 1968;118(1):19-35. doi:10.1002/macp.1968.021180102

29. Yasuda H, Peterlin A, Colton CK, Smith KA, Merrill EW. Permeability of solutes through hydrated polymer membranes. Part III. Theoretical background for the selectivity of dialysis membranes. *Makromol Chem*. 1969;126(1):177-186. doi:10.1002/macp.1969.021260120

30. Ju H, Sagle AC, Freeman BD, Mardel JI, Hill AJ. Characterization of sodium chloride and water transport in crosslinked poly(ethylene oxide) hydrogels. *J Membr Sci*. 2010;358(1):131-141. doi:10.1016/j.memsci.2010.04.035

31. Lee HC, Forte JG. A study of H+ transport in gastric microsomal vesicles using fluorescent probes. *Biochim Biophys Acta BBA - Biomembr*. 1978;508(2):339-356. doi:10.1016/0005-2736(78)90336-X

32. Wylie Nichols J, Hill MW, Bangham AD, Deamer DW. Measurement of net proton-hydroxyl permeability of large unilamellar liposomes with the fluorescent pH probe, 9-aminoacridine. *Biochim Biophys Acta BBA - Biomembr*. 1980;596(3):393-403. doi:10.1016/0005-2736(80)90126-1

33. Steudle E, Tyerman SD. Determination of permeability coefficients, reflection coefficients, and hydraulic conductivity ofChara corallina using the pressure probe: Effects of solute concentrations. *J Membr Biol*. 1983;75(1):85-96. doi:10.1007/BF01870802

34. Steudle E, Oren R, Schulze E-D. Water Transport in Maize Roots: Measurement of Hydraulic Conductivity, Solute Permeability, and of Reflection Coefficients of Excised Roots Using the Root Pressure Probe. *Plant Physiol*. 1987;84(4):1220-1232. doi:10.1104/pp.84.4.1220

35. Soltanieh M, Sahebdelfar S. Interaction effects in multicomponent separation by reverse osmosis. *J Membr Sci*. 2001;183(1):15-27. doi:10.1016/S0376-7388(00)00554-8

36. Geise GM, Freeman BD, Paul DR. Characterization of a sulfonated pentablock copolymer for desalination applications. *Polymer*. 2010;51(24):5815-5822. doi:10.1016/j.polymer.2010.09.072

37. Mukoma P, Jooste BR, Vosloo HCM. A comparison of methanol permeability in Chitosan and Nafion 117 membranes at high to medium methanol concentrations. *J Membr Sci*. 2004;243(1):293-299. doi:10.1016/j.memsci.2004.06.032

38. Elabd YA, Napadensky E, Sloan JM, Crawford DM, Walker CW. Triblock copolymer ionomer membranes: Part I. Methanol and proton transport. *J Membr Sci*. 2003;217(1):227-242. doi:10.1016/S0376-7388(03)00127-3

39. Pivovar BS, Wang Y, Cussler EL. Pervaporation membranes in direct methanol fuel cells. *J Membr Sci*. 1999;154(2):155-162. doi:10.1016/S0376-7388(98)00264-6

40. Tricoli V, Carretta N, Bartolozzi M. A Comparative Investigation of Proton and Methanol Transport in Fluorinated Ionomeric Membranes. *J Electrochem Soc*. 2000;147(4):1286-1290. doi:10.1149/1.1393351

41. Villaluenga JPG, Seoane B, Barragán VM, Ruiz-Bauzá C. Permeation of electrolyte water–methanol solutions through a Nafion membrane. *J Colloid Interface Sci*. 2003;268(2):476-481. doi:10.1016/S0021-9797(03)00585-X

42. Elabd YA, Walker CW, Beyer FL. Triblock copolymer ionomer membranes: Part II. Structure characterization and its effects on transport properties and direct methanol fuel cell performance. *J Membr Sci*. 2004;231(1):181-188. doi:10.1016/j.memsci.2003.11.019

43. Diaz LA, Abuin GC, Corti HR. Methanol sorption and permeability in Nafion and acid-doped PBI and ABPBI membranes. *J Membr Sci*. 2012;411-412:35-44. doi:10.1016/j.memsci.2012.04.013

44. Bowen TC, Li S, Noble RD, Falconer JL. Driving force for pervaporation through zeolite membranes. *J Membr Sci*. 2003;225(1):165-176. doi:10.1016/j.memsci.2003.07.016

45. Cox RA, Smith CR, Yates K. The excess acidity method. The basicities, and rates and mechanisms of enolization, of some acetophenones and acetone, in moderately concentrated sulfuric acid. *Can J Chem*. 1979;57(22):2952-2959. doi:10.1139/v79-480

46. Baij L, Hermans JJ, Keune K, Iedema PD. Time-Dependent ATR-FTIR Spectroscopic Studies on Solvent Diffusion and Film Swelling in Oil Paint Model Systems. *Macromolecules*. 2018;51(18):7134-7144. doi:10.1021/acs.macromol.8b00890

47. Volkov AV, Parashchuk VV, Stamatialis DF, Khotimsky VS, Volkov VV, Wessling M. High permeable PTMSP/PAN composite membranes for solvent nanofiltration. *J Membr Sci*. 2009;333(1):88-93. doi:10.1016/j.memsci.2009.01.050

48. Godino MP, Barragán VM, Villaluenga JPG, Izquierdo-Gil MA, Ruiz-Bauzá C, Seoane B. Liquid transport through sulfonated cation-exchange membranes for different water–alcohol solutions. *Chem Eng J*. 2010;162(2):643-648. doi:10.1016/j.cej.2010.06.013

49. Ji Y, Luo H, Geise GM. Specific co-ion sorption and diffusion properties influence membrane permselectivity. *J Membr Sci*. 2018;563:492-504. doi:10.1016/j.memsci.2018.06.010

50. Zhang D, Pan B, Wu M, et al. Cosorption of organic chemicals with different properties: Their shared and different sorption sites. *Environ Pollut*. 2012;160:178-184. doi:10.1016/j.envpol.2011.08.053

51. Pan B, Xing B. Competitive and Complementary Adsorption of Bisphenol A and 17α-Ethinyl Estradiol on Carbon Nanomaterials. *J Agric Food Chem*. 2010;58(14):8338-8343. doi:10.1021/jf101346e

52. Yong JS, Phillip WA, Elimelech M. Coupled reverse draw solute permeation and water flux in forward osmosis with neutral draw solutes. *J Membr Sci*. 2012;392-393:9-17. doi:10.1016/j.memsci.2011.11.020

53. Su X, Li W, Palazzolo A, Ahmed S. Concentration polarization and permeate flux variation in a vibration enhanced reverse osmosis membrane module. *Desalination*. 2018;433:75-88. doi:10.1016/j.desal.2018.01.001

54. Geise Geoffrey M., Lee Hae-Seung, Miller Daniel J., Freeman Benny D., McGrath James E., Paul Donald R. Water purification by membranes: The role of polymer science. *J Polym Sci Part B Polym Phys*. 2010;48(15):1685-1718. doi:10.1002/polb.22037

55. Kamcev J, Paul DR, Manning GS, Freeman BD. Accounting for frame of reference and thermodynamic non-idealities when calculating salt diffusion coefficients in ion exchange membranes. *J Membr Sci*. 2017;537:396-406. doi:10.1016/j.memsci.2017.05.034

56. Ren X, Springer TE, Zawodzinski TA, Gottesfeld S. Methanol Transport Through Nation Membranes. Electro-osmotic Drag Effects on Potential Step Measurements. *J Electrochem Soc*. 2000;147(2):466-474. doi:10.1149/1.1393219

Chapter 6: Multicomponent transport of methanol and sodium acetate in poly(ethylene glycol) diacrylate membranes of varied fractional free volume

Reproduced in part from Dobyns BM, Kim JM, Beckingham BS. Multicomponent transport of methanol and sodium acetate in poly(ethylene glycol) diacrylate membranes of varied fractional free volume. *Eur Polym J.* 2020;134:109809. doi:10.1016/j.eurpolymj.2020.109809 with permission from Jung Min Kim and Bryan S. Beckingham.

6.1. Introduction

Polymeric membranes are an important class of applied polymer materials of extensive, and increasing, interest due to their potential to dramatically impact industrial separation processes and improve the efficiency of emerging energy applications with low carbon footprints and low energy requirements compared to traditional technologies.[1–5] Critically, adequately designed and fabricated membranes can favor the transport of certain types of molecules over others; for example, water transport over alcohol transport for dehydration of high concentration azeotropic alcohol/water mixtures.[6,7] Permselective ion-containing polymer membranes are an integral component of many energy generation and storage devices, including fuel cells, electrolyzers, and solar fuels devices. For instance, in solar-fuels devices, ion-containing polymer membranes are responsible for permitting the selective transport of ions between electrodes to maintain overall charge neutrality, yet limit the transport of oxidation and reduction products produced at the electrodes.[8–12] The transport behavior of molecules or ions through a membrane is thereby essential and is typically characterized by the membrane's permeability to these species, which can be extracted from diffusion-cell experiments.[8,9,13–17] The permeability, P_i, of a membrane is the product of the thermodynamic solubility, K_i, and the kinetic diffusivity, D_i. The solubility quantifies a membrane's ability to partition a solute from an equilibrium solution, and the diffusivity quantifies the rate of solute transport through the membrane, shown in Equation 6.1.

$$P_i = K_i \times D_i \tag{6.1}$$

A critical characteristic of these membranes is the interplay between ion content and water uptake; and thereby their ion exchange capacity and ionic conductivity.[18–21] Generally, as the ion content

within such membranes increases, the water uptake correspondingly increases.[22–24] While this leads to increased efficiency in ionic conductivity, it also facilitates the transport of other molecular species through the resulting water channels, including the gases and reduction liquid products in solar fuels devices.[11] Consequently, the overall device performance decreases due to this unwanted molecular crossover.[11] Therefore, the water uptake, solute uptake and permeabilities of CO_2 reduction products through these films is very important for their potential use in fuel cells and has been a topic of recent interest in the literature.[23,25–28] For instance, Diao et al. characterized the transport of methanol through high-performance poly(2-acrylamido-2-methylpropanesulfonic acid)-based membranes utilizing a diffusion cell apparatus.[28] In these diffusion cell experiments, the membrane of interest is held between a donor cell and a receiver cell. The donor cell is charged with a known, and higher, concentration of the solute of interest and the concentration of the transporting species in the receiver cell is monitored over time, generally through either a probe-based system or via aliquotic sampling.[8,9,13–16] Conductivity[29–32] or pH[33,34] are commonly-employed probes that, unfortunately, can monitor only an overall change in the solution over time and, therefore, cannot be used to quantify the transport behavior of complex mixtures due to the lack of species-specific information. In the case of Diao et al., they found methanol permeability increased with increasing sulfonic acid content, while methanol permeability decreased with increasing crosslink density.[28] In the case of multicomponent transport, effects such as flux coupling and competitive sorption make predictions of actual mixture transport behavior challenging from such single-component experiments.[8,9,35] Aliquotic sampling can characterize multiple components in the downstream receiver-cell by examining each aliquot using gas chromatography[36–38], mass spectrometry[39,40], or Fourier-transform infrared (FTIR) spectroscopy[41,42] ex situ. However, aliquotic sampling techniques are quite arduous on the

researcher, in addition to imparting a continuously decreasing receiver cell volume, among other complications.

Recently, and in this work, we have employed diffusion-cell experiments and fiber optic probe-based ATR FTIR spectroscopy to monitor multi-solute diffusion cell experiments in situ.[8,9] This approach leverages the advantages of probe-based systems (in situ monitoring and facile data collection), while also yielding speciation information through the collected FTIR spectra.[8,9] Previously, we utilized this technique to examine multi-solute transport in Nafion™ 117[9] and Selemion AMV[8], as these membranes are commercially valuable and have been extensively tested for permeability and selectivity for a range of solutes in the literature.[25,43–47] In these previous studies, distinct differences in permeabilities were observed between single-solute and multi-solute experiments motivating further experimentation, such as our work herein, towards understanding multi-solute transport behavior in polymeric membranes.[8,9]

In this work, we're interested in understanding the role of fractional free volume on the co-transport of two relevant CO_2 reduction products, methanol and sodium acetate.[10,11] As mentioned above, we have previously examined the co-transport of these two species in Nafion™ 117, where interesting emergent transport behavior was observed.[9] In particular, permeability to sodium acetate increased in the multicomponent experiment compared to the single component experiment, while methanol's decreased.[9] In this case, these changes were found to be primarily due to thermodynamic solubility effects based on sorption-desorption experiments.[9]

In this study, the influence of membrane-bound ionic species is removed, and the impact of varied fractional free volume (FFV) on the transport of aqueous methanol, sodium acetate, and methanol-sodium acetate mixtures in a series of hydrated dense polymer membranes is examined. Freeman and coworkers have demonstrated the variation of fractional free volume of UV photopolymerized poly(ethylene glycol diacrylate) (PEGDA)-based membranes through control of the pre-polymerization mixture compositions.[13–15,18,48–53] In particular, by increasing the water content in the pre-polymerization mixture, the fractional free volume of the subsequent membranes could be increased (as demonstrated by increasing water uptake).[15,18,50] Herein, we apply this strategy to synthesize a series of PEGDA-based polymer membranes with varied fractional free volume and characterize the resulting water uptake, dimensional swelling, and diffusive permeability of these membranes to methanol, sodium acetate, and their binary mixture. This study aims to isolate the impact of fractional free volume on transport behavior and, interestingly, emergent behavior is observed for membrane permselectivity as fractional free volume is varied.

6.2. Results and Discussion

6.2.1. Membrane Synthesis, Water Uptake, and Solute Uptake

PEGDA is an amorphous, water-soluble polymer with acrylate functional chain ends facilitating crosslinking when mixed with a photoinitiator (in this work HCPK) and exposed to ultraviolet light. Upon UV exposure, PEGDA photopolymerizes to produce a crosslinked network; Scheme 6.1. To produce free-standing membranes of desired film thickness, pre-polymerization mixtures containing PEGDA, water, and photoinitiator were prepared, sonicated, and sandwiched between quartz plates with spacers of desired thickness, and exposed to UV-light to induce photopolymerization. Pre-polymerization mixtures were visually transparent, homogeneous, and

produced optically clear membranes. Here, a series of model PEGDA-based membranes with varied fractional free volume are synthesized by varying the water content of the pre-polymerization mixture (mixture compositions given in Table 6.1). It has been previously shown that increasing the water content in the pre-polymerization mixture leads to higher fractional free volume in the fabricated membranes.[15,17,50,54] For the membranes synthesized here, water uptake was found to be linearly correlated to the pre-polymerization water content, Figure 6.1, such that pre-polymerization water content is an adequate representation of the varying FFV within the membranes.

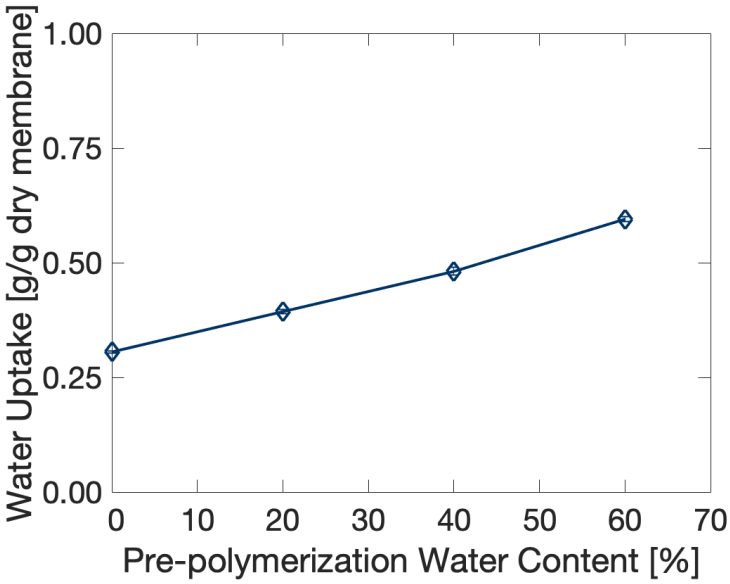

Figure 6.1. Water uptake versus pre-polymerization water content

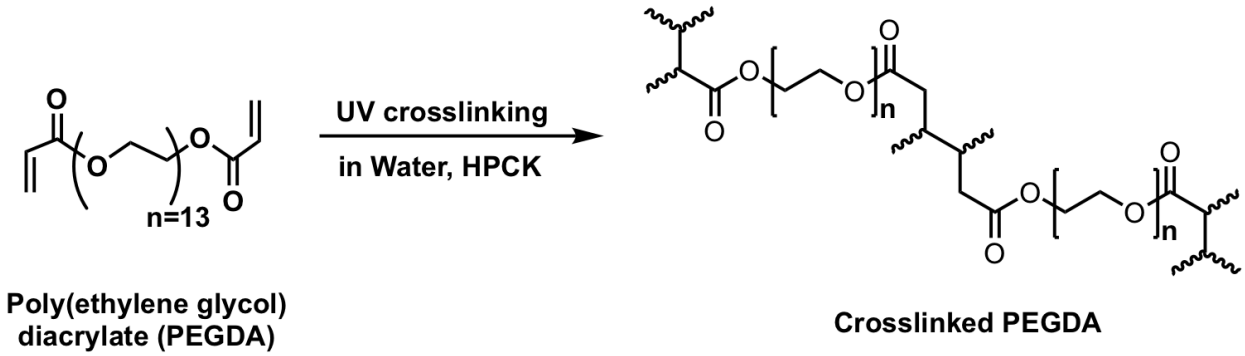

Scheme 6.1. PEGDA photopolymerization to form a crosslinked network

Table 6.1. Composition and water uptake for the range of PEGDA-water membranes

Membrane	Water [g]	PEGDA [g]	HCPK [g]	Water uptake [g/g dry membrane]
PEGDA00	0	9.978	0.010	0.35 ± 0.01
PEGDA20	1.997	8.130	0.011	0.53 ± 0.02
PEGDA40	4.022	5.980	0.011	0.76 ± 0.05
PEGDA60	5.998	4.081	0.010	1.23 ± 0.2

The ability of films to uptake water and/or solutes of interest is a fundamental characteristic for ion exchange polymer membranes for application in devices such as fuel cells, as it is closely linked with ion uptake and diffusion behavior.[16,55,56] Measurement of equilibrium water content provides a useful basis for understanding differences in transport behavior by giving a relative description of membrane fractional free volume, as water occupies the available fractional free volume in dense, hydrated polymer membranes.[16] Equilibrium water content was calculated from membrane hydrated after equilibration in DI water and after drying under vacuum[19]; shown in Figure 6.2 and Table 6.1. The gravimetric solute uptakes are shown in Figure 6.2a and given in Table 6.2.

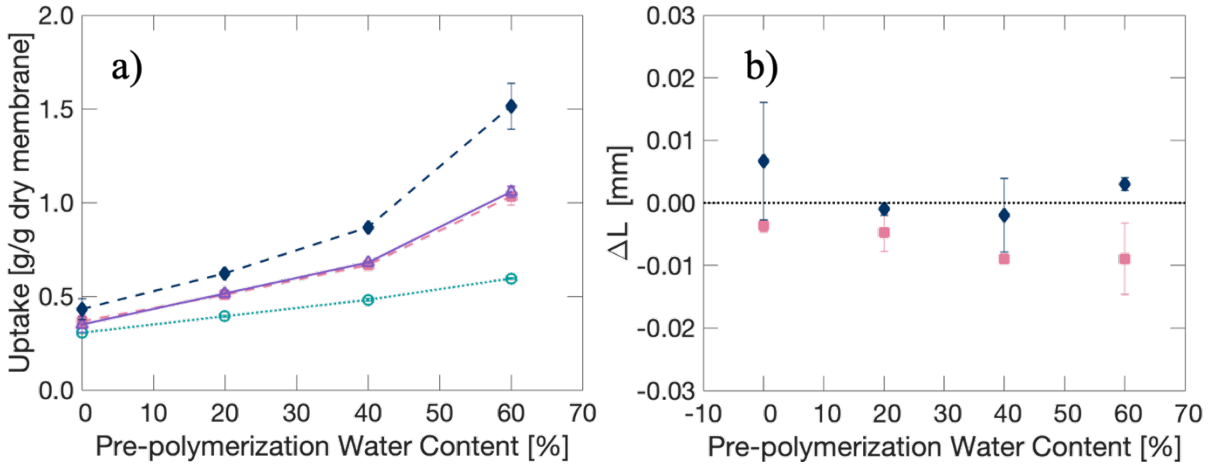

Figure 6.2. a) Gravimetric water and solution uptake as a function of water percentage and b) dimensional swelling in membrane thickness (ΔL, mm) as a function of pre-polymerization water content; (○) water uptake, (♦) methanol uptake/swelling, (■) sodium acetate uptake/swelling, and (△) methanol and sodium acetate simultaneous uptake/swelling. The lines in a) are strictly to guide the eye and the dotted line in b) is at 0 mm swelling. The error bars are the standard deviations between triplicate measurements.

Table 6.2. Water uptake and solute uptake for the range of PEGDA-water membranes

Membrane	Water uptake [g/g dry membrane]	Methanol uptake [g/g dry membrane]	Acetate uptake [g/g dry membrane]	Methanol and acetate uptake [g/g dry membrane]
PEGDA00	0.35 ± 0.01	0.43 ± 0.05	0.37 ± 0.03	0.35 ± 04
PEGDA20	0.53 ± 0.02	0.62 ± 0.01	0.51 ± 0.02	0.51 ± 0.02
PEGDA40	0.76 ± 0.05	0.87 ± 0.01	0.67 ± 0.02	0.68 ± 0.01
PEGDA60	1.23 ± 0.2	1.67 ± 0.3	1.03 ± 0.05	1.06 ± 0.05

As the pre-polymerization water content increases, the equilibrium water uptake also increases (Figure 6.2a and Table 6.2). This observed increasing equilibrium water uptake confirms the expected increasing fractional free volume across our series of membranes as the pre-polymerization water content increases.[15,17,18,48,50,54,57] In general, the solution uptake is based upon the membrane's equilibrium sorption of the solutes and solvent. Here, we do not quantify this equilibrium solubility but rather examine the relative gravimetric uptake from 1 M aqueous solutions of our solutes of interest where uptake is measured as strictly the difference between the swollen and dry membranes; values shown in Figure 6.1a for methanol, sodium acetate, and methanol/sodium acetate. Every solution uptake is higher than water uptake, and we observe comparable gravimetric uptakes for 1 M sodium acetate and 1 M methanol/sodium acetate mixture, while for 1 M methanol, we observe distinctly higher gravimetric uptake. This behavior meets expectations as each of these solutes has a higher molecular mass compared to water, and analogous relative uptake behavior has been previously observed for methanol and sodium acetate in Nafion 117.[9] Dimensional swelling in membrane thickness (ΔL) for the membranes used for methanol and sodium acetate uptake was measured using Equation 6.2,

$$\Delta L = L_S - L_W \tag{6.2}$$

where L_S is the membrane thickness after solution uptake equilibration and L_W is the membrane thickness after equilibration with water; Figure 6.2b. The dotted line in Figure 6.2b represents no change in membrane thickness after equilibration in the 1 M solution of interest. Equilibration with 1 M methanol solutions resulted in little to slight swelling of the membrane. In contrast, equilibration with 1 M sodium acetate solutions resulted in slight membrane deswelling across all pre-polymerization water contents. The minor swelling and higher gravimetric uptake for methanol over sodium acetate is consistent with a higher membrane solubility for methanol (higher

mass uptake, lower molecular mass) as well as results for these solutes in other polyether-based membranes.[7,55,58–62] For instance, analogous results were observed for methanol and sodium acetate in Nafion^{TM} 117, where osmotic deswelling was observed for sodium acetate osmotically, and methanol displayed over an order of magnitude higher solubility than sodium acetate.[9] Overall, salts such as sodium acetate typically deswell hydrated membranes, and have lower membrane solubility than neutral solutes like methanol.[63–65]

6.2.2. Permeability of PEGDA to methanol and sodium acetate

To investigate how fractional free volume impacts transport of these species, we synthesized membranes of varying fractional free volume and characterized their single and multicomponent permeability to methanol and sodium acetate via in situ ATR FTIR spectroscopy, as detailed in Chapter 5. Briefly, a known concentration of solute(s), 1 M for this work, is placed in the donor cell and pure DI water in the receiver cell. The PEGDA membrane is fixed between the two thermally jacketed cells, and they are stirred continuously to ensure complete mixing. We denote these membranes as PEGDAXX, where XX denotes the pre-polymerization mixture weight percent of water; i.e., PEGDA20 has a pre-polymerization water content of 20 wt. %. The ATR FTIR spectroscopy probe is held within the receiver cell to measure the changing absorbance spectra of the solution over time. The single-component downstream receiver-cell concentrations of methanol and acetate, shown in Figure 6.5 as the filled markers, both increase with increasing pre-polymerization water content or increasing FFV. This is anticipated as increasing water content leads to a more open network structure, increasing fractional free volume and correspondingly, permeability to solutes. This finding is in good agreement with the results of Freeman and coworkers[17,48], where increasing fractional free volume via larger PEGDA molecular

weight or increased pre-polymerization mixture water content led to increasing methanol[48] and salt (NaCl)[17] transport in single-solute diffusion cell experiments.

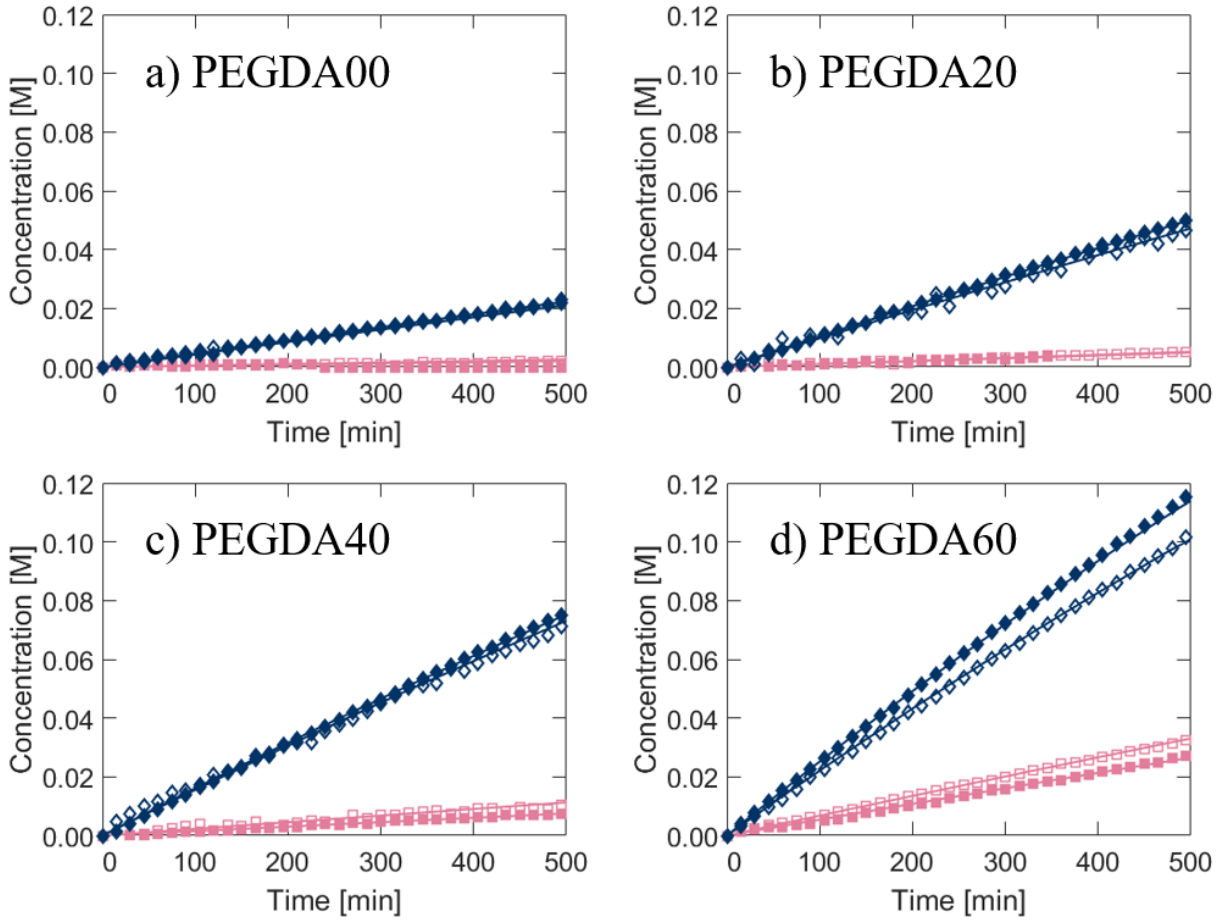

Figure 6.3. Methanol and acetate concentrations over time. a) PEGDA00, b) PEGDA20, c) PEGDA40, and d) PEGDA60. (♦) methanol and (■) acetate. Filled markers are methanol and acetate multicomponent experiments and open markers are single component experiments. Only 15% of the experimental data is shown for clarity.

For PEGDA00, Figure 6.3a, the single and multicomponent receiver cell concentration curves for both methanol and acetate are essentially identical, and therefore, so are the corresponding permeabilities. A small difference appears for PEGDA20, Figure 6.3b, where methanol's single-component receiver cell concentration curve is slightly above that of its multicomponent curve, while the difference for acetate is, again, negligible. Larger deviations arise for methanol within

the PEGDA40 and PEGDA60 membranes, as well as the emergence, and increasing difference, for acetate with increasing pre-polymerization water content. This is most pronounced for the largest FFV PEGDA60 membranes in Figure 6.3d, where methanol's single-component receiver cell concentrations are significantly below, and acetate's single-component receiver cell concentrations are considerably above the multicomponent experimental data. These trends are clearly shown in Figure 6.4a, where the extracted permeabilities are plotted against pre-polymerization water content.

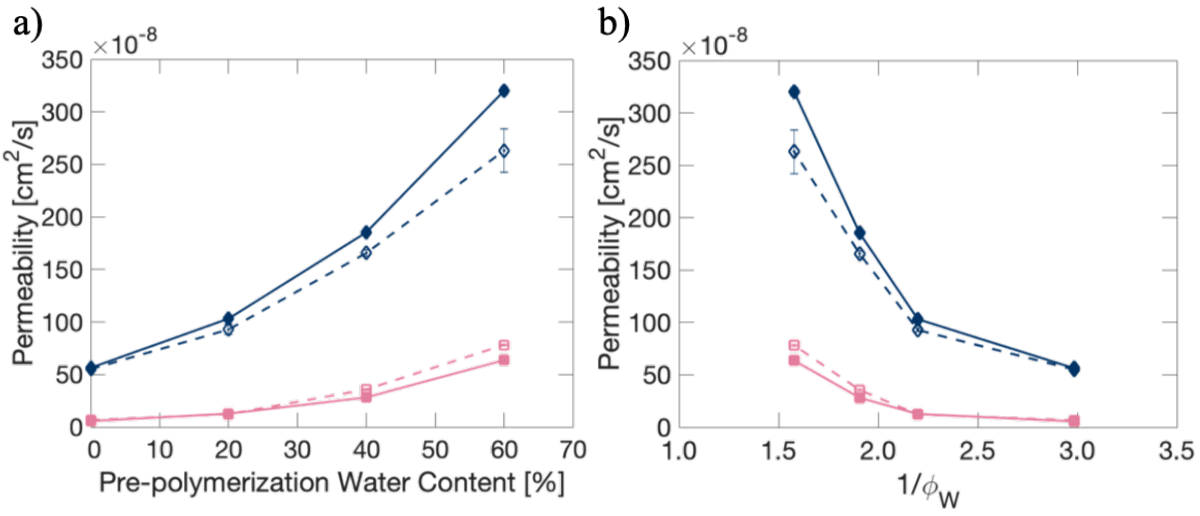

Figure 6.4. a) Permeability as a function of water content b) and permeability as a function of water volume fraction. (♦) methanol and (■) acetate. Filled markers are methanol and acetate single component experiments and open markers are multicomponent experiments. Error bars are standard deviations for triplicate measurements.

The increasing curves observed in Figure 6.4a for permeability as a function of pre-polymerization water content follow the expectation that as pre-polymerization water content increases, crosslink density decreases, indicating that there is an expansion in transport area between polymer chains.[48,52] Galizia et al. and Lin et al. observed similar results for liquid methanol and gas transport, respectively, through crosslinked PEGDA films of varied FFV.[15,48] They found that as the FFV increased, so too did the permeability of the respective solutes.[15,48] Here, we see an

exponential increase in permeability as the pre-polymerization water content, or FFV, increases. This result is consistent with free volume theory when comparing permeability and FFV (v_f), shown in Equation 6.3,

$$P_i = Cexp^{-\frac{\gamma v_f^*}{v_f}} \quad 6.3$$

where C is a constant for the system, γ is a numerical factor between 0.5 and 1 based on Cohen and Turnbull's definition[66], v_f* is the critical free volume, and v_f is the fractional free volume of the system.[67]

While permeability increases as pre-polymerization water content increases, so too does the difference between single and multicomponent permeability for both methanol and acetate. These differences between single and multicomponent permeability increase as FFV increases (i.e., PEGDA00 < PEGDA20 < PEGDA40 < PEGDA60) with PEGDA60 resulting in the most considerable difference between single and multicomponent permeability for both methanol and acetate. This can also be visualized as a function of water volume fraction or, more typically, inverse water volume fraction (Figure 6.4b) as this parameter is highly utilized in the membrane literature for characterizing membrane mesh size.[48,68–75] Water volume fraction, ϕ_W, is calculated utilizing measured densities of the films (between 1.15 and 1.29 g/mL, shown in Figure 6.5), and measured water uptakes via Equation 6.4,

$$\phi_W = \frac{(m_W - m_D)/\rho_L}{(m_W - m_D)/\rho_L + m_D/\rho_P} \quad 6.4$$

where m_W is the mass of the hydrated membrane, m_D is the mass of the dry membrane, r_L is the density of the liquid, and r_P is the density of the membrane. As the inverse water volume fraction increases (as fractional free volume decreases), the permeabilities of both methanol and acetate decrease. For comparison, the permeability of Nafion™ 117 to methanol has been reported with a

range of 5 x 10^{-7} to 5 x 10^{-6} cm^2/s in the literature, such that trends observed here relating changes in permeability to FFV would likely correlate to these or other membranes.[9,27,44,76–82]

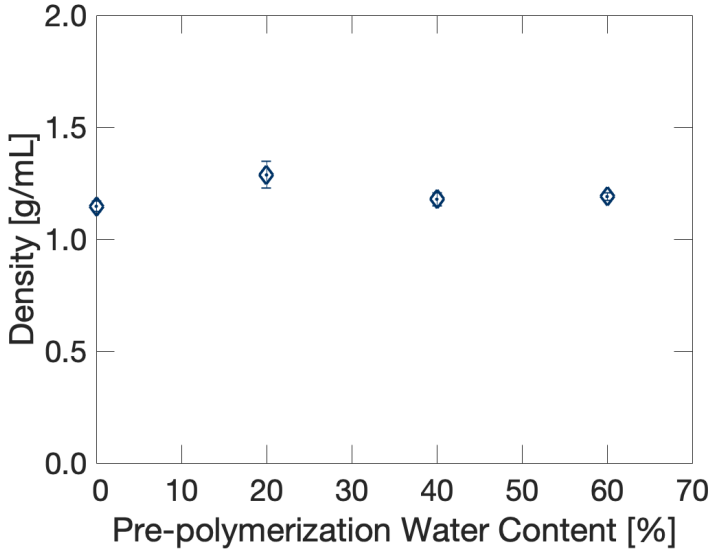

Figure 6.5. Density versus pre-polymerization water content.

Table 6.3. Membrane permeability to methanol and acetate from single and multicomponent diffusion-cell experiments

	P_i [cm^2/s *10^8]			
	Single Component		**2 Component**	
Membrane	**Methanol**	**Acetate**	**Methanol**	**Acetate**
PEGDA00	56.4 ± 0.7	5.6 ± 0.2	55.8 ± 0.7	5.6 ± 0.8
PEGDA20	103 ± 2	12.4 ± 0.1	94 ± 1	13 ± 2
PEGDA40	185 ± 3	29 ± 2	174 ± 3	31 ± 2
PEGDA60	320 ± 4	64 ± 3	266 ± 3	75 ± 2

Examining the permeability values shown in Table 6.3, permeabilities for methanol and acetate in PEGDA00 membranes are consistent from single to multicomponent experiments but are themselves an order of magnitude different from methanol to acetate, as described above and expected from previous work with these solutes.[9] The relative difference between these permeabilities (i.e., methanol/acetate) is important as this ratio describes membrane permselectivity, α, as shown in Equation 6.5. This parameter is commonly used to compare and select membranes for a particular process or set of solutes.

$$\alpha_{M/A} = \frac{P_M}{P_A} \tag{6.5}$$

In this work, we define the membrane permselectivity as the ratio of methanol permeability (P_M) to acetate permeability (P_A) such that all permselectivities are greater than one. We denote "ideal" selectivity, α_{Ideal}, as the ratio between permeabilities extracted from single component diffusion cell experiments. Alternatively, "true" selectivity, α_{True}, is the ratio between permeabilities extracted from diffusion cell experiments of the solute mixture. This "true" selectivity incorporates the complex interactions between solutes (solute-solute interactions) as well as between multiple solutes and the membrane (multiple solute-membrane interactions).

As shown in Figure 6.6 and Table 6.4, distinct differences arise between the "ideal" and "true" selectivities of up to 47%, and these differences between the "ideal" and "true" selectivity can be attributed to both assisted and competitive transport behavior. Methanol likely assists acetate transport due to methanol's higher solubility and higher flux through the membrane. Conversely, presence of the comparably larger acetate molecules occupying the FFV and momentum transfer to acetate from methanol's higher flux, leads to overall decreasing methanol transport.[72-73] Interestingly, this behavior varies with fractional free volume.

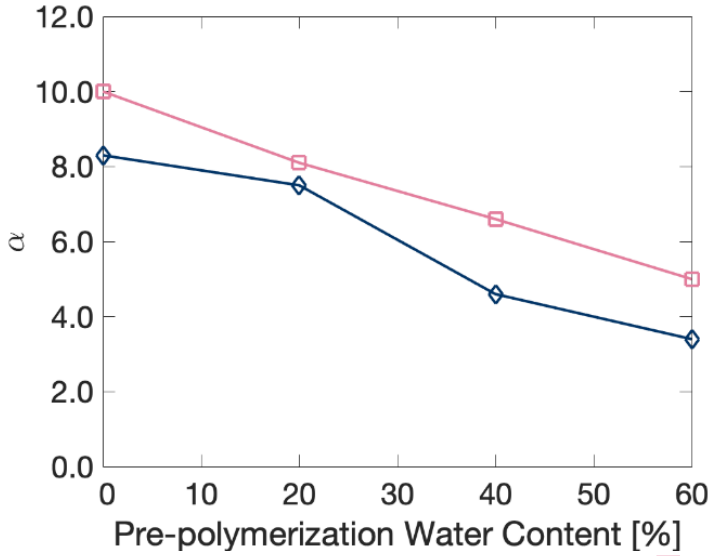

Figure 6.6. Selectivity versus pre-polymerization water content. □ are the "ideal" single component selectivity values and ◊ are the "true" selectivity values.

Table 6.4. Ideal selectivities, true selectivities and percent difference between them with varying pre-polymerization water content

Membrane	α_{Ideal}	α_{True}	% Difference
PEGDA00	10.0	8.3	20
PEGDA20	8.1	7.5	8
PEGDA40	6.6	4.6	43
PEGDA60	5.0	3.4	47

As the fractional free volume increases, facilitating increased overall transport, the presence of methanol molecules assists acetate transport to a greater extent. However, when there is little water content (PEGDA00 and PEGDA20), the difference between the two permeabilities themselves is smaller, and we observe little to no impact on transport due to the presence of a cosolute. This relationship between the physiochemical membrane property (water uptake/fractional free volume) and the resulting multicomponent transport behavior may prove to be a useful handle for understanding or identifying membrane-solute systems where emergent transport behavior should be considered.

6.3. Conclusions

A model system of UV-photopolymerized polyethylene glycol diacrylate (PEGDA) membranes was synthesized with varying pre-polymerization water content to vary the fractional free volume within otherwise chemically analogous membranes. Water and solute uptake, membrane swelling, and permeabilities to these membranes were characterized and compared for two different CO_2 reduction products, methanol and sodium acetate. One and two-component permeabilities to methanol and sodium acetate were measured in custom-build diffusion cells with the receiver cell solute concentrations monitored by in situ ATR FTIR spectroscopy. Permeabilities varied up to a factor of six as the FFV of the PEGDA membranes increased. We observe distinct, and increasing, differences in the magnitude of extracted permeabilities between single solute and combined solute experiments as the FFV increases and attribute these differences to a combination of assisted and competitive transport. Overall, the observed structure-property relationship where increasing pre-polymerization water content (increasing FFV) leads to more divergent transport behavior is potentially a useful tool for identifying membrane-solute systems where this behavior must be understood prior to membrane selection.

6.4. References

1. Lawson KW, Lloyd DR. Membrane distillation. *J Membr Sci*. 1997;124(1):1-25. doi:10.1016/S0376-7388(96)00236-0

2. Cabassud C, Wirth D. Membrane distillation for water desalination: How to chose an appropriate membrane? *Desalination*. 2003;157(1):307-314. doi:10.1016/S0011-9164(03)00410-7

3. Drioli E, Curcio E. Membrane engineering for process intensification: a perspective. *J Chem Technol Biotechnol*. 2007;82(3):223-227. doi:10.1002/jctb.1650

4. Samtleben W, Randerson DH, Blumenstein M, Habersetzer R, Schmidt B, Gurland HJ. Membrane plasma exchange: Principles and application techniques. *J Clin Apheresis*. 1984;2(2):163-169. doi:10.1002/jca.2920020204

5. Zhang LZ, Jiang Y. Heat and mass transfer in a membrane-based energy recovery ventilator. *J Membr Sci*. 1999;163(1):29-38. doi:10.1016/S0376-7388(99)00150-7

6. Lively RP, Sholl DS. From water to organics in membrane separations. *Nat Mater*. 2017;16:276-279.

7. Lue SJ, Ou JS, Kuo CH, Chen HY, Yang T-H. Pervaporative separation of azeotropic methanol/toluene mixtures in polyurethane–poly(dimethylsiloxane) (PU–PDMS) blend membranes: Correlation with sorption and diffusion behaviors in a binary solution system. *J Membr Sci*. 2010;347(1):108-115. doi:10.1016/j.memsci.2009.10.012

8. Carter BM, Dobyns BM, Beckingham BS, Miller DJ. Multicomponent transport of alcohols in an anion exchange membrane measured by in-situ ATR FTIR spectroscopy. *Polymer*. 2017;123:144-152. doi:10.1016/j.polymer.2017.06.070

9. Beckingham BS, Lynd NA, Miller DJ. Monitoring multicomponent transport using in situ ATR FTIR spectroscopy. *J Membr Sci*. 2018;550:348-356. doi:10.1016/j.memsci.2017.12.072

10. Singh MR, Clark EL, Bell AT. Effects of electrolyte, catalyst, and membrane composition and operating conditions on the performance of solar-driven electrochemical reduction of carbon dioxide. *Phys Chem Chem Phys*. 2015;17(29):18857-19676. doi:10.1039/C5CP03283K

11. R. Singh M, T. Bell A. Design of an artificial photosynthetic system for production of alcohols in high concentration from CO2. *Energy Environ Sci*. 2016;9(1):193-199. doi:10.1039/C5EE02783G

12. Kusoglu A, Weber AZ. New insights into perfluorinated sulfonic-acid ionomers. *Chem Rev*. 2017;117(3):987-1104. doi:10.1021/acs.chemrev.6b00159

13. Freeman B, Yampolskii Y, Pinnau I. *Materials Science of Membranes for Gas and Vapor Separation*. John Wiley & Sons; 2006.

14. Lin H, Freeman BD. Gas Permeation and Diffusion in Cross-Linked Poly(ethylene glycol diacrylate). *Macromolecules*. 2006;39(10):3568-3580. doi:10.1021/ma051686o

15. Lin H, Kai T, Freeman BD, Kalakkunnath S, Kalika DS. The Effect of Cross-Linking on Gas Permeability in Cross-Linked Poly(Ethylene Glycol Diacrylate). *Macromolecules*. 2005;38(20):8381-8393. doi:10.1021/ma0510136

16. Yasuda H, Lamaze CE, Ikenberry LD. Permeability of solutes through hydrated polymer membranes. Part I. Diffusion of sodium chloride. *Macromol Chem Phys*. 1968;118(1):19-35. doi:10.1002/macp.1968.021180102

17. Ju H, Sagle AC, Freeman BD, Mardel JI, Hill AJ. Characterization of sodium chloride and water transport in crosslinked poly(ethylene oxide) hydrogels. *J Membr Sci*. 2010;358(1):131-141. doi:10.1016/j.memsci.2010.04.035

18. Wu Y-H, Park HB, Kai T, Freeman BD, Kalika DS. Water uptake, transport and structure characterization in poly(ethylene glycol) diacrylate hydrogels. *J Membr Sci*. 2010;347:197-208. doi:10.1016/j.memsci.2009.10.025

19. Zawodzinski TA, Smith VT, Springer TE. Water Uptake by and TransportThrough Nafion 117 Membranes. *J Electrochem Soc*. 1993;140(4):7. doi:https://doi.org/10.1149/1.2056194

20. Ren X, Springer TE, Gottesfeld S. Water and Methanol Uptakes in Nafion Membranes and Membrane Effects on Direct Methanol Cell Performance. *J Electrochem Soc*. 2000;147(1):92-98. doi:10.1149/1.1393161

21. Zheng Y, Ash U, Pandey RP, Ozioko AG, Ponce-Gonzalez J, Handl M, Weissback T, Varcoe JR, Holdroft S, Liberatore MW, Hiesgen R, Dekel D. Water Uptake Study of Anion Exchange Membranes. *Macromolecules*. 2018;51(9):3264-3278. doi:10.1021/acs.macromol.8b00034

22. Kopitzke RW, Linkous CA, Anderson HR, Nelson GL. Conductivity and Water Uptake of Aromatic-Based Proton Exchange Membrane Electrolytes. *J Electrochem Soc*. 2000;147(5):1677-1681. doi:10.1149/1.1393417

23. Zawodzinski Jr TAZ, Springer TE, Davey J, Jestel R, Lopez C, Valerio J, Gottesfeld S. A Comparative Study of Water Uptake By and Transport Through Ionomeric Fuel Cell Membranes. *J Electrochem Soc*. 1993;140(7):1981. doi:10.1149/1.2220749

24. Kim YS, Hickner MA, Dong L, Pivovar BS, McGrath JE. Sulfonated poly(arylene ether sulfone) copolymer proton exchange membranes: composition and morphology effects on the methanol permeability. *J Membr Sci*. 2004;243(1):317-326. doi:10.1016/j.memsci.2004.06.035

25. Broka K, Ekdunge P. Oxygen and hydrogen permeation properties and water uptake of Nafion® 117 membrane and recast film for PEM fuel cell. *J Appl Electrochem*. 1997;27(2):117-123. doi:10.1023/A:1018469520562

26. Baschuk JJ, Li X. Modeling of ion and water transport in the polymer electrolyte membrane of PEM fuel cells. *Int J Hydrog Energy*. 2010;35(10):5095-5103. doi:10.1016/j.ijhydene.2009.10.032

27. Heinzel A, Barragan VM. A review of the state-of-the-art of the methanol crossover in direct methanol fuel cells. *J Power Sources*. 1999;84:70-74. doi:10.1016/S0378-7753(99)00302-X

28. Diao H, Yan F, Qiu L, Lu J, Lu X, Lin B, Li Q, Shang S, Liu W, Liu J. High Performance Cross-Linked Poly(2-acrylamido-2-methylpropanesulfonic acid)-Based Proton Exchange Membranes for Fuel Cells. *Macromolecules*. 2010;43(15):6398-6405. doi:10.1021/ma1010099

29. Daniel David E. In Situ Hydraulic Conductivity Tests for Compacted Clay. *J Geotech Eng*. 1989;115(9):1205-1226. doi:10.1061/(ASCE)0733-9410(1989)115:9(1205)

30. Hamilton J, Daniel D, Olson R. Measurement of Hydraulic Conductivity of Partially Saturated Soils. In: Zimmie T, Riggs C, eds. *Permeability and Groundwater Contaminant Transport*. ASTM International; 1981:182-196. doi:10.1520/STP28324S

31. Steudle E, Tyerman SD. Determination of permeability coefficients, reflection coefficients, and hydraulic conductivity ofChara corallina using the pressure probe: Effects of solute concentrations. *J Membr Biol*. 1983;75(1):85-96. doi:10.1007/BF01870802

32. Kuchuk FJ, Onur M. Estimating permeability distribution from 3D interval pressure transient tests. *J Pet Sci Eng*. 2003;39(1):5-27. doi:10.1016/S0920-4105(03)00037-8

33. van de Vossenberg JLCM, Driessen AJM, da Costa MS, Konings WN. Homeostasis of the membrane proton permeability in Bacillus subtilis grown at different temperatures. *Biochim Biophys Acta BBA - Biomembr*. 1999;1419(1):97-104. doi:10.1016/S0005-2736(99)00063-2

34. Wohnsland F, Faller B. High-Throughput Permeability pH Profile and High-Throughput Alkane/Water log P with Artificial Membranes. *J Med Chem*. 2001;44(6):923-930. doi:10.1021/jm001020e

35. Koros WJ, Chern RT, Stannett V, Hopfenberg HB. A model for permeation of mixed gases and vapors in glassy polymers. *J Polym Sci Polym Phys Ed*. 1981;19(10):1513-1530. doi:10.1002/pol.1981.180191004

36. Dumas F, Aussel C, Pernet P, Martin C, Giboudeau J. Gas chromatography applied to the lactulose—mannitol intestinal permeability test. *J Chromatogr B Biomed Sci App*. 1994;654(2):276-281. doi:10.1016/0378-4347(94)00041-7

37. Farhadi A, Keshavarzian A, Holmes EW, Fields J, Zhang L, Banan A. Gas chromatographic method for detection of urinary sucralose: application to the assessment of intestinal permeability. *J Chromatogr B*. 2003;784(1):145-154. doi:10.1016/S1570-0232(02)00787-0

38. Bruet V, Bourdeau P, Bizzarri M, Martin L, Dumon H. Rapid blood sampling method for measuring intestinal permeability by gas chromatography in dogs. *Rev Méd Vét*. 2008;159:276-281.

39. Breemen RB van, Li Y. Caco-2 cell permeability assays to measure drug absorption. *Expert Opin Drug Metab Toxicol*. 2005;1(2):175-185. doi:10.1517/17425255.1.2.175

40. Wang Z, Hop CECA, Leung KH, Pang J. Determination of in vitro permeability of drug candidates through a Caco-2 cell monolayer by liquid chromatography/tandem mass spectrometry. *J Mass Spectrom*. 2000;35(1):71-76. doi:10.1002/(SICI)1096-9888(200001)35:1<71::AID-JMS915>3.0.CO;2-5

41. Casiraghi A, Minghetti P, Cilurzo F, Selmin F, Gambaro V, Montanari L. The effects of excipients for topical preparations on the human skin permeability of terpinen-4-ol contained in Tea tree oil: Infrared spectroscopic investigations. *Pharm Dev Technol*. 2010;15(5):545-552. doi:10.3109/10837450903338387

42. McAuley WJ, Mader KT, Tetteh J, Lane ME, Hadgraft J. Simultaneous monitoring of drug and solvent diffusion across a model membrane using ATR-FTIR spectroscopy. *Eur J Pharm Sci*. 2009;38(4):378-383. doi:10.1016/j.ejps.2009.09.002

43. Chiou JS, Paul DR. Gas permeation in a dry Nafion membrane. *Ind Eng Chem Res*. 1988;27(11):2161-2164. doi:10.1021/ie00083a034

44. Xue S, Yin G. Methanol permeability in sulfonated poly(etheretherketone) membranes: A comparison with Nafion membranes. *Eur Polym J*. 2006;42(4):776-785. doi:10.1016/j.eurpolymj.2005.10.008

45. Oei D-G. Permeation of vanadium cations through anionic and cationic membranes. *J Appl Electrochem*. 1985;15(2):231-235. doi:10.1007/BF00620938

46. Isono Y, Fukushima K, Kawakatsu T, Nakajima M. Integration of charged membrane into perstraction system for separation of amino acid derivatives. *Biotechnol Bioeng*. 1997;56(2):162-167. doi:10.1002/(SICI)1097-0290(19971020)56:2<162::AID-BIT5>3.0.CO;2-N

47. Igawa M, Fukushi Y, Hayashita T, Hoffmann MR. Selective transport of aldehydes across an anion-exchange membrane via the formation of bisulfite adducts. *Ind Eng Chem Res*. 1990;29(5):857-861. doi:10.1021/ie00101a021

48. Galizia M, Paul DR, Freeman BD. Liquid methanol sorption, diffusion and permeation in charged and uncharged polymers. *Polymer*. 2016;102:281-291. doi:10.1016/j.polymer.2016.09.010

49. Geise Geoffrey M., Lee Hae-Seung, Miller Daniel J., Freeman Benny D., McGrath James E., Paul Donald R. Water purification by membranes: The role of polymer science. *J Polym Sci Part B Polym Phys*. 2010;48(15):1685-1718. doi:10.1002/polb.22037

50. Kalakkunnath Sumod, Kalika Douglass S., Lin Haiqing, Freeman Benny D. Viscoelastic characteristics of UV polymerized poly(ethylene glycol) diacrylate networks with varying extents of crosslinking. *J Polym Sci Part B Polym Phys*. 2006;44(15):2058-2070. doi:10.1002/polb.20873

51. Kamcev J, Freeman BD. Charged Polymer Membranes for Environmental/Energy Applications. *Annu Rev Chem Biomol Eng*. 2016;7:111-133. doi:10.1146/annurev-chembioeng-080615-033533

52. Lin H, Freeman BD. Gas and Vapor Solubility in Cross-Linked Poly(ethylene Glycol Diacrylate). *Macromolecules*. 2005;38(20):8394-8407. doi:10.1021/ma051218e

53. Lin H, Freeman BD. Gas solubility, diffusivity and permeability in poly(ethylene oxide). *J Membr Sci*. 2004;239(1):105-117. doi:10.1016/j.memsci.2003.08.031

54. Ju H, McCloskey BD, Sagle AC, Kusuma VA, Freeman BD. Preparation and characterization of crosslinked poly(ethylene glycol) diacrylate hydrogels as fouling-resistant membrane coating materials. *J Membr Sci*. 2009;330(1):180-188. doi:10.1016/j.memsci.2008.12.054

55. Geise GM, Park HB, Sagle AC, Freeman BD, McGrath JE. Water permeability and water/salt selectivity tradeoff in polymers for desalination. *J Membr Sci*. 2011;369(1):130-138. doi:10.1016/j.memsci.2010.11.054

56. Yan N, Paul DR, Freeman BD. Water and ion sorption in a series of cross-linked AMPS/PEGDA hydrogel membranes. *Polymer*. 2018;146:196-208. doi:10.1016/j.polymer.2018.05.021

57. La Y-H, McCloskey BD, Sooriyakumaran R, Vora A, Freeman B, Nassar M, Hedrick J, Nelson A, Allen R. Bifunctional hydrogel coatings for water purification membranes: Improved fouling resistance and antimicrobial activity. *J Membr Sci*. 2011;372(1):285-291. doi:10.1016/j.memsci.2011.02.005

58. Koros WJ, Coleman MR, Walker DRB. Controlled permeability polymer membranes. *Annu Rev Mater Sci*. 1992;22:47-89.

59. Yan X, He G, Gu S, Wu X, Du L, Wang Y. Imidazolium-functionalized polysulfone hydroxide exchange membranes for potential applications in alkaline membrane direct alcohol fuel cells. *Int J Hydrog Energy*. 2012;37(6):5216-5224. doi:10.1016/j.ijhydene.2011.12.069

60. Geise GM, Paul DR, Freeman BD. Fundamental water and salt transport properties of polymeric materials. *Prog Polym Sci*. 2014;39(1):1-42. doi:10.1016/j.progpolymsci.2013.07.001

61. Li J, Xiong B, Yin C, Zhang X, Zhou Y, Wang Z, Fang P, He C. Free volume characteristics on water permeation and salt rejection of polyamide reverse osmosis membranes investigated by a pulsed slow positron beam. *J Mater Sci*. 2018;53(23):16132-16145. doi:10.1007/s10853-018-2740-3

62. Zhang S, Zhang R, Jean YC, Paul DR, Chung T-S. Cellulose esters for forward osmosis: Characterization of water and salt transport properties and free volume. *Polymer*. 2012;53(13):2664-2672. doi:10.1016/j.polymer.2012.04.024

63. Okorafor OC. Solubility and Density Isotherms for the Sodium Sulfate−Water−Methanol System. *J Chem Eng Data*. 1999;44(3):488-490. doi:10.1021/je980243v

64. Randová A, Hovorka Š, Izák P, Bartovská L. Swelling of Nafion in methanol–water–inorganic salt ternary mixtures. *J Electroanal Chem*. 2008;616(1):117-121. doi:10.1016/j.jelechem.2007.12.018

65. Bhattarai A, Nandi P, Das B. The Effects of Concentration, Relative Permittivity and Temperature on the Transport Properties of Sodium Polystyrenesulphonate in Methanol–Water Mixed Solvent Media. *J Polym Res*. 2006;13(6):475-482. doi:10.1007/s10965-006-9070-x

66. Cohen MH, Turnbull D. Molecular Transport in Liquids and Glasses. *J Chem Phys*. 1959;31(5):1164-1169. doi:10.1063/1.1730566

67. Ito K, Saito Y, Yamamoto T, Ujihira Y, Nomura K. Correlation Study between Oxygen Permeability and Free Volume of Ethylene−Vinyl Alcohol Copolymer through Positronium Lifetime Measurement. *Macromolecules*. 2001;34(18):6153-6155. doi:10.1021/ma001813a

68. Carter BM, Keller L, Wessling M, Miller DJ. Preparation and characterization of crosslinked poly(vinylimidazolium) anion exchange membranes for artificial photosynthesis. *J Mater Chem A*. 2019;7(41):23818-23829. doi:10.1039/C9TA00498J

69. Sagle AC, Ju H, Freeman BD, Sharma MM. PEG-based hydrogel membrane coatings. *Polymer*. 2009;50(3):756-766. doi:10.1016/j.polymer.2008.12.019

70. Sagle AC, Van Wagner EM, Ju H, McCloskey BD, Freeman BD, Sharma MM. PEG-coated reverse osmosis membranes: Desalination properties and fouling resistance. *J Membr Sci*. 2009;340(1):92-108. doi:10.1016/j.memsci.2009.05.013

71. Chen Z, Rand RP. The influence of cholesterol on phospholipid membrane curvature and bending elasticity. *Biophys J*. 1997;73(1):267-276. doi:10.1016/S0006-3495(97)78067-6

72. Li JY, Nemat-Nasser S. Micromechanical analysis of ionic clustering in Nafion perfluorinated membrane. *Mech Mater*. 2000;32(5):303-314. doi:10.1016/S0167-6636(00)00002-8

73. Alexandre B, Langevin D, Médéric P, Aubry T, Couderc H, Nguyen QT, Saiter A, Marais S. Water barrier properties of polyamide 12/montmorillonite nanocomposite membranes: Structure and volume fraction effects. *J Membr Sci*. 2009;328(1):186-204. doi:10.1016/j.memsci.2008.12.004

74. Schaetzel P, Vauclair C, Nguyen QT, Bouzerar R. A simplified solution–diffusion theory in pervaporation: the total solvent volume fraction model. *J Membr Sci*. 2004;244(1):117-127. doi:10.1016/j.memsci.2004.06.060

75. Gebel G. Structural evolution of water swollen perfluorosulfonated ionomers from dry membrane to solution. *Polymer*. 2000;41(15):5829-5838. doi:10.1016/S0032-3861(99)00770-3

76. Mukoma P, Jooste BR, Vosloo HCM. A comparison of methanol permeability in Chitosan and Nafion 117 membranes at high to medium methanol concentrations. *J Membr Sci*. 2004;243(1):293-299. doi:10.1016/j.memsci.2004.06.032

77. Elabd YA, Napadensky E, Sloan JM, Crawford DM, Walker CW. Triblock copolymer ionomer membranes: Part I. Methanol and proton transport. *J Membr Sci*. 2003;217(1):227-242. doi:10.1016/S0376-7388(03)00127-3

78. Pivovar BS, Wang Y, Cussler EL. Pervaporation membranes in direct methanol fuel cells. *J Membr Sci*. 1999;154(2):155-162. doi:10.1016/S0376-7388(98)00264-6

79. Tricoli V, Carretta N, Bartolozzi M. A Comparative Investigation of Proton and Methanol Transport in Fluorinated Ionomeric Membranes. *J Electrochem Soc*. 2000;147(4):1286-1290. doi:10.1149/1.1393351

80. Elabd YA, Walker CW, Beyer FL. Triblock copolymer ionomer membranes: Part II. Structure characterization and its effects on transport properties and direct methanol fuel cell performance. *J Membr Sci*. 2004;231(1):181-188. doi:10.1016/j.memsci.2003.11.019

81. Huang QM, Zhang QL, Huang HL, Li WS, Huang YJ, Luo JL. Methanol permeability and proton conductivity of Nafion membranes modified electrochemically with polyaniline. *J Power Sources*. 2008;184(2):338-343. doi:10.1016/j.jpowsour.2008.06.013

82. Chaabane L, Dammak L, Grande D, Larchet C, Huguet P, Nikonenko SV, Nikonenko VV. Swelling and permeability of Nafion®117 in water–methanol solutions: An experimental and modelling investigation. *J Membr Sci*. 2011;377(1):54-64. doi:10.1016/j.memsci.2011.03.037

Chapter 7: Multicomponent transport in PEGDA-PEA-AMPS Membranes of Varied Charge Content

7.1. Introduction

The preceding chapters examine the multicomponent transport behavior in neutral PEGDA membranes and the commercially available cation exchange membrane, Nafion™ 117. The investigation on Nafion™ 117 was able to probe the interplay of solubility, diffusivity, and permeability for alcohol transport and transport of complex mixtures of alcohols. However, as a commercial membrane, it is not possible to vary membrane properties to investigate the structural roots of the observed behavior. This led to our work on PEGDA-based membranes of varied pre-polymerization water content. This platform allowed for the investigation of the role of fractional free volume on multicomponent transport; however, these membranes are less complex as they do not also incorporate membrane-bound ionic moieties. Here, these efforts are extended by synthesizing and investigating multicomponent transport behavior PEGDA-based membranes that incorporate both a hydrophobic comonomer, 2-phenoxyethyl acrylate (PEA), and a cation exchange comonomer, 2-acrylamido-2-methyl-1-propanesulfonic acid (AMPS), that features a bound sulfonate group analogous to that in Nafion™ 117. PEA, shown in Figure 7.1a, was selected as a comonomer as it is readily incorporated into the structure, and is more hydrophobic than PEGDA and AMPS, which should lead to reduced water uptake and thereby lower permeability of solutes such as the CO_2 reduction products of interest. PEGDA is maintained as the core bifunctional platform to provide network formation via crosslinking. AMPS was selected as the ionic comonomer as it contains a bound sulfonate side chain, shown in Figure 7.1b, which is incorporated as a pendant moiety from the polymer membrane network. These membrane-bound sulfonate groups are analogous to the sulfonate groups bound to Nafion membranes and make

these materials cation exchange membranes of controlled ion content through the AMPS content in the synthesis step.

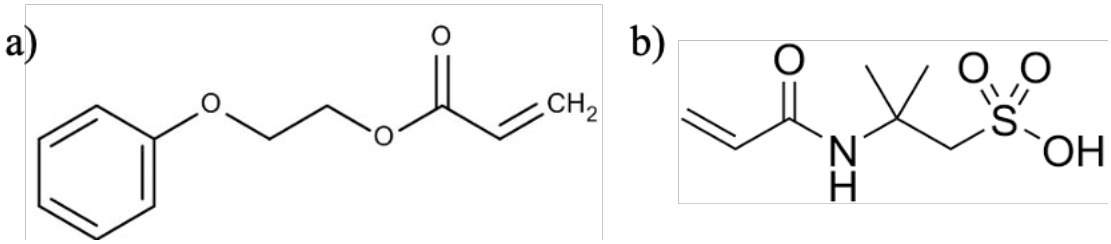

Figure 7.1. Chemical structure of a) 2-phenoxyethyl acrylate (PEA) and b) 2-acrylamido-2-methyl-1-propanesulfonic acid (AMPS).

The inclusion of two comonomers (PEA and AMPS) to the PEGDA membranes investigated in Chapter 6, in addition to variation in the pre-polymerization water content, dramatically expands the compositional space for synthesizing membranes. Here, a constant PEGDA and water content in the pre-polymerization mixtures were maintained, and the relative amount of PEA and AMPS varied. In this way, membranes with similar network structures are compared through analogous pre-polymerization water content, difunctional monomer content, and monofunctional comonomer content, but modify the hydrophobicity (PEA) and ion content (AMPS).

Methanol and sodium acetate, two very important CO_2 reduction products, are the solutes of interest for this work. Methanol was selected as it is the smallest neutral product, and therefore, generally the most common neutral solute in the reduction product stream. Sodium acetate was selected to relate this work to the results in Chapter 6 (varied FFV PEGDA[1]) and separate collaborative work on PEGDA-AMPS membranes[2].

Analogous to the work presented in Chapters 5 and 6, in situ ATR FTIR spectroscopy is employed to monitor the permeation of a series of CO_2 reduction products. Permeability experiments were

conducted for unary and binary mixtures using the custom-built diffusion cells outfitted with in situ ATR FTIR spectroscopy to monitor the temporal receiver cell solution concentrations of methanol and sodium acetate. Solute sorption/desorption experiments are also performed to evaluate solute solubility for each of the solute feed combinations and used to calculate solute diffusivities using the solution-diffusion model. The relative changes in alcohol permeability and permselectivity are discussed, as are how these changes are related to changes in the membrane structure.

7.2 Results and Discussion

To extend previous work on PEGDA membranes of varied FFV[1] and PEGDA-AMPS membranes of varied AMPS content[2], a series of PEGDA-PEA-AMPS membranes were synthesized with varied relative content of AMPS and PEA. PEGDA and pre-polymerization water content were both kept constant. Both PEA and AMPS readily polymerize into the membrane in the presence of HCPK, due to their reactive double bonds; chemical structures are shown in Figure 7.1. Unfortunately, inclusion of PEA at very high contents was precluded by solubility issues using our current membrane fabrication scheme. At a PEA content of 52 mol %, the solution, even after prolonged sonication, was cloudy, indicating phase separation (Figure 7.2a). This set the compositional window of our membranes as we found 44 mol % to form homogeneous pre-polymerization mixtures. PEGDA content in the synthesized membranes was thus set at 56 mol %, while the remaining 44 mol % of the membrane species were composed of PEA and AMPS contents of varying relative amounts; Table 7.1. A constant mass (8 g) of the membrane-forming species was maintained for preparing the pre-polymerization mixtures in addition to a constant amount of water. We denote these membranes as PEAXX, where XX denotes the pre-

polymerization mixture mole percent of PEA; i.e., PEA22 has a pre-polymerization PEA content of 22 mol %. The PEA and AMPS contents varied from 0 to 44 mol % (0, 11, 22, 33, and 44 mol % PEA, the remainder AMPS). All solutions and membranes synthesized were homogeneous and optically transparent. It was also noticed that as the PEA content increased, the membranes become more mechanically robust as they were easier to handle, but further mechanical characterization was not performed.

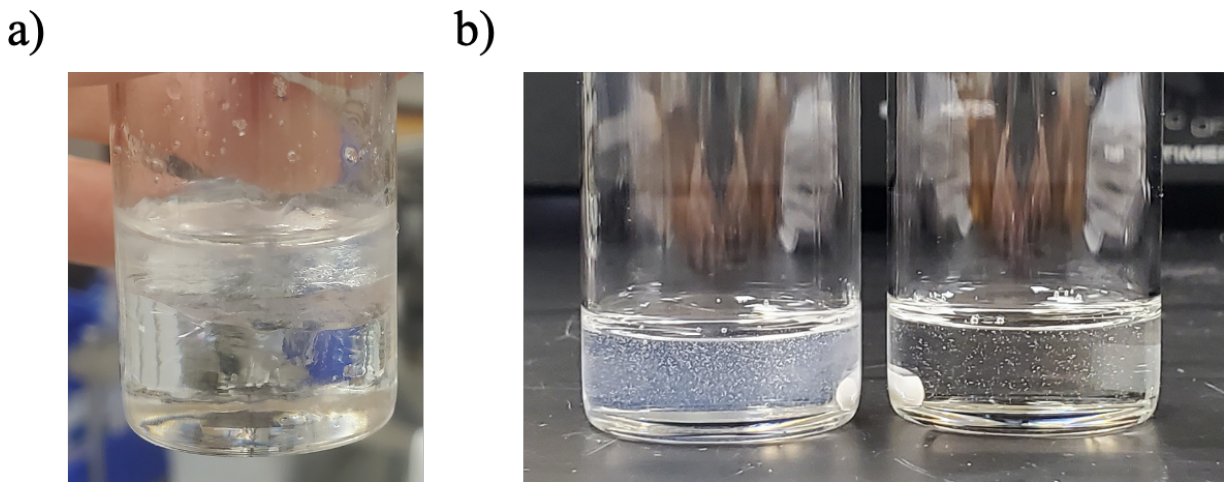

Figure 7.2. Photographic images of a) PEA-PEGDA solution of 56-44 mol% before sonication and b) PEA-PEGDA of 56-44 mol% on the left and PEA-PEGDA of 44-56 mol% on the right, after sonication. All solutions contain 2 g water per 8 g of monomer solution.

Table 7.1. PEGDA-PEA-AMPS Membrane Compositions

Membrane	PEGDA [mol%]	PEA [mol%]	AMPS [mol%]
PEA00	**56.0**	**0.0**	**44.0**
PEA11	**55.9**	**11.1**	**33.0**
PEA22	**55.7**	**22.2**	**22.0**
PEA33	**54.9**	**34.3**	**10.8**
PEA44	**55.7**	**44.3**	**0.0**

The observed solubility issue for PEA is consistent with the differences in the solubility parameters between PEGDA, AMPS, and PEA. The closer the solubility parameters, the more likely two species are to form a homogeneous phase. PEGDA and water both have relatively high solubility parameters (32.9[3] and 47.8[3] $MPa^{1/2}$, respectively), while AMPS and PEA much lower (18.7[4] and 11.03[5] $MPa^{1/2}$, respectively) for an overall solubility parameter ordering of Water>PEGDA>AMPS>PEA. Therefore, it is unsurprising that at relatively high PEA content (here 52 mol % was tested), miscibility was an issue; as shown in Figure 7.2.

Water uptake was measured gravimetrically, as discussed in Chapter 3, as a measure of the fractional free volume of these membranes as the composition is varied; higher water uptake being indicative of greater fractional free volume. Figure 7.3a shows the water-swollen membrane weight compared to vacuum dried membrane weight, and Figure 7.3b shows the methanol uptake (filled blue diamonds), sodium acetate uptake (filled pink squares), and simultaneous uptake (open purple triangles). The dotted black line in Figure 7.3b indicates no change in water swollen and solvent swollen weight. There is an increase in water uptake between the PEA00 and PEA11 in Figure 7.3a, potentially due to the bulkier PEA sidechain compared to the and more linear AMPS molecule, as can be seen from the 3D figures of the molecules shown in Figure 7.4, resulting in increased fractional free volume. From there, the water uptake decreases with increasing PEA content, expected based on the relative hydrophobicity of PEA compared to AMPS. Recall PEA has the farthest solubility parameter from water, in the order Water>PEGDA>AMPS>PEA. The solute solution uptakes, Figure 7.3b, for PEA11 displays analogous single component uptakes (filled blue diamonds and pink squares, respectively) and the PEA22 solute solution uptakes for each are also very similar. With increasing PEA content, the difference between methanol solution

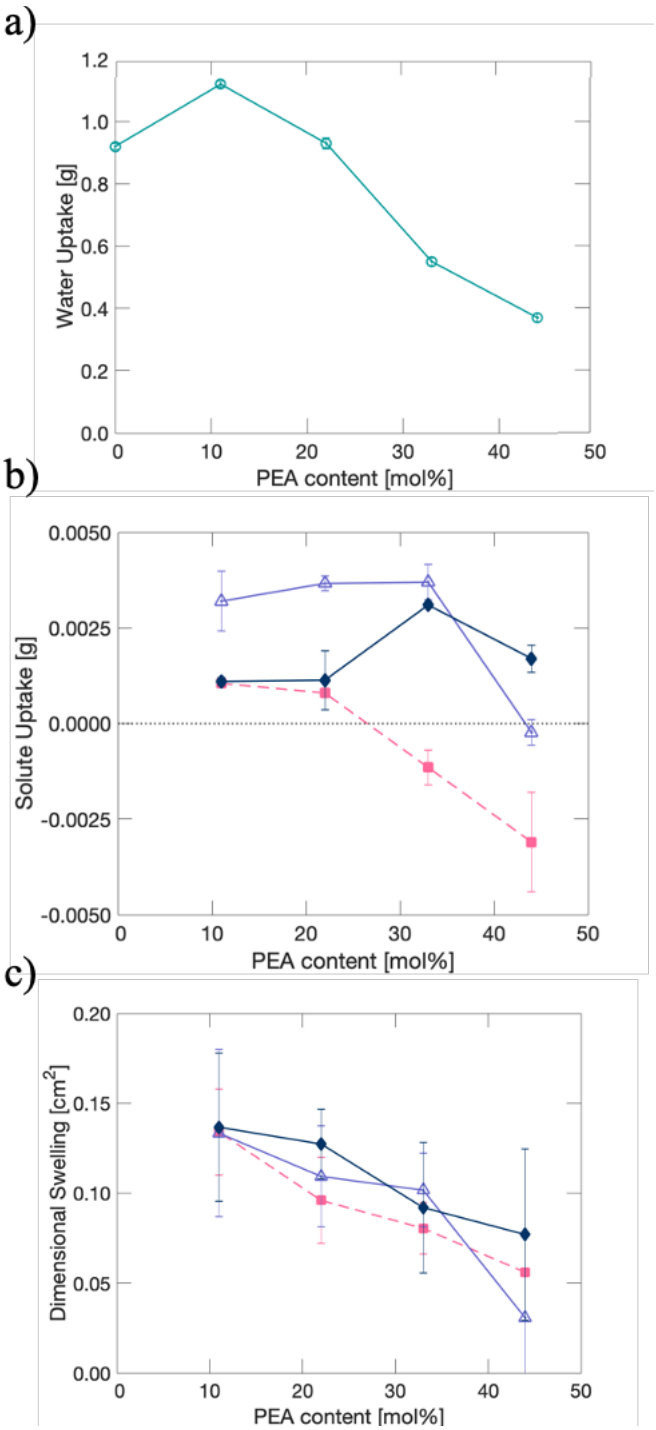

Figure 7.3. Uptake and swelling for varying PEA content within the PEGDA-PEA-AMPS membranes a) water uptake, b) solute uptakes, and c) dimensional swelling. (♦) methanol uptake, (■) sodium acetate uptake, and (△) methanol and sodium acetate simultaneous uptake, and (○) water uptake. Lines connecting experimental points are to guide the eye, and the dotted black line is at 0 g, where the membrane doesn't change from water-swollen to solvent swollen. Error bars are standard deviations from triplicate measurements, where error bars are smaller than the data points.

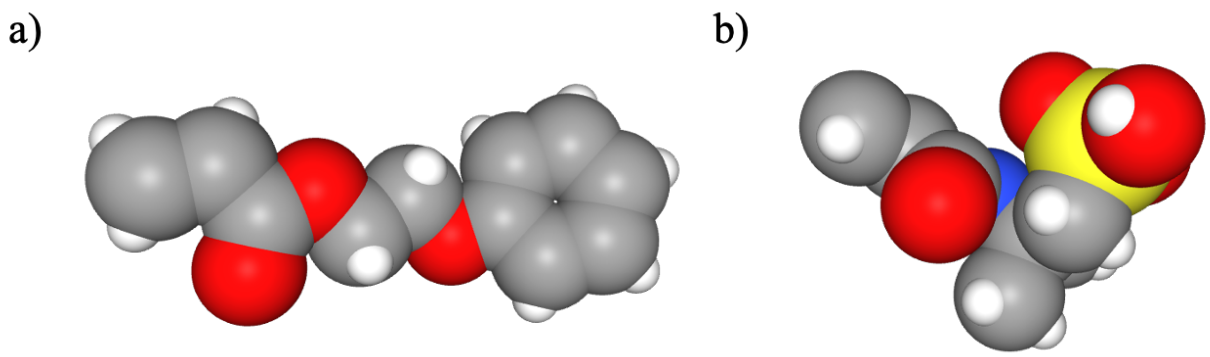

Figure 7.4. 3D structures of a) PEA and b) AMPS.

Table 7.2. Water uptake, solute uptake, and dimensional swelling.

	Water Uptake [g]	**Methanol Uptake [g]**	**Sodium Acetate Uptake [g]**	**Methanol and Sodium Acetate Uptake [g]**	**Methanol Swelling [cm^2]**	**Sodium Acetate Swelling [cm^2]**	**Methanol and Sodium Acetate Swelling [cm^2]**
PEA00	0.92						
PEA11	1.12	0.0011	0.0011	0.0032	0.14	0.13	0.13
PEA22	0.93	0.0011	0.0008	0.0037	0.13	0.10	0.11
PEA33	0.55	0.0031	-0.0012	0.0037	0.09	0.08	0.10
PEA44	0.37	0.0017	-0.0031	-0.0002	0.08	0.06	0.03

and sodium acetate solution uptakes increase extensively. Methanol solution uptake for both PEA33 and PEA44 was higher, with PEA33 displaying the highest methanol solution uptake. Sodium acetate solution uptake (filled pink squares) decreases continuously with increasing PEA content. The increasing methanol and decreasing sodium acetate uptakes result in an essentially flat mixture solution uptake (open purple triangles), until the highest PEA content (PEA44), where the significant membrane deswelling (relative to water uptake) from the sodium acetate likely dominates. This is clear from the dimensional swelling in Figure 7.3c, where the increase in membrane area after equilibration in 1.0 M solute solutions was most significant for PEA11 and decreases with increasing PEA content for a swelling trend of PEA11>PEA22>PEA33>PEA44 for methanol, sodium acetate, and the binary mixture. Unfortunately, the standard deviations for these solute solution uptake experiments are extensive and generally overlap at each PEA/AMPS content muddling any possible conclusions. Additional replicates of these experiments are to be carried out, in addition to solubility studies analogous to those discussed in Chapter 5 for Nafion^{TM} 117. These solubility studies were unfortunately disrupted by laboratory shutdown and subsequent instrumentation issues and will be performed in future to complete the characterization of the transport behavior of these membranes.

The transport of methanol and sodium acetate through these varied membranes was characterized via ATR FTIR spectroscopy, as described extensively in Chapters 3-5. Briefly, a known concentration of solute is placed in the donor cell (1.0 M), and pure DI water is placed in the receiver cell. The cells are jacketed for temperature control and well mixed with magnetic stir bars. The membrane is sandwiched between the cells with a hand-tightened metal clamp. The ATR FTIR spectroscopy probe (ReactIR 15 from Mettler Toledo (Columbus, OH) with a 9.5 mm AgX

Dicomp probe (Au, diamond, C22)) is placed in the receiver cell to characterize the increase in solute concentration that has passed through the membrane over time.

The extracted permeability values are shown in Table 7.3 and plots of permeability versus PEA content compared to water uptake are included in Figure 7.5 a and b, respectively. The permeabilities of these membranes follow expectations based on water uptake and previous work with these solutes. PEA11 had the largest permeability to methanol with decreasing permeability as PEA content increases. Methanol is a neutral molecule, while sodium acetate is similarly charged to the AMPS moieties such that Donnan exclusion is a factor. Also, sodium acetate is much larger than methanol and requires more polymer reptation for diffusion to occur, both tending to decrease permeability. The approximate order of magnitude higher permeability to methanol compared to sodium acetate is consistent with the relative permeability for these solutes for Nafion™ 117[6] as well as the varied FFV PEGDA membranes[1] described in Chapter 6. Comparing these single component permeabilities to the permeabilities from the binary experiments, distinct behavior is observed. The general trends for both methanol and sodium acetate in the binary experiments are analogous to the patterns observed for the single component experiments. The observed overall decreases in permeability are consistent with the decreasing water uptake as the PEA content increases and the membranes become more hydrophobic. Methanol permeability generally decreases in the binary case compared to the single component case, while sodium acetate remains essentially unchanged. This seems to suggest that the transport of sodium acetate, in this case, is unaffected by the methanol co-solute. Meanwhile, at higher AMPS content (lower PEA content, higher ion content, higher water uptake), methanol experiences a decrease, and most considerable difference, compared to the single component

experiments. This suggests that the presence of membrane-bound ions is impacting the transport behavior. The inclusion of increasing PEA, and decreasing AMPS, results in a decreasing, and eventually no difference, in permeability to methanol. As discussed above, determination of membrane solubility to these solutes and the solutes from the binary mixture are to be conducted to further examine this behavior.

As discussed in Chapters 5 and 6, membrane permselectivity is an important and useful metric for examining changes in membrane transport behavior. The 'ideal' selectivity is the ratio of membrane permeability to each solute extracted from single component permeability experiments, while the 'true' selectivity utilizes the permeability values extracted from multicomponent transport experiments. The membrane permselectivity (both 'ideal' and 'true') to methanol and sodium acetate are shown in Table 7.4.

As was observed for Nafion^{TM} 117 and PEGDA membranes of varied FFV in Chapters 5 and 6, the permselectivity can vary greatly between the 'ideal' and 'true' values. The 'ideal' selectivities here for methanol to sodium acetate range from 6.77 to 32.03, while 'true' values only range between 5.26 and 9.74. Interestingly, for PEA-containing membranes, the difference between the ideal and true selectivity increases with increasing PEA content with the largest percent difference observed for PEA44, where the ideal and true selectivity differs by a factor of about four! Again, these multicomponent experiments are incredibly important for determining true transport behavior.

Table 7.3. Permeability values of methanol and sodium acetate in single and multicomponent experiments.

P_i x 10^6 [cm^2/s]				
	Single Component		**Multicomponent**	
Membrane	**Methanol**	**Acetate**	**Methanol**	**Acetate**
PEA00	1.63	0.18	1.48	0.24
PEA11	2.82	0.36	2.48	0.36
PEA22	2.39	0.35	1.73	0.33
PEA33	1.43	0.20	1.31	0.13
PEA44	0.72	0.02	0.64	0.07

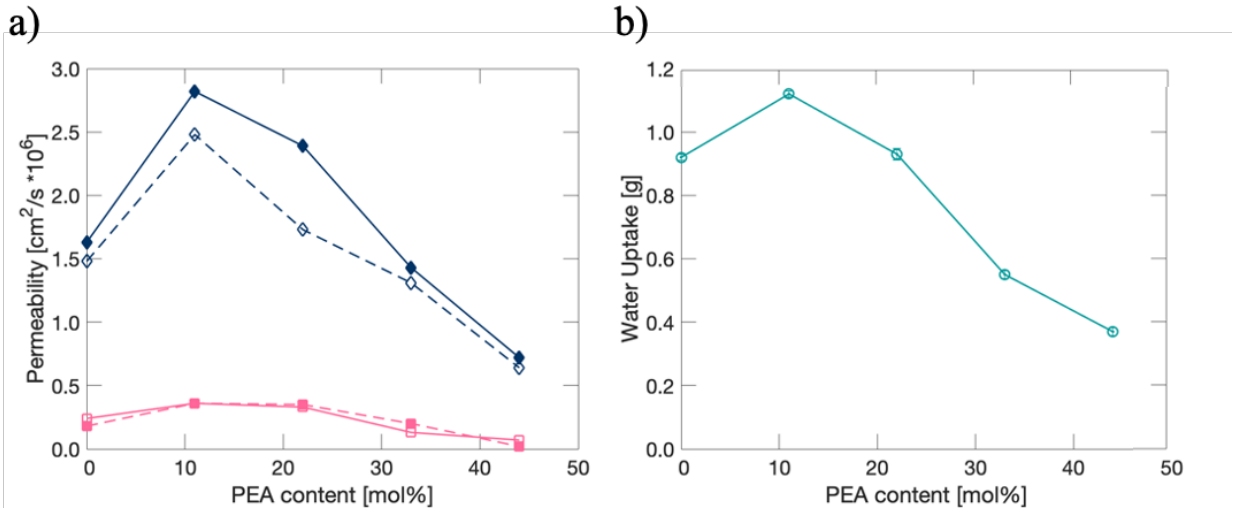

Figure 7.5. Permeability and water uptake as a function of PEA mol%. a) Single and multicomponent permeabilities and b) water uptake. (♦) methanol, (■) acetate, and (○) water uptake. Filled markers are methanol and acetate multicomponent experiments and open markers are single component experiments. Only 15% of the experimental data is shown for clarity. Lines are strictly to guide the eye.

Table 7.4. Selectivity of varied PEA-AMPS content membranes to methanol over sodium acetate. Ideal selectivity is based upon single component experiments and true selectivity is based upon simultaneous, multicomponent transport experiments.

$\alpha_{M/S}$	Ideal	True	% Diff
PEA00	8.96	6.24	30
PEA11	7.73	6.82	12
PEA22	6.77	5.26	22
PEA33	7.18	9.74	36
PEA44	32.03	8.75	73

7.3. Conclusions

PEGDA-PEA-AMPS membranes were synthesized similar to the PEGDA varied FFV membranes, but with additional monomers. The inclusion of PEA increases hydrophobicity and inclusion of AMPS introduces increasing membrane-bound ion content. Water uptake, solute uptake, and permeability to methanol and sodium acetate in single and multicomponent solutions were characterized, as well as permselectivity. The permeabilities followed the water uptake with decreasing water uptake corresponding to decreasing permeability. In comparison, ideal to true selectivity variation of up to 73% (or a factor of about four) was observed, again indicating how important these experiments are for complex multicomponent transport behavior characterization. Future characterization of solute solubilities for these membranes and solutes will provide additional insights into the cause of this behavior.

7.4. References

1. Dobyns BM, Kim JM, Beckingham BS. Multicomponent transport of methanol and sodium acetate in poly(ethylene glycol) diacrylate membranes of varied fractional free volume. *Eur Polym J*. 2020;134:109809. doi:10.1016/j.eurpolymj.2020.109809

2. Kim JM, Dobyns BM, Zhao R, Beckingham BS. Multicomponent transport of Methanol and Acetatein a series of crosslinked PEGDA-AMPS cation exchange membranes. *J Membr Sci*. Published online 2020.

3. Hansen CM. *Hansen Solubility Parameters: A User's Handbook, Second Edition*. CRC Press; 2007.

4. Durmaz S, Okay O. Acrylamide/2-acrylamido-2-methylpropane sulfonic acid sodium salt-based hydrogels: synthesis and characterization. *Polymer*. 2000;41(10):3693-3704. doi:10.1016/S0032-3861(99)00558-3

5. Sutton D, Stanford JL, Ryan AJ. Structure-Property Relations in Reaction-Induced, Phase-Separated Poly(2-Phenoxyethyl Acrylate)/Polystyrene Blends. *J Macromol Sci Part B*. 2001;40(3-4):485-506. doi:10.1081/MB-100106172

6. Beckingham BS, Lynd NA, Miller DJ. Monitoring multicomponent transport using in situ ATR FTIR spectroscopy. *J Membr Sci*. 2018;550:348-356. doi:10.1016/j.memsci.2017.12.072

8. Conclusions and Future Work

The scientific community greatly needs improved separation techniques, as 10-15 % of the total energy used within the United States is for separations. These separations enable our current medication, water purification, energy production, harmless food, and chemical separation sectors.[1] Synthetic polymeric membranes are widely used in research today as they can be tailored to the specifications desired for a particular application. However, the characterization of simultaneous transport of multiple species through polymer membranes is widely needed, due to poor understanding of the array of complex interactions present in such systems. Unfortunately, common speciation techniques have a range of involved complications which has precluded investigation; a deficiency this dissertation seeks to remedy.

This dissertation has detailed a technique for determining multicomponent permeabilities in situ (Figure 8.1) and leveraged this technique to interrogate the transport and multicomponent transport behavior of both commercially available (Nafion™ 117) and tailored polymer membranes (PEGDA membranes of varied fractional free volume and PEGDA-PEA-AMPS membranes of varied composition).

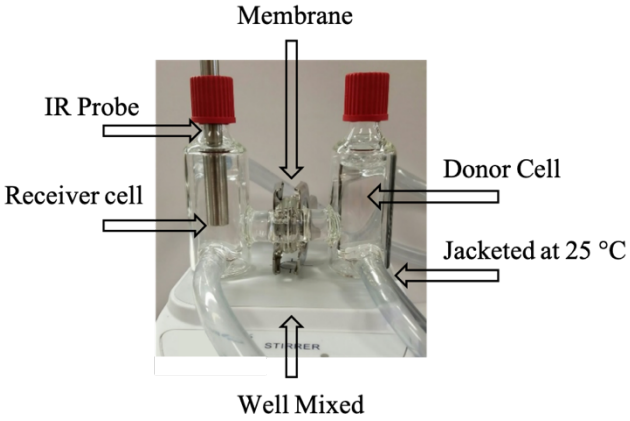

Figure 8.1. Diffusion Cell Apparatus.

Critically, this work demonstrates both the utility of in situ ATR FTIR spectroscopy as a technique and the need to perform multicomponent transport experiments to capture solute behavior for complex mixtures; one of the most needed areas of investigation for membranes in the water purification and energy production, particularly solar fuels, research communities.[2,3] This work furthers the capabilities of the membrane research community by showing the importance of these multicomponent experiments for probing fundamental membrane behavior concerning applications of interest, and moving toward a better mechanistic understanding of complex transport. This fundamental research has been largely neglected and is required for membrane processes to move forward. Indeed, differences between single and multicomponent permselectivity for select solute pairs varied by up to 73 %. To select a membrane based upon the 'ideal' or single component permselectivity, would thereby not perform as sought.

In the end, this work can help science save the world! With this new, facile, accurate technique, the water purification and energy production sectors can benefit greatly, were they to adopt and implement the techniques developed herein. The following provides brief summative conclusions of each topic discussed in the dissertation and a summary of potential extensions of this work in future; some of which are already underway.

8.1. Multicomponent transport of alcohols in Nafion ™117 measured by in situ ATR FTIR spectroscopy

The permeability of Nafion™ 117 to methanol, ethanol, n-propanol, and acetone was investigated through single, double, triple, and quadruple component permeability experiments. The permeability to methanol was found to be well within the literature range, indicating that the proposed technique for facile, multicomponent, in situ characterization is an adequate technique for determining solute transport. From there, multicomponent validation mixtures were prepared to determine if the found effective extinction coefficients held for multiple components in solution. The permeabilities to these solutes were characterized and the observed changes were complex and, in some cases, significant. This was exemplified by comparison of 'ideal' and 'true' permselectivity determined from single solute and two-solute diffusion cell experiments, respectively, and were found to vary by as much as 60% (for ethanol/n-propanol). Changes in solute solubility and diffusivity were inversely correlated (as expected) through the solution-diffusion model, and changes in solubility and diffusivity were both found to impact the changes in observed permeability. For the series of solutes here, changes in their permeation behavior in Nafion™ 117 are a result of changes in a combination of solubility and diffusivity and had a significant impact on the resulting permselectivity.

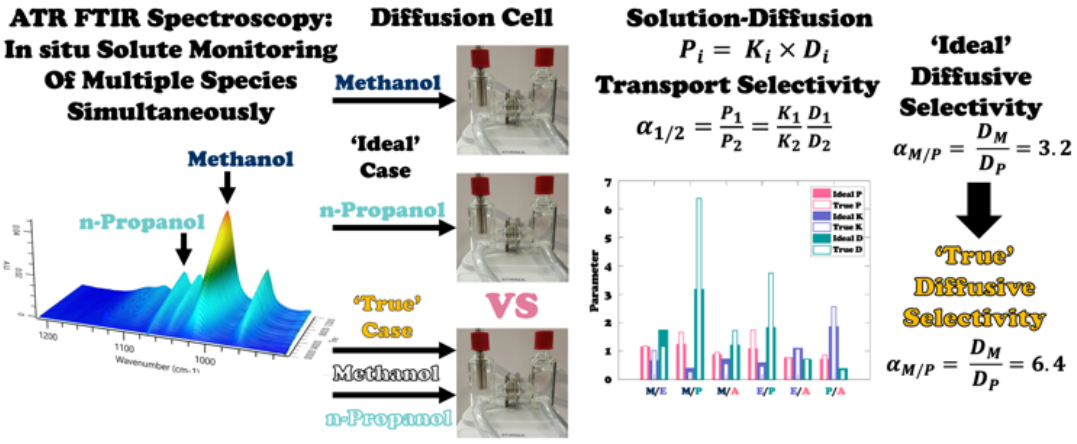

Figure 8.2. Graphical overview of Nafion™ 117 research in this dissertation.

8.2. Multicomponent transport in PEGDA membranes of varied fractional free volume (FFV)

A series of PEGDA membranes were synthesized with varied fractional free volume via pre-polymerization water content and their permeability to methanol, sodium acetate, and their binary mixture investigated. Water uptake was characterized as a measure of fractional free volume, which was found to increase with increasing pre-polymerization water content. Membrane permeability to methanol and sodium acetate was varied by up to a factor of 6 and 11, respectively, as the pre-polymerization water content and thereby FFV of the membranes was increased. Furthermore, distinct, and increasing, differences in the magnitude of extracted permeabilities between single solute and combined solute experiments were observed as the FFV increases. These differences are attributed to a combination of assisted and competitive transport.

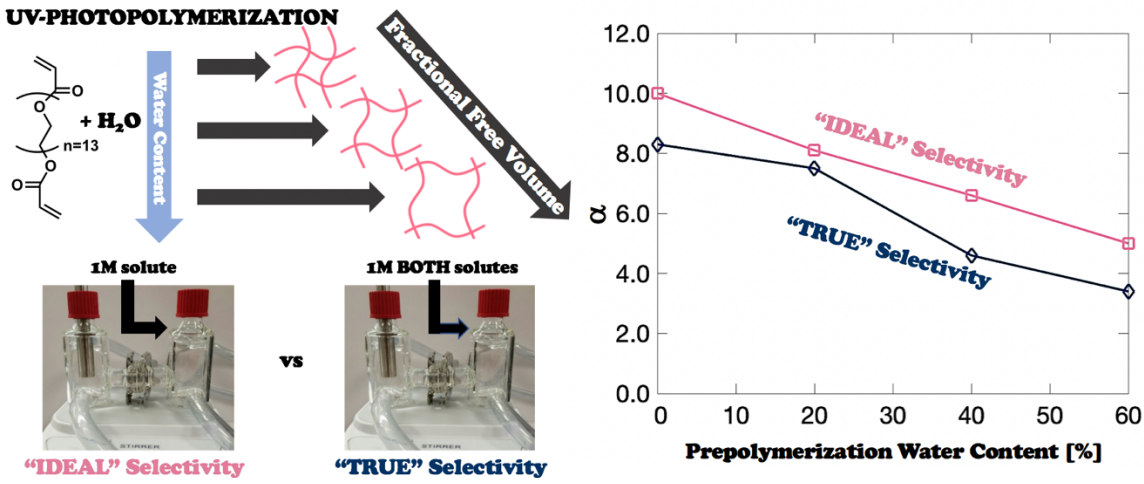

Figure 8.3. Graphical overview of varied FFV PEGDA membrane research in this dissertation.

8.3. Multicomponent transport PEGDA-PEA-AMPS membranes of varied hydrophobicity and ion content

PEGDA-PEA-AMPS membranes were photopolymerized of varied relative PEA (hydrophobic monomer) and AMPS content (cation exchange monomer) with otherwise analogous composition (identical PEGDA, water, and photoinitiator concentrations). Water uptake, solute uptake, and permeability of these membranes to methanol and sodium acetate were measured to characterize structure-property relationships. Water uptake and permeability followed similar trends: as PEA content increases, both decrease as the membranes become more hydrophobic. These trends follow our expectations based on monomer solubility parameters. PEA00 demonstrated lower permeability to both solutes and lower water uptake than the PEA11 and PEA22 membranes, possibly due to higher fractional free volume as PEA is a bulkier molecule compared to AMPS, resulting in additional fractional free volume in PEA-containing membranes. Lastly, single and multiple component permeability and permselectivity were compared. Overall, the 'ideal' to 'true' selectivities varied by up to a factor of about four with the magnitude of this difference increasing with increasing AMPS content.

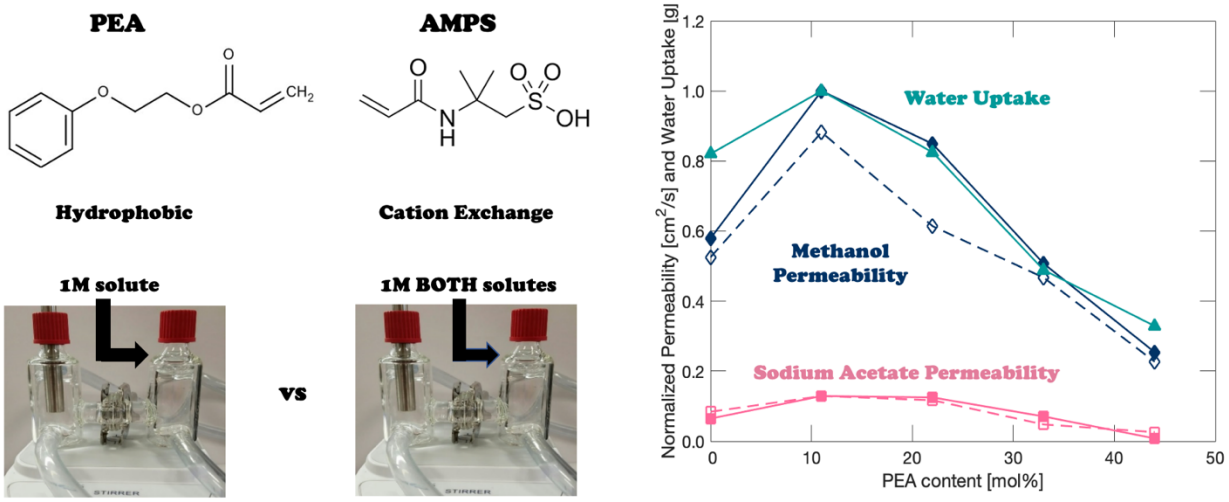

Figure 8.4. Graphical overview of PEGDA-PEA-AMPS research in this dissertation.

8.4. Future work

Transport of single components through dense polymer membranes has been relatively well described, yet binary and multicomponent transport is poorly understood due to the myriad of interactions that occur in these systems (i.e., between co-permeants and between permeants and the membrane). This dissertation attempts to begin answering some of the many questions in this area through careful measurement of membrane physiological properties, and evaluation of transport and multicomponent transport behavior. Many questions remain. For instance, the role of ion content (or ionic conductivity) on transport behavior is complex and essentially unstudied for multicomponent transport. To address the impact of ion content, additional investigation of PEGDA-AMPS membranes and PEGDA-PEA-AMPS membranes should be performed. These investigations could vary the ion content more thoroughly than explored herein, as well as modulating the pre-polymerization water content to evaluate the simultaneous impact of FFV. Further characterization is also needed to examine the solubility of solutes of interest in these systems, coupled with the permeability as examined for the Nafion^{TM} 117 membranes in this dissertation. Additionally, evaluation of these membranes should be extended to permeability to the other neutral alcohols studied herein. Another extension on this membrane chemistry platform is to incorporate dimethylaminoethyl acrylate (ammonium side chains) in lieu of AMPS (sulfonate side chains, similar to Nafion^{TM}) to prepare anion exchange membranes analogous to Selemion AMV. From there, these two chemistries could be combined to prepare bipolar membranes to control the local pH for catalyst stability, product selectivity, and overall performance for solar fuels devices. To extend on my work with PEA, other phenyl-terminal acrylates of varied chain length (such as benzyl acrylate) could be used as the hydrophobic comonomer. This would provide insights into the role of pendant chain length on transport behavior for these rather bulky end groups.

Overall, there remains many questions and challenges in understanding the behavior of complex mixtures and solute transport behavior. This dissertation and the examples above are just a few of the plethora of different possible membrane chemistries and solutes of interest to investigate to further our fundamental understanding of this complex behavior. This dissertation takes a solid first step towards understanding the complex behavior of complex mixtures in dense polymer membranes.

8.5. References

1. National Academies of Sciences, Engineering, and Medicine. *A Research Agenda for Transforming Separation Science*. The National Academies Press; 2019. doi:10.17226/25421
2. Tumas B, Dempsey J, Mallouk T, et al. Basic Energy Sciences Roundtable Liquid Solar Fuels. *Oak Ridge Natl Lab Publ*; 2019. doi:10.2172/1615599
3. Tirrell M, Hubbard S, Sholl D. Basic Research Needs for Energy and Water. *US Dep Energy*; 2017.